A Chiral Symmetric Calculation of Pion-Nucleon Scattering

U Ne Oo

M Sc (Rangoon University)

A thesis submitted in fulfillment of the

requirements for the degree of

Doctor of Philosophy

at the

University of Adelaide

Department of Physics and Mathematical Physics

University of Adelaide

South Australia

February 1993

Contents

List of Figures

List of Tables

Abstract

Within quark models of hadron structure which respect chiral symmetry (like the cloudy bag) it is possible to guarantee that well known soft-pion theorems are satisfied in Born approximation. The most famous example is the Weinberg-Tomozawa result for S-wave πN scattering. However when one goes beyond Born approximation to solve the problems to all orders it has not yet proven possible to satisfy both soft-pion theorems and unitarity. We intend to test a recent suggestion that the problem can be solved with a particular choice of relativistic wave equation.

Acknowledgements

First and foremost, I would like to express my sincere gratitude to my supervisor, Professor A.W.Thomas. The present work would not have materalised without his close guidance and encouragement. He was & is always kind and patient with his teaching, especially in the earlier days of my thesis work when I didn't have enough background knowledge. I am also indebted to his attitude of constant striving for the developments of the subject that consequently inspires me to do more work.

To a physicist of any social background, for the requirement of a degree or any other reasons, carrying out research presents him as a means *and* an end. However, the implications of rewarding a degree will vary from one to the other. One may be considered as an academic achievement that would serve as an avenue to make a living. However, to a citizen of Burma, carrying out research and then being rewarded a degree means something rather different. Under the profound political repression, which combined with grinding poverty, doing research for a Burmese means a rare opportunity to get research experience from leading scientists. The degree then rewarded is not simply a symbol of academic achievement, it is rather a symbol of overcoming all the odds which serve as an inspiration for the oppressed academics. The authorities in Burma certainly ought to learn such implications to avoid unnecessary conflicts.

In the midst of such conflict between the Burmese Military Government and myself, I am grateful to a number of people for their helps; Ms Tania Utkin, the Regional Director of South Australian branch of AIDAB; Dr A.J. Blake, the Head of Department of Physics and Mathematical Physics and Prof. Thomas, my supervisor. Without their help it would have been far more difficult to face the "*Long Days in Australia*". My hearty thanks also for my friends and colleagues; Martin C Palm, Than Htun Aung, Andrew R Rawlinson, Alex C Kalloniatis and the members of the Burma Action Group, who showed their support. The University is also thanked

for waiving their tuition fees in the last semester of 1992.

My thanks are, of course, not only to those who provided help in the turbulent year of 1992. It should be dating back to 1988, the year I commenced my research programme. The visitors and staff members of the Adelaide University Physics Department are thanked for their time and patience given to my questions. Dr Lindsay Dodd is especially thanked for his help. I wish to express my gratitude to Johann Haidenbauer,Guo Liu, Andrew A Rawlinson and Bruce C Pearce for reading my thesis. Their criticism and comments are undoubtedly beneficial to this work. My special thanks to Ms Arlene Shaw and Mark Ferraretto, who were always cheerful and willingly giving help. Staff members of AIDAB are thanked for their supports and services throughout those years.

Finally, my mother and my family in Burma are thanked for their support for my education.

Declarations

This work contains no material which has been accepted for the award of any other degree or diploma in any university or other tertiary institution and, to the best of my knowledge and belief, contains no material previously published or written by another person, except where due reference has been made in the text.

I give consent to this copy of my thesis, when deposited in the University Library, being available for loan and photocopying.

SIGNED:. . DATE: 9/2/93

Chapter 1

Introduction

The interaction of pions and nucleons has been studied extensively with many different approaches since the early days of nuclear physics. In those early days, there were limitations in the capabilities of both experimental and theoretical techniques with regard to πN physics [Kol 69, Eric70, EW 88]. The nucleon is accepted as an extended object but has to be treated as elementary particle. The study of the πN system was motivated by the aim to explain a more complex system, the nucleus. Although there was some success in explaining strong interactions there are still many unanswered questions. The S-wave pion-nucleon interaction near the energy threshold has been one of them.

In the eyes of present day's maturity of field theory and technology, studying the πN system represents not just a means to explain the nuclear structure but also serves as a system to test theories at a more fundamental level, such as quark models [Tho 84, Klu 91]. The developments in both theoretical and experimental strong interaction physics in the past two decades brings this subject to the forefront of our interest. The experimental confirmation of the quarks and the theory of Quantum Chromodynamics can be viewed as the major developments of the past two decades. Deep Inelastic Scattering (DIS) experiments certainly show the trails of quarks and gluons. Quantum Chromodynamics(QCD) is considered a most orthodox theory

for the subnuclear structure. The problem of confinement is unresolved and still stands as a profound barrier in understanding nuclear structure and nuclear physics. Therefore, there is a need to bridge the gap between traditional nuclear physics and QCD. Our study of the pion-nucleon system has the objective of building such a bridge.

In this work, attempts are made to test two concepts: unitarity and chiral symmetry. By now, considerable effort has been made to satisfy unitarity in strong interaction physics. Because of the non-convergence of the S-matrix in usual perturbation theory, an alternative formulation was required to describe strong interactions. Such divergences are unavoidable when we use field theory and calculate higher order graphs in order to describe interactions consistently. After the work of Bethe and Salpeter [BS 51], followed by that of Blankenbecler and Sugar [BbS 66] there is a method that can guarantee unitarity in field theory. The use of relativistic 3-dimensional propagators developed by Blankenbecler and Sugar in studying the NN interaction enable the successful application of field theory to the strong interaction [Erk 74, Hol+87, PL 70, Gro 82].

The success of One Boson Exchange potentials with unitarity preserving propagators in the NN interaction is rather elegant when compared with the remaining sectors of strong interaction. For example, in the πN system, the one particle exchange (tree diagrams) doesn't seem to provide a reasonable agreement with experiment when we unitarize the scattering equation. Especially for the S-wave interaction near threshold, the experimental phase shifts are not well reproduced and the scattering lengths are wrongly calculated when we attempt to unitarize the wave equation [Tho+87, CJ 86].

There is another concept of profound importance concerning with the symmetry of subnuclear particles: quarks and gluons. It is chiral symmetry. Historically, this symmetry was inspired by the smallness of the pion mass on the hadronic scale.

The partially conserving axial current(PCAC), the current algebra and soft-pion theorems were the major achievements in the 60s. These theorems, of course, build on the concept that both nucleon and pion are structureless (which is a somewhat simple picture compared with present day knowledge) were proved to be consistent with experiment [AD 68, EW 88]. These traditional soft-pion theorems should, perhaps, be considered as a successful test for the Chiral symmetry in the context of nucleons and pions.

Chiral symmetry continues to play a role in modern field theory in a more fundamental way. Nucleons consist of quarks and gluons which are confined to a spatial region. The QCD Lagrangian in the limit of massless quarks is found to be invariant under chiral transformations. This QCD Lagrangian is known to be highly non-linear and very difficult to solve. On the other hand, as we study low energy nuclear physics, the relevant degrees of freedom are not those of quarks and gluons, but mesons and nucleons. At first it seems for low energy nuclear physics there is no reason to take into account the dynamics of quarks and gluons. However, from the results of many workers, the interaction of pion and nucleon in low energy regime follows the dictate of the dynamics of the subnuclear particles [Tho 81, Tho 84, Klu 91].

It is rather interesting, from my point of view, to mention a brief account of the physics of chiral symmetry developed to this date. In the mid-70's the difficulty in applying exact QCD to calculations has led physicists to consider other alternatives. The bag model of the MIT group provides such alternative. In the MIT bag model, one uses the phenomenological confining force and can explain the nucleon structure. The quarks are seen as Dirac particles confined to a spherical cavity. This model, however, is not invariant under chiral symmetry. There is also no mention of how to include mesons in the scheme [Hey 77].

This drawback of MIT bag model is rectified by considering the pion (mesons) as a compensating field required by Chiral symmetry. The pion is considered an

elementary particle and nucleons as combined 3-quark states. It is important to point out that such a scheme not only provides links between traditional low energy nuclear physics and QCD but may also provide further theoretical clues regarding confinement. As we've just said, in traditional nuclear physics the approximate conservation of axial vector currents that resulted from smallness of pion mass in hadronic scales gave various low energy theoretical predictions. The soft-pion theorems are a good example. Within the context of chiral bag models, the smallness of the pion mass is also found to be crucial [Jaf 79, Tho+80, Tho 84].

As far as S-wave pion nucleon scattering is concerned, Weinberg's nonlinear Lagrangian satisfactorily predicts the isovector scattering length. The volume coupling version of Cloudy Bag Model (CBM) has been found to provide the same results [Tho 81]. However, our attitude is that we are not satisfied with the tree level calculation which is consistent with experiment only at threshold. We must be able to evaluate scattering lengths as well as phase shifts at finite energy.

Initially, it was assumed that the non-linear CBM lagrangians are reliable only to lowest order in the πN coupling. However, Kalbermann and Eisenberg proved that the CBM Lagrangians are also reliable for higher order calculations, such as pion production [KE 83]. In their work, Kalbermann and Eisenberg successfully calculated M1 photoproduction amplitude in the $\Delta(1232)$ energy region. This encourages us to use the CBM Lagrangian in higher order calculations.

The calculation for the S-wave πN interaction using higher order graphs has been done by [Tho+87, CJ 86]. In their work, Thomas et al. used the driving potential to order $\frac{1}{(2f)^4}$. However, the experimental isovector form factors were used instead of those given by the model and only the isoscalar contributions were calculated explicitly. The Lippmann-Schwinger equation was used to iterate the potential to preserve the unitarity.

In our work, we calculate the driving potential for S-wave to order $\frac{1}{(2f)^4}$, with

both the isoscalar and isovector contributions derived from the CBM Lagrangian. Various 3-dimensional relativistic propagators are used in solving the scattering equation.

The outline of this thesis is as follows. In Chapter 2, we discuss the relevance of chiral symmetry to nuclear physics. Attention has been given to the S-wave πN scattering at threshold. Firstly, the related problems encountered in explaining the S-wave threshold behaviour using covariant field theory are described. We then discuss how the approximate conservation of the axial current is used in solving this problem. Next we discuss the linear sigma model and how the PCAC results are reproduced in this model. Then we discuss Weinberg's non-linear representation of the sigma model and show how the purely isovector scattering lengths for πN S-wave are obtained(Weinberg-Tomozawa results).

In Chapter 3, we discuss the question of unitarity in field theory. In particular, attention has been given to the methods of approximations for the Bethe-Salpeter equation which ensure covariance and unitarity. We discuss the methods to deduce various three dimensional relativistic propagators. We also give attention to the so called "smooth" propagators that are consistent with Dirac phenomenology. The advantage of using such a propagator in systems of non-equal masses are discussed. We list the propagators used in testing the scattering equation.

Our major contribution to this work can be found in Chapter 4. In Chapter 4, the formalism used in deriving πN interactions is discussed. The examples of how the interaction of pion and quarks are transformed to those of pion and nucleon are discussed in detail. We then calculate the S-wave interaction to order of $\frac{1}{(2f)^4}$ using the Cloudy Bag Lagrangian.

In Chapter 5 we calculate the P-wave interaction to order $\frac{1}{(2f)^2}$ using the CBM Lagrangian. It is mainly a repetition of work done by previous researchers. We just include this for completeness.

In Chapter 6, we carry out renormalization for the S-wave πN interactions. We first give detailed derivations of the nucleon self energy, vertex renormalization and bare bag probability. After this presentation, which is a review of the renormalization procedure, we show how the renormalization is carried out for the Weinberg-Tomozawa interaction.

All of our numerical results are presented in Chapter 7. The various phase shifts and scattering lengths for S-wave and P-waves are given. The comparison for different relativistic propagators is also made. The threshold behaviour for the S-wave interactions are discussed.

We close the work with a general discussion and give an outlook for the πN S and P waves in Chapter 8.

Chapter 2

Chiral Symmetry in Nuclear Physics

2.1 Introduction

In this chapter, we will discuss how chiral symmetry plays an important role in the understanding of the strong interaction. We will first focus our attention on the traditional field theoretic methods in studying the S-wave interaction. In Section 2.2 we will firstly look at the covariant calculation of Feynman diagrams to lowest order. It will be seen that the use of pseudoscalar and pseudovector πN interactions in tree diagrams do not give correct scattering lengths for S-wave. In Section 2.3 the Partially Conserved Axial Current (PCAC) and soft-pion theorems are discussed. We then show how the bad results for the S-wave scattering lengths in Section 2.2 are rectified by soft-pion theorems. We discuss the linear σ models in Section 2.4 and show how S-wave scattering lengths are obtained. In Section 2.4.4, we discuss the Weinberg's non-linear σ model and show how the S-wave isovector scattering lengths (Weinberg-Tomozawa Results) are obtained.

2.2 Pseudoscalar and Pseudovector pion-nucleon interactions

The interaction between pions and nucleons can be described by an interaction Hamiltonian of the form (which is consistent with parity and charge conservation):

$$\mathcal{H}_{\pi NN}^{(ps)} = ig\bar{\Psi}_N\gamma_5\boldsymbol{\tau}\cdot\boldsymbol{\pi}\Psi_N \tag{2.1}$$

$$\mathcal{H}_{\pi NN}^{(pv)} = -(\frac{f}{m_\pi})\bar{\Psi}_N\gamma^\mu\gamma_5\boldsymbol{\tau}\Psi_N\cdot\partial_\mu\boldsymbol{\pi} \tag{2.2}$$

where g is the pseudoscalar coupling constant and f the pseudovector coupling constant(dimensionless):

$$\frac{g^2}{4\pi} = 14.3 \pm 0.08\ , \qquad \frac{f^2}{4\pi} = 0.097 \pm 0.001\ , \tag{2.3}$$

and f and g are related by

$$\frac{f}{m_\pi} = \frac{g}{2m_N}\ . \tag{2.4}$$

The two interactions,(2.1) and (2.2) are equivalent in the non-relativistic limit for P-wave scattering but not for S-wave.

2.2.1 The S-wave interaction

Using the pseudoscalar interaction (2.1), we can calculate the S-wave scattering amplitude by the usual covariant method [MS 88, BD 62, IZ 88, AH 84]. The S-matrix amplitude to order g^2 for the process

$$\pi_i(q) + N(p,s) \to \pi_j(q') + N(p',s')$$

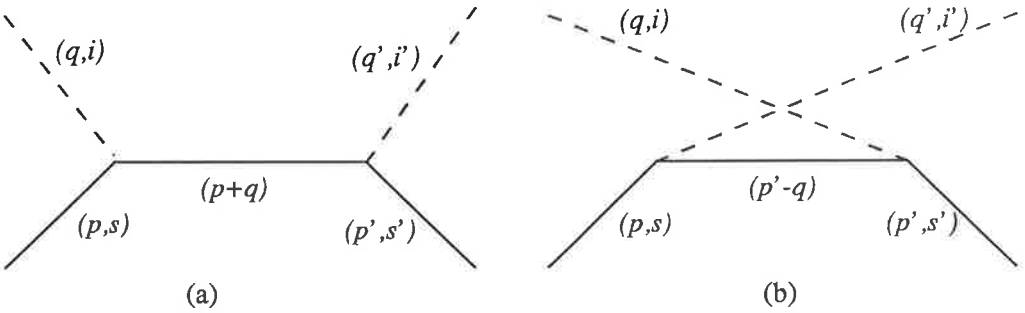

Figure 2.1: Diagrams contributing to the S-wave pion nucleon scattering: solid line represents nucleon and dash line pion.

is given by (in this chapter we use the normalization convention of Aitchison and Hey [AH 84])

$$\begin{aligned}\langle p',s';q',j|S^{(2)}-1|p,s;q,i\rangle &= (2\pi)^4\delta^4(p'+q'-p-q) \\ &\quad (2\pi)^{-6}\left[\frac{1}{2E_p}\frac{1}{2E_{p'}}\frac{1}{2\omega_{\mathbf{q}}}\frac{1}{2\omega_{\mathbf{q}'}}\right]^{\frac{1}{2}}(M_a(ps)+M_b(ps)),\end{aligned} \tag{2.5}$$

where i,j are pion isospin labels and the covariant amplitudes $M_a(ps), M_b(ps)$ are given by

$$M_a(ps) = g^2\bar{u}(p',s')\tau_j\gamma_5\left[\frac{(\not{p}+\not{q}+m_N)}{(s-{m_N}^2)}\right]\gamma_5\tau_i u(p,s) \tag{2.6}$$

and

$$M_b(ps) = g^2\bar{u}(p',s')\tau_i\gamma_5\left[\frac{(\not{p}'-\not{q}+m_N)}{(u-{m_N}^2)}\right]\gamma_5\tau_j u(p,s). \tag{2.7}$$

In (2.6) and (2.7), s and u are usual Mandelstam variables

$$s = p+q = p'+q'$$

$$u = p-q' = p'-q.$$

Using $\tau_i\tau_j = \delta_{ij} + i\epsilon_{ijk}\tau_k$, we can easily show that

$$M_a(ps)+M_b(ps) = \delta_{ij}T^{(+)}(ps) + i\epsilon_{ijk}\tau_k T^{(-)}(ps)\ , \tag{2.8}$$

where

$$T^{(\pm)}(ps) = \mp g^2 \bar{u}(p',s') \left[\frac{\not{q}}{s - m_N^2} \mp \frac{\not{q}'}{u - m_N^2} \right] u(p,s) \ . \tag{2.9}$$

By noting that in the non-relativistic limit (i.e. all momenta are nearly zero):

$$\bar{u}(p',s') \not{q} u(p,s) \approx 2 m_N m_\pi$$

$$s - m_N^2 = 2 m_N m_\pi (1 + m_\pi / 2 m_N)$$

$$u - m_N^2 = -2 m_N m_\pi (1 - m_\pi / 2 m_N),$$

we can evaluate $T^{(\pm)}(ps)$ at threshold. At threshold $T^{(\pm)}(ps)$ behaves as

$$T^{(+)}(ps) \rightarrow \frac{-2g^2}{1 - m_\pi^2 / 4 m_N^2} \ , \tag{2.10}$$

$$T^{(-)}(ps) \rightarrow \frac{g^2 m_\pi / m_N}{1 - m_\pi^2 / 4 m_N^2} \ . \tag{2.11}$$

From the definition of the scattering lengths we find that for low energies,

$$f^{(\pm)} = \frac{1}{8\pi W} T^{(\pm)} \rightarrow a^{(\pm)} \ , \tag{2.12}$$

and therefore at the threshold energy

$$a_0^{(+)}(ps) \approx -\frac{g^2}{4\pi} \frac{1}{m_\pi + m_N} \approx -1.8 m_\pi^{-1} \tag{2.13}$$

$$a_0^{(-)}(ps) \approx \frac{g^2}{8\pi} \frac{m_\pi}{m_N} \frac{1}{m_\pi + m_N} \approx 0.14 m_\pi^{-1}. \tag{2.14}$$

In eqn (2.12), $W = m_\pi + m_N$ is the total energy and $f^{(\pm)}$ the scattering amplitude which is equal to the scattering length $a^{(\pm)}$ at threshold. $a_0^{(+)}(ps)$ in (2.13) and $a_0^{(-)}(ps)$ in (2.14) corresponds to S-wave isoscalar and isovector scattering lengths respectively. The pseudovector interaction (2.2) can also be used to calculate the S-

wave scattering length at threshold. Following similar algebra which led to equations (2.6) and (2.7) the invariant amplitudes for the diagrams shown in Fig.2.1a and Fig. 2.1b are

$$M_a(pv) = -(\frac{f}{m_\pi})^2 \bar{u}(p',s')\gamma_5 \not{q}' \tau_j \left[\frac{(\not{p}+ \not{q} + m_N)}{s - m_N^2 + i\epsilon}\right] \not{q}\gamma_5\tau_i u(p,s) \ , \tag{2.15}$$

and

$$M_b(pv) = -(\frac{f}{m_\pi})^2 \bar{u}(p',s')\gamma_5 \not{q}\tau_i \left[\frac{i(\not{p}- \not{q} + m_N)}{s - m_N^2 + i\epsilon}\right] \not{q}'\gamma_5\tau_j u(p,s) \ . \tag{2.16}$$

For threshold energy where the 3-momenta are nearly zero one finds that

$$\bar{u}(p',s')\gamma_5 \ \not{q}'(\not{p}+ \not{q} + m_N)\gamma_5 \ \not{q}u(p,s) \approx 2m_N m_\pi^3,$$

$$\bar{u}(p',s')\gamma_5 \ \not{q}(\not{p}- \not{q}' + m_N)\gamma_5 \ \not{q}u(p,s) \approx -2m_N m_\pi^3,$$

and therefore the amplitude for the pseudovector interaction is given by

$$M_a(pv)/M_b(pv) \approx -f^2 \frac{1}{(1 \pm m_\pi/2m_N)}(\delta_{i,j} \mp i\epsilon_{ijk}\tau_k).$$

Since we have

$$M_a(pv) + M_b(pv) = \delta_{ij}T^{(+)}(pv) + i\epsilon_{ijk}\tau_k T^{(-)}(pv) \ , \tag{2.17}$$

The scattering lengths $a^{(\pm)}$ for the pseudovector interaction are

$$a_0^{(+)}(pv) \approx -\frac{f^2}{4\pi}\frac{1}{m_\pi + m_N} \approx -0.010 m_\pi^{-1} \tag{2.18}$$

$$a_0^{(-)}(pv) \approx -\frac{f^2}{8\pi}\frac{m_\pi}{m_N}\frac{1}{m_\pi + m_N} \approx 0 \tag{2.19}$$

It is immediately noted that the results (2.13) and (2.19) do not agree with experimental values:

$$a_0^{(+)}(exp) = -0.010 \ \ m_\pi^{-1}; \qquad\qquad a_0^{(-)}(exp) = -0.091 \ \ m_\pi^{-1} \ . \tag{2.20}$$

It is interesting, however, to note that the results $a_0^{(+)}(pv)$ in eqn (2.18) and $a_0^{(-)}(ps)$ given in eqn (2.14) do agree with $a_0^{(+)}(exp)$ and $a_0^{(-)}(exp)$ respectively. The large value of $a_0^{(+)}(ps)$ resulted from the large contribution of the isoscalar part of (2.8). We shall now examine what mechanism can be used to reduce this value.

2.3 Soft-pion Theorems

In studying low energy strong interactions, the soft-pion theories are a time honoured subject. In this section we will discuss the implication of the approximate conservation of the axial current. In particular, we show how the soft-pion theorems can be used to rectify the bad piece of the isoscalar scattering length $a_0^{(+)}(ps)$ in eqn (2.13). For the discussion in this section, we closely follow those of Adler [Adl 65], Scadron [Sca 79, Sca 81] and T.D. Lee [Lee 88].

2.3.1 Partially Conserved Axial Current(PCAC)

The vacuum to one pion transition amplitude can be written as

$$\langle 0|J^i_{\mu 5}(\mathbf{x})|\pi^j(q)\rangle = \delta^{ij} i f_\pi q_\mu e^{-iq.x} \tag{2.21}$$

where

$$J^i_{\mu 5}(\mathbf{x}) = \bar{\psi}_{\mathrm{N}} \gamma_\mu \gamma_5 \boldsymbol{\tau} \cdot \boldsymbol{\pi} \psi_{\mathrm{N}} \tag{2.22}$$

is the axial vector current and f_π is the pion decay constant. Taking the divergence of this equation leads to

$$\partial^\mu J^i_{\mu 5} = \delta^{ij} f_\pi m_\pi^2 \tag{2.23}$$

From this, we can see that axial vector current is not conserved since f_π and m_π^2 are non zero. However, since the ratio of pion mass to nucleon mass squared is small, $m_\pi^2/m_N^2 \approx 0.02$, to a good approximation we can take the divergence of the axial current to be zero, i.e.

$$\partial^\mu J^i_{\mu 5} \approx 0. \tag{2.24}$$

This is one version of the hypothesis of the partial conservation of the axial current (PCAC).

In order to see how the soft pion theorem is used in pion-nucleon scattering, let us consider the general pion transition $A \rightarrow B + \pi$ (A, B=hadrons) in the soft pion case [Sca 81]. One can separate the matrix element of the axial current, $T^i_\mu = \langle B|J^i_{\mu 5}|A\rangle$, into pion pole dominant part and a background part [Lee 88, Adl 65, Sca 79, Sca 81]. Graphically, it can be presented as in Figure 2.2.

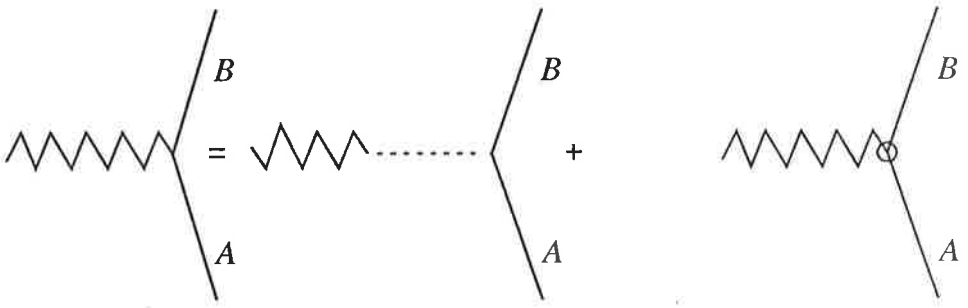

Figure 2.2: Pion pole dominant at low energy

The matrix element for this process can be written as

$$T^i_\mu = (-i)(-f_\pi q_\mu)\frac{i}{q^2 - m_\pi^2} T^i_\pi(q) + \bar{T}^i_\mu, \tag{2.25}$$

Where $T^i_\pi(q)$ can be identified as pion current matrix element and $\bar{T}^i_\mu$ is the back-

ground current. Equation (2.25) with the condition $m_\pi^2 \approx 0, \partial_\mu J^\mu \approx 0$ provides the so called S-matrix version of PCAC [Sca 81]

$$if_\pi T_\pi^i(q) = q^\mu \bar{T}_\mu^i \tag{2.26}$$

Equation (2.26) is found to be insensitive to the $m_\pi^2 \approx 0$ or $q^2 \approx 0$ limit. One can further remove the bremmstrahlung type pole in eqn (2.26). The result being the soft pion version of PCAC [Sca 81]. In soft pion limit ($m_\pi^2, q^2 \to 0$ and$q \to 0$)

$$T_\pi^i \Longrightarrow -if_\pi^{-1} q^\mu \bar{T}_\mu^i(pole) + O(q) \tag{2.27}$$

2.3.2 Adler's Consistency condition

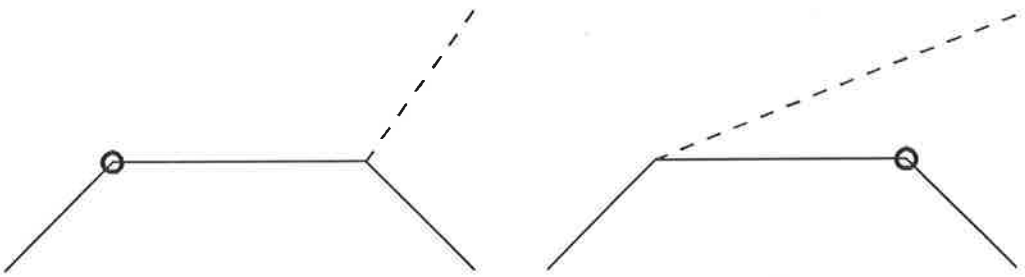

Figure 2.3: Diagrams for the generalized Born matrix element $\langle \pi N | J_{\mu 5}^i | N \rangle$. The heavy dots marks for the axial current interaction.

One can further pursue the PCAC in order to apply it to the interaction of the pion-nucleon system. Starting from generalized Born approximation, i.e. the axial currents between $|N\rangle$ and $|\pi N\rangle$ states, one can derive the so-called Consistency Conditions for strong interactions [Adl 65]. As in the previous Section one can separate the matrix element $M_\mu = \langle \pi N | J_{\mu 5} | N \rangle$ into the pion pole contribution part

M_π and Background part $\bar{M}_\mu$.

$$M_\mu^i = (-i)(-if_\pi q_\mu)(\frac{1}{q^2 - m_\pi^2 + i\epsilon})M_\pi^i(q) + \bar{M}_\mu^i \tag{2.28}$$

In the limit $m_\pi^2 \approx 0$ the approximate axial current conservation $\partial^\mu j_{\mu 5} \approx 0$ implies:

$$if_\pi M_\pi^i(q) \approx q^\mu \bar{M}_\mu^i \tag{2.29}$$

From this one can identify the nucleon pole part of $q^\mu \bar{M}_\mu^i$ as the pseudoscalar interaction of Fig. 2.3 while the non pole term has the form

$$\tau^i \gamma_5 M_0 + M_0 \gamma_5 \tau^i \ ,$$

where M_0 denotes the background amplitude. In the limit $q^\mu \to 0$, we have soft pion theorems;

$$M_\pi^i(q) \approx M_{psNpoles}^i(q) + \bar{M}_\pi^i(q \to 0) \tag{2.30}$$

where

$$\bar{M}_\pi^i(q \to 0) = \frac{g}{2m_N}(\tau^i \gamma_5 M_0 + M_0 \gamma_5 \tau^i) \tag{2.31}$$

In the case of final pion being soft, the hadronic background amplitude M_0 becomes $-g\tau^j\gamma_5$. This results in the background amplitude for the pion nucleon case [Sca 81]:

$$\bar{M}_\pi^{ij}(q \to 0) = \frac{g^2}{m_N}\delta^{ij} \tag{2.32}$$

Therefore this background amplitude modifies the $T^{(+)}(ps)$ as follows:

$$T^{(+)}(ps) \rightarrow \frac{-2g^2}{1 - m_\pi^2/4m_N^2} + 2g^2$$
$$= \frac{-g^2 m_\pi^2/2m_N^2}{1 - m_\pi^2/4m_N^2} \tag{2.33}$$

With this modification, the scattering length $a_0^{(+)}(ps)$ becomes

$$a_0^{(+)} = -0.0092 \ \ m_\pi^{-1} \tag{2.34}$$

which is comparable with the experimental value.

2.4 The Sigma Model

In the previous section we showed how current algebra and soft pion theorems are applied to get correct scattering lengths for the S-wave interaction. We saw that the large and attractive isoscalar contribution in the interaction is neutralised by the background amplitude $\bar{M}_\pi^{ij}(q \rightarrow 0)$. We will now discuss how such cancellations occur naturally in the context of the sigma model.

2.4.1 The Linear Sigma Model

In 1961 Gell-Mann and Levy introduced the linear σmodel [GL 60] In this model, they postulated an isoscalar-scalar field (σ) in addition to the pion field, which is isovector-pseudoscalar. Together they form a so called chiral 4 vector $\{\sigma, \boldsymbol{\pi}\}$ for which the scalar product with $\{\bar{\psi}_N \psi_N, \bar{\psi}_N \gamma_5 \boldsymbol{\tau} \psi_N \ \}$ is invariant under chiral transformation. The Lagrangian of the linear σ model can be written as

$$\mathcal{L} = \mathcal{L}_0 + c\sigma, \tag{2.35}$$

where $\mathcal{L}_0$ in (2.35) is given as

$$\mathcal{L}_0 = \bar{\psi}_N[i\gamma_\mu\partial^\mu - g(\sigma + i\boldsymbol{\pi}\cdot\boldsymbol{\tau}\gamma_5)]\psi_N + U(\sigma,\boldsymbol{\pi}) + \frac{1}{2}[(\partial_\mu\sigma)^2 + (\partial_\mu\pi)^2], \quad (2.36)$$

with the potential term

$$U(\sigma,\boldsymbol{\pi}) = -\frac{1}{4}\lambda^2\{(\sigma^2+\pi^2) - \lambda_2^2\}^2, \quad (2.37)$$

where λ and λ_2 arbitrary constants. In eqn (2.35) $c\sigma$ is the chiral symmetry breaking term. Under an infinitesimal isospin rotation, $\boldsymbol{\pi}$ and ψ_N transform as

$$\sigma \to \sigma, \qquad \boldsymbol{\pi} \to \boldsymbol{\pi} - \boldsymbol{\alpha}\times\boldsymbol{\pi}, \quad (2.38)$$

$$\psi_N \to \psi_N + i\frac{\boldsymbol{\tau}\cdot\boldsymbol{\alpha}}{2}\psi_N, \qquad \bar{\psi}_N \to \bar{\psi}_N - i\bar{\psi}_N\frac{\boldsymbol{\tau}\cdot\boldsymbol{\alpha}}{2}, \quad (2.39)$$

while under an infinitesimal chiral transformation

$$\sigma \to \sigma - \boldsymbol{\beta}\cdot\boldsymbol{\pi}, \qquad \boldsymbol{\pi} \to \boldsymbol{\pi} + \sigma\boldsymbol{\beta}, \quad (2.40)$$

$$\psi_N \to \psi_N - i\frac{\boldsymbol{\tau}\cdot\boldsymbol{\beta}}{2}\gamma_5\psi_N, \qquad \bar{\psi}_N \to \bar{\psi}_N - i\bar{\psi}_N\gamma_5\frac{\boldsymbol{\tau}\cdot\boldsymbol{\beta}}{2}. \quad (2.41)$$

With these two transformations we have vector and axial vector currents ,

$$\begin{aligned}\boldsymbol{V}_\mu &= -\frac{\delta\mathcal{L}}{\delta(\partial_\mu\boldsymbol{\alpha})} \\ &= \bar{\psi}_N\gamma_\mu\boldsymbol{\tau}/2\psi_N + \boldsymbol{\pi}\times\partial_\mu\boldsymbol{\pi}, \end{aligned} \quad (2.42)$$

and

$$\begin{aligned}\boldsymbol{A}_\mu &= -\frac{\delta\mathcal{L}}{\delta(\partial_\mu\boldsymbol{\beta})} \\ &= \bar{\psi}_N\gamma_5\gamma_\mu\frac{\boldsymbol{\tau}}{2}\psi_N + (\partial_\mu\sigma)\boldsymbol{\pi} - \partial_\mu\boldsymbol{\pi}\sigma, \end{aligned} \quad (2.43)$$

and their divergences are

$$\partial_\mu \boldsymbol{V}_\mu = 0; \qquad \partial^\mu \boldsymbol{A}_\mu = c\boldsymbol{\pi}. \tag{2.44}$$

2.4.2 Broken Symmetry Mode

It should be noted that in the potential term in the Lagrangian, $U(\sigma, \boldsymbol{\pi})$, we can choose one of the constants, λ_2, as the pion decay constant f_π . It is chosen so that the vacuum expectation of the σ field in the absence of the pion field is

$$\langle 0|\sigma|0\rangle = f_\pi, \tag{2.45}$$

and the nucleon masses are generated according to the Goldberger-Treimann relation

$$\begin{aligned} \langle 0|g\bar{\psi}_N\sigma\psi_N|0\rangle &= g f_\pi \bar{\psi}_N\psi_N \\ &= m_N\bar{\psi}_N\psi_N. \end{aligned} \tag{2.46}$$

The $\boldsymbol{\pi}-\sigma$ interaction is also generated by the potential term $U(\sigma, \boldsymbol{\pi})$. In the absence of a nucleon field one may expand the σ field so that [Bro 90]

$$U(f_\pi + \phi_\sigma, \boldsymbol{\pi} = 0) = \lambda^2 f_\pi^2\phi_\sigma^2 + \lambda^2 f_\pi^2\phi_\sigma^3 + \frac{1}{4}\lambda^2\phi_\sigma^4, \tag{2.47}$$

from which we can identify the mass of ϕ_σ as

$$\frac{1}{2}m_\sigma^2\phi_\sigma^2 = \lambda^2 f_\pi^2\phi_\sigma^2. \tag{2.48}$$

For a non-zero pion field, the potential term becomes

$$U(f_\pi + \phi_\sigma, \boldsymbol{\pi}) = \frac{1}{4}\lambda^2[((f_\pi + \phi_\sigma)^2 + \boldsymbol{\pi}^2) - f_\pi^2]^2, \tag{2.49}$$

which leads to an interaction Lagrangian of the form

$$\mathcal{L}_{\sigma-\pi\pi} = \frac{m_\sigma^2}{2f_\pi}\phi_\sigma \boldsymbol{\pi}^2. \tag{2.50}$$

2.4.3 Correction to the S-wave amplitude

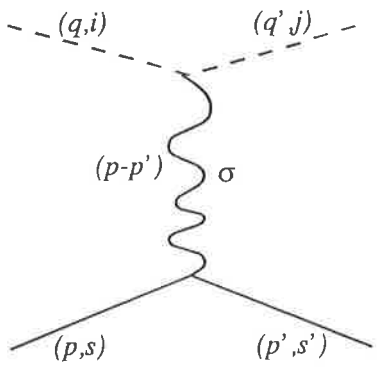

Figure 2.4: t-channel σ exchange diagram for S-wave πN interactions

Using eqn (2.50), we can write down the amplitude associated with Fig. 2.4 as generated by the sigma field

$$M_\sigma = -\left(\frac{m_\sigma^2 g}{f_\pi}\right)\bar{u}(p',s')\frac{1}{t-m_\sigma^2+i\epsilon}u(p,s)\delta_{ij} \tag{2.51}$$

In the non-relativistic limit, $t=(p-p')^2 \approx 0$, therefore

$$M_\sigma \approx +g\frac{2m_N}{f_\pi}\delta_{ij} = 2g^2\delta_{ij} \tag{2.52}$$

where use has been made of the Goldberger-Treimann relation $m_N = gf_\pi$ in (2.52). In our discussion for soft pion theory in Section 2.3, we have seen that in eqn (2.33) the background amplitude $\bar{M}_\pi^{ij}(q\to 0)$ in (2.32) modifies the large piece of pseudoscalar result $T^{(+)}(ps)$ of eqn (2.13). Here we can see that the t- channel σ exchange diagram shown in Fig. 2.4 provides the same modification to the pseudoscalar result(2.13), as the three diagrams shown in Fig. 2.1a, 2.1b and Fig. 2.4

must be taken together in linear sigma model.

2.4.4 The Non-linear sigma model

The σ model of Gell-Mann and Levy provides a good theoretical foundation for explaining chiral symmetry, spontaneous symmetry breaking and the generation of nucleon masses. As we have demonstrated in the previous section it is also consistent with the soft-pion theorems in explaining the S-wave scattering behaviour at threshold energy. A drawback of the σ model is that the σ particle has not been observed in nature. However Weinberg has shown that the σ field can be transformed away by defining a new pion field (ϕ) as follows [Wei 67, Wei 69, Wei 79, Bro 90].

$$\boldsymbol{\phi} = 2f_\pi tan(\frac{\theta}{2})\ \hat{\boldsymbol{\pi}}, \tag{2.53}$$

where $\hat{\boldsymbol{\pi}} = \boldsymbol{\pi}/\pi$ and θ is related to σ and π through

$$\sigma = f_\pi \cos\theta, \qquad\qquad \boldsymbol{\pi} = f_\pi \hat{\boldsymbol{\pi}} \sin\theta. \tag{2.54}$$

When we apply this transformation to the Lagrangian of the linear σ model (2.35), we get the Weinberg Lagrangian

$$\begin{aligned} \mathcal{L}_W &= \bar{\psi}_N(i\gamma^\mu D_\mu - m_N)\psi_N - (\frac{f}{m_\pi})\bar{\psi}_N\gamma_5\gamma^\mu\boldsymbol{\tau}\psi_N \cdot D_\mu\boldsymbol{\phi} \\ &\quad -\frac{1}{2}D_\mu\boldsymbol{\phi}\cdot D^\mu\boldsymbol{\phi} - \frac{1}{2}m_\pi^2\frac{\boldsymbol{\phi}^2}{(1+\frac{\boldsymbol{\phi}^2}{4f_\pi^2})^2} \end{aligned} \tag{2.55}$$

The boson kinetic energy term of (2.35) becomes

$$-\frac{1}{2}[(\partial_\mu\boldsymbol{\pi})^2 + (\partial_\mu\sigma)^2] \rightarrow -\frac{1}{2}D_\mu\boldsymbol{\phi}\cdot D^\mu\boldsymbol{\phi} \tag{2.56}$$

where covariant derivatives are defined as

$$D_\mu \boldsymbol{\phi} = \frac{\partial_\mu \boldsymbol{\phi}}{(1+\frac{\boldsymbol{\phi}^2}{4f_\pi^2})} \ , \tag{2.57}$$

and

$$\begin{aligned} D_\mu \psi_N &= [\partial_\mu + i(4f_\pi^2 + \boldsymbol{\phi}^2)^{-1} \boldsymbol{\tau} \cdot (\boldsymbol{\phi} \times \partial_\mu \boldsymbol{\phi})]\psi_N \\ &= \partial_\mu \psi_N + \frac{i}{(4f_\pi^2 + \boldsymbol{\phi}^2)} \boldsymbol{\tau}\psi_N \cdot (\boldsymbol{\phi} \times \partial_\mu \boldsymbol{\phi}) \ . \end{aligned} \tag{2.58}$$

In eqn (2.55), the pseudovector coupling term is written by using the relation $\frac{1}{2f_\pi} \approx \frac{f}{m_\pi}$. The Weinberg Lagrangian (2.55) is particularly convenient in dealing with S-wave scattering at threshold. We noticed that the empirical isoscalar piece of (2.20) is nearly zero and that therefore the pion-nucleon scattering length at threshold is purely isovector. We see that the Lagrangian (2.55) has an interaction term known as the Weinberg-Tomozawa term (2.58) in addition to the usual pseudovector coupling term . The Weinberg-Tomozawa term gives the correct scattering length at threshold energy as follows.

The usual covariant S-matrix expansion to order (1) is

$$\begin{aligned} S^{(1)} &= \int d^4x \mathcal{H}_{WT}(x) \\ &= -\frac{1}{4f_\pi^2} \int d^4x \bar{\psi}_N(x) \gamma_0 \boldsymbol{\tau} \psi_N(x) \cdot (\boldsymbol{\phi}(x) \times \partial^0 \boldsymbol{\phi}(x)). \end{aligned} \tag{2.59}$$

To this order we find the S-matrix amplitude for Weinberg-Tomozawa interaction as

$$\begin{aligned} \langle f|S^{(1)} - 1|i\rangle &= (2\pi)^4 \delta^4(p' + q' - p - q) \\ &\quad \frac{1}{(2\pi)^6} \left[\frac{1}{2E_{\mathbf{p}'}} \frac{1}{2E_{\mathbf{p}}} \frac{1}{2\omega_{\mathbf{q}'}} \frac{1}{2\omega_{\mathbf{q}}}\right]^{\frac{1}{2}} M_{WT}(i_{B'}, j; i_B, i) \end{aligned} \tag{2.60}$$

Where, the covariant amplitude $M_{WT}(i_{B'}, j; i_B, i)$ is given by (we rather writing this amplitude by showing explicit isospin dependence)

$$M_{WT}(i_{B'}, j; i_B, i) = -\frac{1}{4f_\pi^2}(\omega_{\mathbf{q}} + \omega_{\mathbf{q}'})u^\dagger(p', s')u(p, s)\langle I_{B'} i_{B'}|\tau_k(-i\epsilon_{kji})|I_B i_B\rangle \quad ,(2.61)$$

where $\omega_{\mathbf{q}} = \sqrt{m_\pi^2 + \mathbf{q}^2}$ the pion energy and $i\epsilon_{kji}$ the pion isospin matrix elements [Wick55]. In order to have a covariant amplitude for total isospin I, rather than an amplitude for definite isospin state for pion and nucleon, we transform (2.61) as follows:

$$\begin{aligned} M_{WT}^I &= \sum_{i_{B'} j} \sum_{i_B i} C_{I_{B'} I_{M'} I}^{i_{B'} j \; I_3} C_{I_B I_M I}^{i_B i \; I_3} M_{WT}(i_{B'} j; i_B i) \\ &= -\frac{1}{4f_\pi^2}(\omega_{\mathbf{q}} + \omega_{\mathbf{q}'})u^\dagger(p', s')u(p, s)\lambda_{WT}^I \quad , \end{aligned} \tag{2.62}$$

where $\lambda_{WT}^{\frac{1}{2}} = -2$ and $\lambda_{WT}^{\frac{3}{2}} = 1$ (see also Table 4.4). At threshold the scattering length is

$$\begin{aligned} a_{2I} &= \frac{1}{8\pi W} M_{WT}^I \\ &= -\frac{m_\pi}{8\pi f_\pi^2 (1 + m_\pi/m_N)} \lambda_{WT}^I \end{aligned} \tag{2.63}$$

This is the famous Weinberg-Tomozawa result:

$$\begin{aligned} a_1 &= +\frac{m_\pi}{4\pi f_\pi^2} = 0.18 \;\; m_\pi^{-1} \\ a_3 &= -\frac{m_\pi}{8\pi f_\pi^2} = -0.09 \;\; m_\pi^{-1} \quad , \end{aligned} \tag{2.64}$$

which agrees well with experiment since the isoscalar scattering length $a^{(+)}$ and isovector scattering length $a^{(-)}$ are related to a_1 and a_3 via

$$a^{(+)} = \frac{1}{3}(a_1 + 2a_3) \approx 0.0$$

$$a^{(-)} = \frac{1}{3}(a_3 - a_1) \approx -0.09 \ m_\pi^{-1}$$

The contribution from the usual pseudovector coupling term (2.19), as we have shown in Section 2.2.1, is indeed negligible.

2.5 Summary

In this chapter we have shown that usual pion-nucleon interactions, i.e. pseudoscalar and pseudovector interactions, cannot give correct scattering lengths for the S-wave interaction. We then discussed how the S-wave scattering lengths are evaluated correctly by soft-pion theorems. Next we showed that in the linear sigma model, the t-channel sigma exchange gives the necessary cancellation in the isoscalar component and consequently yields the correct result for the S-wave scattering lengths. We also discussed the non-linear σ model and Weinberg-Tomozawa results.

Chapter 3

Relativistic Two-Body Propagators

3.1 Introduction

In this chapter we would like to discuss the methods used to ensure unitarity in two body scattering theory. It has long been clear that use of the non-relativistic Lippmann-Schwinger equation with non-relativistic potentials satisfies the unitarity condition. When one describes the scattering process in a relativistic framework, it is natural to use relativistic propagators (Greens Functions) and to treat the interaction in terms of fields. This poses problems which make it difficult to solve the scattering equations exactly. Firstly, we have to take the negative energy states into account in propagation as well as interaction. Furthermore, the 4-dimensional scattering equations are more difficult to solve numerically. The convergence of the equation is not readily guaranteed, especially in strong interactions. However after numerous approximations and reductions, and encouraged by the success of non-relativistic formulations, it is reasonable to believe that one may ensure the unitarity by using relativistic propagators. In Sections 3.2 and 3.3, we will outline

how the relativistic equations for a scattering process are deduced. In Section 3.3.1 we discuss how the 4-dimensional relativistic scattering equations can be reduced to 3-dimensions, by removing the relative energy variable by means of the dispersion technique. In Section 3.3.2 we employ the instantaneous interaction approximation to obtain the relativistic three dimensional equations.

Relativistic 3-dimensional two body propagators have been used for systems of two equal mass particles (with or without spin) since Blankenbecler and Sugar invented that technique. For the πN system, where the masses are different, these relativistic propagators cannot be applied. There are additional restrictions that must be imposed on these relativistic equations in order to give correct physics when the particles are of unequal mass.

In this context, we discuss more recent developments in this field. In Sect. 3.4, the concept of short range structures is introduced and its relevance to relativistic scattering is also discussed. Then, in Sect. 3.5, we show how a smooth relativistic 3-dimensional propagator for the πN system can be deduced by applying the short range method. The one body limit is discussed in 3.6 and 3.7 and it is proven that the smooth propagators do not violate one body limits.

3.2 Bethe-Salpeter Equation

In field theory, one can write down the covariant amplitude for the interaction of two particles in accordance with perturbation theory to any order in the coupling constant. However, it is impossible to calculate all of these diagrams exactly. A remedy for this is to use the Bethe-Salpeter(BS) equation, which is covariant and describes the relativistic interaction of two particles. The variables for the BS equations are those of 4-momentum (or 4-coordinates) of the interacting fields. The Bethe Salpeter equation for the scattering of two particles with initial(final) 4-momenta

$q_1, q_2(p_1, p_2)$ is given by [BS 51]

$$M(p_1, p_2; q_1, q_2) = K(p_1, p_2; q_1, q_2) + \int \frac{d^4k}{(2\pi)^4} \frac{d^4k_2}{(2\pi)^4} K(p_1, p_2; k_1, k_2) G_1(k_1) G_2(k_2) M(k_1, k_2; q_1, q_2) \tag{3.1}$$

where $M(p_1, p_2; q_1, q_2)$ is the relativistic scattering amplitude and the interaction kernel K is the sum of all connected two-particle irreducible diagrams (to infinite order). The G_i's are relativistic, one particle, free propagators. The structure of the Bethe-Salpeter equation (3.2) can be represented schematically by Fig.3.1. It

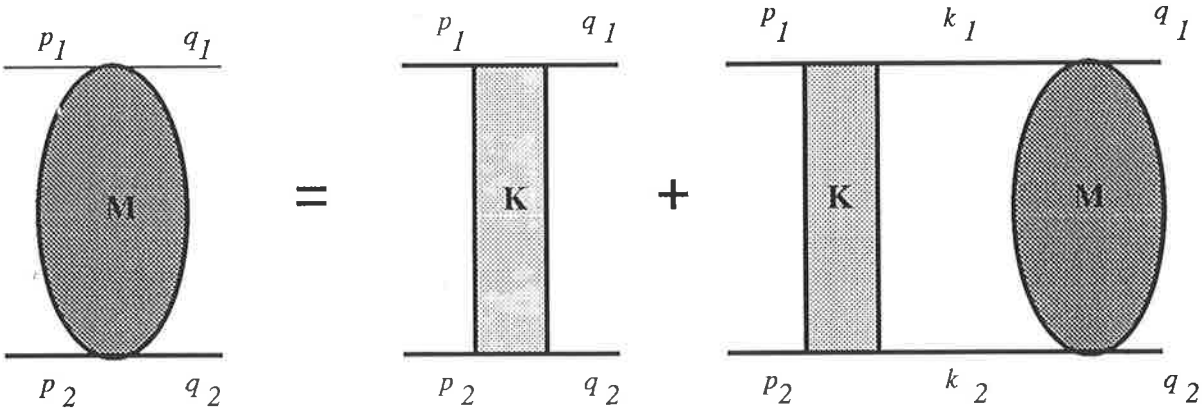

Figure 3.1: Schematic Diagram of Bethe Salpeter equation

is advantageous to describe the 4-momentum variables, p_1, p_2, q_1, q_2, in relativistic Jacobi coordinates [CJ 89]. For two spinless particles of different masses, the total 4-momenta P, and relative 4-momenta p, are given by (see more detail in Appendix B),

$$\begin{aligned} P &= q_1 + q_2 = p_1 + p_2 = k_1 + k_2 \\ P &= p_1 + p_2, p = \frac{\epsilon_2(S) p_1 - \epsilon_1(S) p_2}{\epsilon_1(S) + \epsilon_2(S)} \\ p_1 &= \frac{\epsilon_1(S) P}{\epsilon_1(S) + \epsilon_2(S)} + p, p_2 = \frac{\epsilon_2(S) P}{\epsilon_2(S) + \epsilon_2(S)} - p \end{aligned} \tag{3.2}$$

where the energy of particle 1 and 2 is,

$$\begin{aligned} \epsilon_1(S) &= \frac{S+m_1^2-m_2^2}{2\sqrt{S}} \\ \epsilon_2(S) &= \frac{S+m_2^2-m_1^2}{2\sqrt{S}} \end{aligned} \tag{3.3}$$

The Bethe Salpeter equation in terms of relative coordinates p, k and q becomes

$$M(p,q|S) = K(p,q|S) - i\int \frac{d^4k}{(2\pi)^4} K(p,k|S)G(k,S)M(k,q|S). \tag{3.4}$$

The Kernel K is the sum of all two particle irreducible diagrams, i.e.

$$K(p,k|S) = \sum_{n=1}^{\infty} K^{(2n)},$$

where $K^{(2n)}$ represents the covariant Feynman amplitude of order $2n$. It is the usual practice to approximate the infinitely summed kernel with a one particle exchanged diagram, meaning the kernel can be approximated by

$$K(p,k|S) \approx K^{(2)}.$$

The resulting equation where K is replaced with $K^{(2)}$ is known as the ladder approximated Bethe-Salpeter equation. It is normally assumed to be the best equation to describe strong interactions (see however Gross [Gro 82]).

The obvious advantage in using the Bethe-Salpeter equation (or ladder approximated version) is that it ensures unitarity. Since the S-matrix element S_{fi} is related to relativistic scattering amplitude via

$$S_{fi} = \delta_{fi} + i(2\pi)^4\delta(P_f - P_i)M_{fi}, \tag{3.5}$$

the unitarity condition,

$$SS^{\dagger} = S^{\dagger}S = I, \tag{3.6}$$

can be satisfied. Another advantage in using Bethe-Salpeter equation is its similarity with the Lippmann-Schwinger(LS) equation. Although the four dimensional Bethe-Salpeter equation,(3.2) or (3.4), cannot be solved easily, we can reduce it to a 3-dimensional equation. Since the reduced form of the Bethe-Salpeter equation is similar to the non-relativistic Lippmann-Schwinger equation, the computational techniques become more tractable. In the next section we will discuss the three dimensional reductions of the ladder approximated Bethe-Salpeter equation (3.4).

3.3 Relativistic Two Particle Propagators

The Bethe-Salpeter equation (3.4) is similar to the Lippmann-Schwinger(LS) equation, where the main feature is that one uses the iterated solution for the scattering amplitude M. However a great deal of care must be taken. Firstly, consider the kernel K of (3.4) which plays the role of the potential. In the non-relativistic LS equation, the potentials are independent of the scattering energy. In the relativistic case, the kernel is the sum of all irreducible diagrams to infinite order, which have singularities. Secondly, the propagator $G(k, S)$ represents not only the propagation of particles but also anti-particles.

In this section, we will discuss how the Bethe-Salpeter equation is reduced to three dimensions by removing the relative energy variable. When one considers relativistic scattering, the scattering amplitude and the propagator possess a complicated analytic structure. Furthermore, the kernel and propagator include negative energy states. There is also a question of how many exchange particles should be included in the kernel. Since it is impossible to solve all problems exactly, an ap-

proximation must be made to the scattering equation which is consistent with the physical picture. To do this, the kernel will be represented by the ladder approximation and we will ignore the anti-particle contributions to the propagator. This will greatly simplify our procedure for calculating the scattering amplitude.

There have been various attempts to construct propagators that incorporate relativistic effects in LS-type scattering equations. Here, we will obtain the three dimensional propagators from the Bethe-Salpeter equation by using two different methods [WJ 73]. First we will discuss the method of Blankenbecler and Sugar [BbS 66] which employed the dispersion technique to obtain an approximated propagator. Then we will discuss the instantaneous-interaction approximation. We will not discuss another derivation-namely- the minimal introduction of relativistic kinematics into LS equation [Bro 79, Bro 69].

3.3.1 Blankenbecler-Sugar Method

The starting point for the Blankenbecler-Sugar reduction [BbS 66] is the requirement that the relativistic propagator must have the same cut structure as its non-relativistic counterpart in the elastic region. The actual situation, however, is complicated by the singularities in the scattering amplitude and the potential(kernel). Therefore, we restrict ourselves to the singularity free region of the scattering amplitude and kernel. We will discuss the scattering of two spinless particles of masses m_1 and m_2. We recall the Bethe-Salpeter equation in the c.o.m frame,

$$M(p,q|S) = K(p,q|S) - i\int \frac{d^4k}{(2\pi)^4}\, K(p,k|S)G(k,S)M(k,q|S) \tag{3.7}$$

where p, k, q are the 4-momenta and S the total scattering energy and

$$G(k,S) = -\frac{1}{[(\frac{1}{2}P+k)^2 - m_1^2][(\frac{1}{2}P-k)^2 - m_2^2]}, \tag{3.8}$$

is the fully relativistic two particle propagator. It must be noted that the total 4-momentum is conserved in each step of the interaction in the ladder, while the total mass varies during interaction(off-mass-shell scattering). It should also be noted that $G(k,S)$ has singularities due to its pole structure. When one imposes certain restrictions, namely that the kernel is independent of the relative energy (and therefore singularity free) the essential difference between the BS equation and the LS equation will be the form of the propagator G and the non-relativistic propagator g. It is also known that G can produce a two-particle cut in the non-physical region(left hand cut), in addition to usual right hand cut in the elastic region. Our aim is to construct the three dimensional propagator $g(k,S)$ from $G(k,S)$ which produces the same two particle cut in the physical region. Now let us rewrite the BS equation as two equations:

$$M = K + KgM, \tag{3.9}$$

$$K = V + V(G-g)K. \tag{3.10}$$

It is hoped that the difference between the two propagators g and G is small enough so that it will give correct result when we iterate (3.9) and (3.10).

Following Aaron [Tho 77], we can prove for a symmetric $K(p,q|S)$,

$$M(p,q|S^+) - M(p,q|S^-) \tag{3.11}$$
$$= (2\pi)^{-4} \int d^4k M(p,k|S^+)[G(k,S^+) - G(k,S^-)]M(k,q|S^-) \ .$$

The statement of unitarity also provides

$$M(p,q|S^+) - M(p,q|S^-) \tag{3.12}$$
$$= (2\pi)^{-4} \int d^4k M(p,k|S^+)[(2\pi)^2\delta^+(k_1^2 - m_1^2)\delta^+(k_2^2 - m_2^2)]M(k,q|S^-)$$

We have from (3.12) and (3.13), the discontinuity of $G(k,S)$

$$\begin{aligned} disc\{G(k,S)\} &= G(k,S^+) - G(k,S^-) \\ &= i(2\pi)^2\delta^+(k_1^2 - m_1^2)\delta^+(k_2^2 - m_2^2) \end{aligned} \tag{3.13}$$

Now the integration over the discontinuity gives

$$G(k,S) = \frac{1}{2\pi i}\int_{(m_1+m_2)^2}^{\infty} dS' \frac{disc\{G(k,S')\}}{(S'-S)} \tag{3.14}$$

Evidently, $g(k,S)$ is defined to have the same elastic unitarity cut structure as $G(k,S)$. One can carry out the integration over S' in (3.14) for $m_1 = m_2$ to get the three dimensional propagator

$$g(k,S) = \frac{1}{4E_k}\frac{\delta(k_0)}{k^2 - q^2 - i\epsilon} \tag{3.15}$$

(The detailed derivation of the propagator for the general case of different masses m_1 and m_2 is given in Appendix B, and (3.15) is only the particular case $m_1 = m_2$.) Equation (3.9) with the choice (3.15) for $g(k,S)$ is known as Blankenbecler-Sugar equation.

3.3.2 Instantaneous-interaction approximation

In Section 3.3.1 we obtained the relativistic 3-dimensional equation which is known as the Blankenbecler-Sugar equation. The basic principle in deriving (3.15) was to remove the relative energy variable from the Bethe-Salpeter equation while maintaining the unitarity condition which is necessary for elastic scattering. In this Section we will obtain the Blankenbecler-Sugar equation by the instantaneous-interaction approximation [Thom70, WJ 73]. In this case, one makes the assumption that the kernel in the Bethe-Salpeter equation is independent of the relative energy. We first

write the homogeneous term of the BS equation as follows

$$\int dk_0 \int d^3k \frac{K(\boldsymbol{p},0;\boldsymbol{k},k_0|S)M(\boldsymbol{k},k_0;\boldsymbol{q},0|S)}{[(\frac{1}{2}\sqrt{S}+k_0)^2-E_k^2+i\epsilon][(\frac{1}{2}\sqrt{S}-k_0)^2-E_k^2+i\epsilon]}. \tag{3.16}$$

We are interested in obtaining the totally on-shell scattering amplitude $M(\boldsymbol{q},0;\boldsymbol{q},0|S)$ for the case of two equal mass particles. When one reduces the integral equation from four to three dimensions, certain information about the amplitude M as a function of relative energy k_0 will be lost. For example, the singularities due to the exchanged particle are neglected for some kinematical regions [WJ 73]. If we make the assumption that the scattering amplitude M is independent of relative energy k_0, we can write the homogeneous term of the BS equation as,

$$\int d^3k M(\boldsymbol{k},0;\boldsymbol{q},0|S) \int dk_0 \frac{K(\boldsymbol{p},0;\boldsymbol{k},k_0|S)}{[(\frac{1}{2}\sqrt{S}+k_0)^2-E_k^2+i\epsilon][(\frac{1}{2}\sqrt{S}-k_0)^2-E_k^2+i\epsilon]}. \tag{3.17}$$

It must be noted that (3.17) does not imply that $M(\boldsymbol{k},k_0;\boldsymbol{q},0|S)$ is equivalent to $M(\boldsymbol{k},0;\boldsymbol{q},0|S)$. We are merely calculating M at particular value of k_0. Since we require the solution for a totally on-shell amplitude, we choose $k_0 = 0$. In (3.17) there is still some k_0 dependence in the kernel K. There have been calculations for which the energy dependence of the kernel K has been taken into account[WJ 73, Coh 70]. One can make a further simplification by assuming the interaction kernel is independent of relative energy variable k_0 which enables us to write the homogeneous term of BS equation as

$$\int \frac{d^3k}{(2\pi)^3} K(\boldsymbol{p},\boldsymbol{k}|S) \left[\int \frac{dk_0}{2\pi i} \frac{1}{[(\frac{1}{2}\sqrt{S}+k_0)-E_k^2+i\epsilon][(\frac{1}{2}\sqrt{S}-k_0)^2-E_k^2+i\epsilon]}\right] M(\boldsymbol{k},\boldsymbol{q}|S) \tag{3.18}$$

The contour integration over dk_0 can be done to give

$$\left[\frac{1}{2E_k\sqrt{S}(2E_k-\sqrt{S})}-\frac{1}{2E_k\sqrt{S}(2E_k+\sqrt{S})}\right] = \frac{1}{4E_k}\frac{1}{E_k^2-S/4} \tag{3.19}$$

Noting that $S/4 = E_{\mathrm{q}}^2$, this equation (3.19) is easily seen to be the same as Blankenbecler-Sugar equation (3.15).

3.4 Short Range Structure in the Propagators

In the preceding section, we outlined how a relativistic three dimensional propagator can be obtained from the Bethe-Salpeter equation. In this section we will introduce the concept of short range structure of the relativistic propagators [CJ+86, CJ 88]. One can obtain the short range structure of the propagator by expressing it as a function of $|\boldsymbol{r}-\boldsymbol{r}'|$. Those pieces which behave like $\delta(\boldsymbol{r}-\boldsymbol{r}')$ or $exp(-m|\boldsymbol{r}-\boldsymbol{r}'|)$ will be defined as short range structure.

For a long time, the short range structure in scattering has been noticed by various authors. For example Barshay et al. pointed out that in pion scattering the iteration of momentum dependent potentials in the Lippmann Schwinger equation can generate a delta function term that corresponds to scattering of these particles at the same point [Bro+74].A similar phenomenon in proton-nucleus scattering has been pointed out by Thies [Thi 85, Thi 86]. Recently, the interpretation for the short range structure and anti-particle contribution in proton-nucleus scattering has been given by Cooper and Jennings [CJ+86].

In order to discuss the relation between short range structure and anti-particle contributions in scattering processes, we will look at the propagator $G_E(\boldsymbol{r}',\boldsymbol{r})$, for a Dirac particle scattering off a local potential $V(\boldsymbol{r}')$ [CJ+86, CJ 88]. The propagator

can be obtained from the full Feynman propagator $S_F(x'-x)$ as follows

$$\begin{aligned} G_E(\boldsymbol{r}',\boldsymbol{r}) &= -\int d(t'-t) S_F(x'-x) e^{-iE(t'-t)} \\ &= \int \frac{d^3p}{(2\pi)^3} \frac{e^{i\mathbf{p}\cdot(\mathbf{r}'-\mathbf{r})}}{\boldsymbol{p}^2 - \boldsymbol{k}^2 - i\epsilon} \begin{pmatrix} E+m & -\boldsymbol{\sigma}\cdot\boldsymbol{p} \\ \boldsymbol{\sigma}\cdot\boldsymbol{p} & m-E \end{pmatrix} \end{aligned} \tag{3.20}$$

where the Feynman propagator is

$$S_F(x'-x) = \int \frac{d^4p}{(2\pi)^4} \frac{e^{-ip\cdot(x'-x)}}{(\not{p}-m)}. \tag{3.21}$$

We obtain the asymptotic Dirac propagator $G_E^{(+)}(\boldsymbol{r}',\boldsymbol{r})$ by performing a contour integration over the momentum $\boldsymbol{p}$. Since the only pole contributing in the asymptotic region is from $|\boldsymbol{p}| = (k \pm i\epsilon)$, we have

$$G_E^{(+)}(\boldsymbol{r}',\boldsymbol{r}) = \begin{pmatrix} E+m & -\boldsymbol{\sigma}\cdot\boldsymbol{k} \\ \boldsymbol{\sigma}\cdot\boldsymbol{k} & m-E \end{pmatrix} \frac{e^{-k|\mathbf{r}'-\mathbf{r}|}}{4\pi|\boldsymbol{r}'-\boldsymbol{r}|}. \tag{3.22}$$

On the other hand, one can also decompose $S_F(x'-x)$ into particle and antiparticle contributions. We then have:

$$\begin{aligned} -S_F(x'-x) &= -\int \frac{d^3p}{(2\pi)^3} e^{i\mathbf{p}\cdot(\mathbf{r}'-\mathbf{r})} \int \frac{dp_0}{(2\pi)} \frac{(\gamma_0 p_0 - \boldsymbol{\gamma}\cdot\boldsymbol{p} + m) e^{-ip_0(t'-t)}}{[p_0 + E_p + i\epsilon][p_0 - E_p - i\epsilon]} \\ &= S_F^{(+)}(x'-x) + S_F^{(-)}(x'-x). \end{aligned} \tag{3.23}$$

Taking the Fourier transform into the scattering energy $E = \sqrt{\boldsymbol{k}^2 + m^2}$, (3.23) becomes,

$$G_E(\boldsymbol{r}',\boldsymbol{r}) = \tilde{S}_F^{(+)}(x'-x) + \tilde{S}_F^{(-)}(x'-x), \tag{3.24}$$

where

$$\tilde{S}_F^{(\pm)} = -\int \frac{d^3p}{(2\pi)^3} \frac{e^{i\mathbf{p}\cdot(\mathbf{r}'-\mathbf{r})}}{2E_{\mathbf{p}}} \left[\frac{\pm\gamma_0 E - \boldsymbol{\gamma}\cdot\boldsymbol{p} + m}{E_{\mathbf{p}} \mp E - i\epsilon} \right]. \tag{3.25}$$

The coordinate representation of the particle propagator $\tilde{S}_F^{(+)}$ can be obtained by integrating over momentum p. We will write the contribution from the pole as $\tilde{S}_F^{(+)}(x'-x)|_{pole}$ and other contributions as $\tilde{S}_F^{(+)}(x'-x)|_{non-pole}$. We can then write $G_E(\boldsymbol{r}', \boldsymbol{r})$ as

$$\begin{aligned} G_E(\boldsymbol{r}', \boldsymbol{r}) &= \tilde{S}_F^{(+)}(x'-x)|_{pole} + \tilde{S}_F^{(+)}(x'-x)|_{non-pole} + \tilde{S}_F^{(-)}(x'-x) \\ &= G_E^{(+)}(\boldsymbol{r}', \boldsymbol{r}) + \tilde{S}_F^{(+)}(x'-x)|_{non-pole} + \tilde{S}_F^{(-)}(x'-x) \end{aligned} \tag{3.26}$$

The second line of (3.26) follows since we can prove that

$$\tilde{S}_F^{(+)}(x'-x)|_{pole} = G_E^{(+)}(\boldsymbol{r}', \boldsymbol{r}).$$

In the asymptotic region, we noticed that $G_E(\boldsymbol{r}', \boldsymbol{r})$ behaves as $G_E^{(+)}(\boldsymbol{r}', \boldsymbol{r})$ in (3.22). The interpretation of the result (3.26) is controversial. In fact, it is not at all clear that the last two terms in (3.26) give a null contribution in the asymptotic region or why they should. However, Cooper and Jennings [CJ+86] justify this numerically. They also argue that the propagator is not only subjected to elastic scattering, but that all physical processes include negative energy states. Therefore, the success of Dirac phenomenology in proton-nucleus scattering is attributed to the cancellation of the spurious short ranged terms in the particle propagators by anti-particle contributions (see discussion in Ref. [PT 87], however).

3.5 Smooth Propagators

We have discussed at length, in Section 3.4, that the short range structure removes the anti-particle contributions in the propagators. In this Section, we will extend the method of removing anti-particle degrees of freedom by means of the short range approach to the two particle propagators. We will derive the pion-nucleon propagators from the so-called box diagram Fig. 3.2, which can be evaluated in accordance with Feynman rules. As has been done in Section 3.3.2, we will apply the instantaneous-interaction approximation to the box diagram and then apply the short range method to this propagator. A similar application has been made to obtain a smooth propagator for the NN scattering [CJ 88]. Our presentation in this section is a follow up application of Cooper and Jenning's work. The model chosen is a pion interacting with a nucleon through ρ meson exchange where the $\rho - \pi$ coupling is of the form

$$(E_\pi + E'_\pi)\gamma_0 \boldsymbol{\pi}^2$$

with only the time component of ρ contributing [CJ 88].The amplitude for Fig.3.2 is,

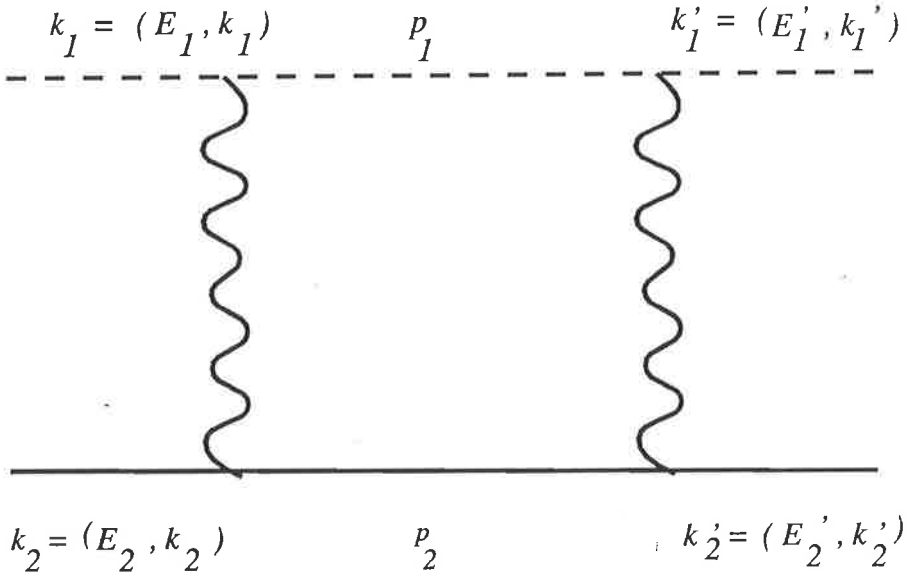

Figure 3.2: Box Diagram for πN system

$$A = \int d^4p_1 d^4p_2 d^4q d^4q' \frac{\delta^4(k_2' - p_2 + q')}{[q'^2 - m_\rho^2 - i\epsilon]} \frac{\delta^4(k_1' - p_1 - q')}{[p_1^2 - m_\pi^2 - i\epsilon]} \frac{\delta^4(p_1 - k_1 - q)}{[q^2 - m_\rho^2 - i\epsilon]}$$
$$\gamma_0(E_1' + p_{10}) \frac{\delta^4(p_2 - k_2 + q)}{[\not{p}_2 - m_N - i\epsilon]} \gamma_0(p_{10} + E_1) \tag{3.27}$$

Integrating over p_2, q, q' gives

$$A = \delta^4(k_1' + k_2' - k_1 - k_2) \int d^4p \frac{1}{[(k_1' - p)^2 - m_\rho^2 - i\epsilon]} \frac{1}{[p^2 - m_\pi^2 - i\epsilon]} \tag{3.28}$$
$$\frac{1}{[(p - k_1)^2 - m_\rho^2 - i\epsilon]} \gamma_0(E_1' + p_0) \frac{1}{[(\not{k}_2 + \not{k}_1 - \not{p}_1) - m_N - i\epsilon]} \gamma_0(p_0 + E_1)$$

As in Section 3.3.2, we integrate over the energy variable p_0. By noting

$$\omega_\rho' = [(\boldsymbol{k}_1' - \boldsymbol{p})^2 + m_\rho^2]^{\frac{1}{2}}$$
$$\omega_\rho = [(\boldsymbol{p} - \boldsymbol{k}_1)^2 + m_\rho^2]^{\frac{1}{2}}$$
$$\omega_\pi = [\boldsymbol{p}^2 + m_\pi^2]^{\frac{1}{2}}$$
$$\omega_N = [(\boldsymbol{k}_1' + \boldsymbol{k}_1 - \boldsymbol{p})^2 + m_N^2]^{\frac{1}{2}}$$

and integrating over p_0, the four poles from (3.28) give

$$A = \delta^4(k_1' + k_2' - k_1 - k_2) \int d^3p$$
$$\Bigg\{ \frac{1}{2\omega_\rho'} \frac{1}{(E_1' + \omega_\rho')^2 - \omega_\pi^2} \frac{1}{(E_1' + \omega_\rho' - E_1)^2 - \omega_\rho^2} \gamma_0(E_1' + E_2' + \omega_\rho')$$
$$\frac{\gamma_0(E_2 + E_1 - E_1' - \omega_\rho') - \boldsymbol{\gamma} \cdot (\boldsymbol{k}_2 + \boldsymbol{k}_1 - \boldsymbol{p}) + m_N}{(E_2 + E_1 - E_1' - \omega_\rho')^2 - \omega_N^2} \gamma_0(E_1' + E_1' + \omega_\rho')$$
$$+ \frac{1}{(E_1' - \omega_\pi)^2 - \omega_\rho'^2} \frac{1}{2\omega_\pi} \frac{1}{(\omega_\pi - E_1)^2 - \omega_\rho^2}$$
$$\gamma_0(E_1' + \omega_\pi) \frac{\gamma_0(E_2 + E_1 - \omega_\pi) - \boldsymbol{\gamma} \cdot (\boldsymbol{k}_2 + \boldsymbol{k}_1 - \boldsymbol{p}) + m_N}{(E_2 + E_1 - \omega_\pi)^2 - \omega_N^2} \gamma_0(E_1' + \omega_\pi)$$
$$+ \frac{1}{(E_1' + E_1 + \omega_\rho)^2 - \omega_\rho'^2} \frac{1}{(E_1 + \omega_\rho)^2 - \omega_\pi^2} \frac{1}{2\omega_\rho}$$

$$\gamma_0(E_1' + E_1 + \omega_\rho)\frac{\gamma_0(E_2 + E_1 - E_1 - \omega_\rho) - \boldsymbol{\gamma}\cdot(\boldsymbol{k}_2 + \boldsymbol{k}_1 - \boldsymbol{p}) + m_N}{(E_2 + E_1 - E_1 - \omega_\rho)^2 - \omega_N^2}\gamma_0(E_1' + E_1 + \omega_\rho)$$
$$+\frac{1}{(E_1' - E_2 - E_1 - \omega_N)^2 - \omega_\rho'^2}\frac{1}{(E_2 + E_1 + \omega_N)^2 - \omega_\pi^2}$$
$$\frac{1}{(E_2 + E_1 + \omega_N - E_1)^2 - \omega_\rho^2}\gamma_0(E_1' + E_2 + E_1 + \omega_N)$$
$$\frac{\gamma_0(-\omega_N) - \boldsymbol{\gamma}\cdot(\boldsymbol{k}_2 + \boldsymbol{k}_1 - \boldsymbol{p}) + m_N}{2\omega_N}\gamma_0(E_1' + E_2 + E_1 + \omega_N)\Bigg\} \tag{3.29}$$

Now let us examine each of the 4-terms in (3.29). The pion propagator in the last term can be written as

$$\frac{1}{(E_2 + E_1 + \omega_N)^2 - \omega_\pi^2} = \frac{E_2 - \sqrt{\boldsymbol{p}^2 + m_N^2}}{2(E_1 + E_2)(\boldsymbol{k}^2 - \boldsymbol{p}^2)}$$

This denominator is not only providing the branch cut in momentum space, but also vanishes when we integrate over $|\boldsymbol{p}|$. The contribution from nucleon part

$$\frac{\gamma_0(-\omega_N) - \boldsymbol{\gamma}\cdot(\boldsymbol{k}_2 + \boldsymbol{k}_1 - \boldsymbol{p}) + m_N}{2\omega_N}$$

will give a branch cut since $\omega_N = \sqrt{\boldsymbol{p}^2 + m_N^2}$. We will therefore regard this term as purely short range.

Similar consideration for the 2nd terms of (3.29) leads to

$$\begin{aligned}\frac{1}{(E_2 + E_1 - \omega_\pi)^2 - \omega_N^2} &= \frac{E_1 + \sqrt{\boldsymbol{p}^2 + m_\pi^2}}{2(E_1 + E_2)(\boldsymbol{k}^2 - \boldsymbol{p}^2)} \\ &= \frac{E_1}{E_1 + E_2}\frac{1}{(\boldsymbol{k}^2 - \boldsymbol{p}^2)}.\end{aligned} \tag{3.30}$$

Following Cooper and Jennings [CJ 88] the 1st and 3rd term in (3.29) cancel. Therefore, in the c.o.m (3.29) becomes

$$A = \delta^4(k_1' + k_2' - k_1 - k_2)\int d^3p\left\{\frac{1}{\omega_\rho'^2}\gamma_0(2E_\pi)\frac{\gamma_0 E_2 + \boldsymbol{\gamma}\cdot\boldsymbol{p} + m_N}{2(E_\pi + E_N)(\boldsymbol{k}^2 - \boldsymbol{p}^2)}\gamma_0(2E_\pi)\frac{1}{\omega_\rho^2}\right\} \tag{3.31}$$

Hence we take the two particle propagator for πN system to be:

$$G(\boldsymbol{p}_N|S) = \frac{\gamma_0 E_2 - \boldsymbol{\gamma}\cdot\boldsymbol{p}_N + m_N}{2\sqrt{S}\,(\boldsymbol{k}^2 - \boldsymbol{p}^2)} \tag{3.32}$$

This is known as smooth propagator, which we will apply in our CBM calculation in Chapter 7

3.6 The One Body Limit

After writing down a fully relativistic scattering equation, such as the Bethe-Salpeter(BS) equation, there is the question of how this equation is consistent with non-relativistic physics. It is a sensible question to ask how an equation will reduce to known results in physics. In the case of the BS equation, which is a relativistic description of the interaction of two particles, we ask the question whether this will reduce to a one particle equation when the mass of one particle becomes large(one body limit). In this limit, the interaction will reduce to an instantaneous one since there will be no energy transfer to the larger mass source. The two particle propagator then reduces to the one particle propagator. Gross [Gro 82] has made such an analysis for the ladder approximated BS equation. Following Gross, we will show that ladder approximated BS equation does not reduce to the correct equation in the one body limit. Let us recall the Bethe-Salpeter equation (3.7) with masses $m_1 << m_2$

$$M(p,q|S) = K(p,q|S) - i\int \frac{d^4k}{(2\pi)^4} K(p,q|S)G_1(k_1)G_2(k_2)M(k,q|S) \tag{3.33}$$

where $G_1(k_1)$ and $G_2(k_2)$ are the relativistic propagators. Denoting $\alpha_1 = \epsilon_1/(\epsilon_1+\epsilon_2)$ and $\alpha_2 = \epsilon_2/(\epsilon_1+\epsilon_2)$, the two body propagator becomes

$$\begin{aligned} G(k,S) &= G_1(k_1)G_2(k_2) \\ &= \frac{1}{[(\alpha_1 P + k)^2 - m_1^2 + i\epsilon]} \frac{1}{[(\alpha_2 P - k)^2 - m_2^2 + i\epsilon]} \end{aligned} \tag{3.34}$$

Consider the particular case of $m_2 \to \infty$. In this limit, the kernel K is free of relative energy variable hence the integration over relative energy variable will be done only on the poles of $G(k,S)$. Firstly we will look at the contribution from the poles of particle 1. The two poles are at

$$k_0 = -\alpha_1 \pm E_1 \pm i\epsilon$$

where $E_1 = \sqrt{m_1^2 + \boldsymbol{k}^2}$. The effect of these poles on G_2 in the limit of $m_2 \to \infty$ is

$$\begin{aligned} G_2(k_2) &= \frac{1}{[(\alpha_2 P - k)^2 - m_2^2]} \\ &= \frac{1}{[(\epsilon_2 + \epsilon_1 - E_1)^2 - E_2^2]} \to 0 \end{aligned} \tag{3.35}$$

where ϵ_1 and ϵ_2 been given in (3.3). For the contributions from the poles of particle 2, we will first write $G_2(k_2)$ in (3.34) as follows:

$$\begin{aligned} G(k,S) &= \frac{1}{[(\alpha_1 P + k_0)^2 - E_1^2 + i\epsilon]} \frac{1}{2E_2} \\ &\quad \left(\frac{1}{E_2 - \alpha_2 P + k_0 - i\epsilon} + \frac{1}{E_2 + \alpha_2 P - k_0 - i\epsilon} \right) \end{aligned} \tag{3.36}$$

In the limit $m_2 \to \infty$

$$E_2 \to m_2$$

$$E_2 - \alpha_2 P \to E_2 - \epsilon_2$$

$$E_2 + \alpha_2 P \to E_2 + \epsilon_2 \approx 2m_2$$

Thus the contribution from 2nd term in (3.36) can be ignored. For the 1st term of (3.36) there will be a significant contribution in the energy integration since $E_2 - \epsilon_2$ is small. Therefore, we cannot ignore this term in the limit $m_2 \to \infty$. It is this term that violates the one body limit.

In relation to smooth propagators, it is worth noting that the troublesome term from the nucleon pole, i.e. the last term in (3.29), is removed by the short range method. Therefore, the smooth propagators naturally satisfy the one body limit.

3.7 One Body Limit, the R factor

In Section 3.3 we demonstrated how the Blankenbecler-Sugar and Instantaneous-interaction approximations can be applied in approximating the Bethe-Salpeter equation. In Section 3.6, we showed that the ladder approximated Bethe-Salpeter equation does not give the correct equation when one of the scattering particle's masses becomes large. It is worth noting that Gross's discussion of the one body limit is based on the instantaneous-interaction approximation of Section 3.3.2. One can equally discuss the one body limit in Blankenbecler-Sugar type propagators [CJ 89] which we will now examine.

Likewise in (3.14), we can write down the Lorentz invariant propagator for the general case of different masses m_1 and m_2. The general two particle propagator G_{gen} which has poles when two particle are on shell is

$$\begin{aligned} G_{gen}(p,P) &= \int_{(m_1+m_2)^2}^{\infty} \frac{dS'}{S-S'} f(S,S') \delta^+ \left(\left(\frac{\epsilon_1(S')P'}{\epsilon_1(S')+\epsilon_2(S')} + p \right)^2 - m_1^2 \right) \\ & \quad \delta^+ \left(\left(\frac{\epsilon_2(S')P'}{\epsilon_1(S')+\epsilon_2(S')} - p \right)^2 - m_2^2 \right) \end{aligned} \tag{3.37}$$

where $P' = \sqrt{\frac{S'}{S}}P$ and $f(S, S')$ represents any function which has the property

$$f(S, S) = 1.$$

The propagator G_{gen} in (3.37) is most general among 3-dimensional propagators that the smooth and BbS propagators can be considered as special case. One can do the integration over S' (see Appendix B for more details). From (3.37) we then have the general case of a two particle propagator for two spinless particles with different masses

$$G_{gen}(P, p) = \frac{\delta(2P \cdot p)}{\boldsymbol{p}^2 - \boldsymbol{k}^2} \frac{(S_p S - (m_1^2 - m_2^2))}{4\sqrt{S S_p}\epsilon_1(S_p)\epsilon_2(S_p)} f(S, S_p), \tag{3.38}$$

where

$$\sqrt{S_p} = \sqrt{m_1^2 - p^2} + \sqrt{m_2^2 - p^2}.$$

Equation (3.38) is the central result for our discussion. Since this is a general case of a propagator for two different mass particles, we can compare with the other two particle propagators and identify the so-called R factor for different propagators. Firstly, we can factor out the smooth propagator G_{sm} in (3.32) and Blankenbecler-Sugar propagator G_{BbS} (3.19) from general propagator (3.38) as follows:

$$\begin{aligned} G_{sm}(P, p) &= \frac{\delta(P_0)}{2\sqrt{S}(\boldsymbol{p}^2 - \boldsymbol{k}^2)} \frac{(S_p S - (m_1^2 - m_2^2))}{4\sqrt{S S_p}\epsilon_1(S_p)\epsilon_2(S_p)} f(S, S_p) \\ &= \frac{\delta(P_0)}{2\sqrt{S}\,(\boldsymbol{p}^2 - \boldsymbol{k}^2)} R_{sm} \end{aligned} \tag{3.39}$$

$$\begin{aligned} G_{BbS}(P, p) &= \frac{\delta(P_0)}{2\sqrt{S_p}(\boldsymbol{p}^2 - \boldsymbol{k}^2)} \frac{S_p}{S} \frac{S S_p - (m_1^2 - m_2^2)^2}{S_p^2 - (m_1^2 - m_2^2)^2} f(S, S_p) \\ &= \frac{\delta(P_0)}{2\sqrt{S_p}(\boldsymbol{p}^2 - \boldsymbol{k}^2)} R_{BbS} \end{aligned} \tag{3.40}$$

From (3.39) and (3.40), it can be seen that for equal masses $m_1 = m_2$, R_{sm} and

R_{BbS} both become unity, the only difference being the square root factors in the denominators. We can now study the properties of different propagators when the mass of one particle become infinite, $m_2 \to \infty$:

$$R_{sm} \approx 1 \tag{3.41}$$

$$R_{BbS} \approx \frac{\epsilon_1 + \epsilon_1(S_p)}{2\epsilon_1(S_p)} \tag{3.42}$$

We can now compare the smooth propagator and BbS propagator in the light of one body limit. In Section 3.6, the one body limit was defined as the ability to reduce to one particle equation when the mass of one particle approaches infinity. When we formulate the 3-dimensional propagator in Blankenbecler and Sugar's approach(used dispersion technique) the potential is instantaneous and we need to ask whether the propagator exhibits the features of one particle propagator. In fact the smooth propagator does become the one particle propagator since $R_{sm} \approx 1$ in the $m_2 \to \infty$ limit. On the other hand R_{BbS} does not reduce to unity when the mass of one particle becomes large and it therefore violates the one body limit.

3.8 Application to the πN system

In Section 3.7, we derived the Blankenbecler Sugar propagator and smooth propagators and examined their one body limits. When we apply these propagators to the πN system, we need to include spin. This is done by introducing the projection operators in eqn (3.37) for one particle as outlined in [Erk 74, Bro 79, CJ 89].

For the Blankenbecler Sugar propagator, we need to make modifications as outlined by Cooper and Jennings [CJ 89] in order to have correct one body limit. The

propagators used in our calculation in Chapter 7 are

$$G_{sm}^{(1/2,0)}(P,p) = \frac{1}{2\sqrt{S}}\frac{\delta(p_0)}{\boldsymbol{p}^2-\boldsymbol{k}^2}D_{sm}^1(P,p) \tag{3.43}$$

$$G_{BbS}^{(1/2,0)}(P,p) = \frac{1}{2\sqrt{S_p}}\frac{\delta(p_0)}{\boldsymbol{p}^2-\boldsymbol{k}^2}D_{sm}^1(P,p), \tag{3.44}$$

where the Dirac factor D_{sm}^1 is given by

$$D_{sm}^1(P,p) = \gamma_\mu\left(\frac{\epsilon_1}{\epsilon_1+\epsilon_2}P^\mu + p^\mu\right) + m_1.$$

3.9 Summary

In this Chapter, we discussed methods to ensure unitarity by using relativistic propagators. Attention has been given to 3-dimensional propagators which are covariant and guarantee unitarity. We first discussed how the interaction of two particles is described using the Bethe-Salpeter equation in ladder approximation. We also focussed our attention on a recently suggested smooth propagator which is consistent with Dirac phenomenology and does not violate one body limits. We also presented the relativistic propagators used in our calculation in Chapter 7.

Chapter 4

The Formalism

4.1 Introduction

In Chapter 3 we presented the relativistic wave equations which can guarantee unitarity in scattering. We shall now discuss in detail how the driving potential for the relativistic scattering equation is obtained in the Cloudy Bag Model(CBM). As we have stated in Chapter 1, the CBM Lagrangian describes interactions of pion and quarks . The main aim of this chapter is to provide the formulation for transforming interaction of pion and quark to those of pion and nucleon. We expect the potentials to be relatively simple at threshold energy and give proper cancellations of the type encountered in Chapter 2. In Section 4.2 we will discuss how the pion-quark interaction can be projected into a pion-nucleon interaction. We give two examples, namely the vertex function and the Weinberg-Tomozawa term. In Section 4.3 we give a detailed account of how the higher order graphs are calculated in the CBM. We also give information on how we can approximate some complicated integral functions.

4.2 Interactions in the Cloudy Bag Model

There are many possible non-linear lagrangians which represent the same physical system and can provide the same result to order of $\frac{1}{(2f)^2}$. From these, we shell use the Kalbermann and Eisenberg's variant of CBM lagrangian [KE 83], and write in Hamiltonian form favoured by [Tho+87, CJ 86]. The full Hamiltonian is given as follows(see Appendix A.2 for details):

$$H(\boldsymbol{x}) = \int d^3x \{\mathcal{H}_{MIT}(\boldsymbol{x}) + \mathcal{H}_{0\pi}(\boldsymbol{x}) + \mathcal{H}_1(\boldsymbol{x}) + \mathcal{H}_3(\boldsymbol{x}) + \mathcal{H}'(\boldsymbol{x}) + \mathcal{H}_{4\pi}(\boldsymbol{x}) + \mathcal{H}_{WT}(\boldsymbol{x})\} , \tag{4.1}$$

where

$$\mathcal{H}_{MIT}(\boldsymbol{x}) = (\frac{1}{2} i\bar{q}\boldsymbol{\gamma}\cdot(\overleftarrow{\nabla} - \vec{\nabla})q + B)\theta_v + \frac{1}{2}\bar{q}q\triangle_s \tag{4.2}$$

$$\mathcal{H}_{0\pi}(\boldsymbol{x}) = \frac{1}{2}\{\boldsymbol{\Pi}^2 + (\vec{\nabla}\,\boldsymbol{\phi})^2 + m_\pi^2\boldsymbol{\phi}^2\} \tag{4.3}$$

$$\mathcal{H}_1(\boldsymbol{x}) = -\frac{\theta_v}{(2f)}\bar{q}\boldsymbol{\gamma}\gamma_5\boldsymbol{\tau}q.\,\vec{\nabla}\,\boldsymbol{\phi} \tag{4.4}$$

$$\mathcal{H}_3(\boldsymbol{x}) = \frac{\theta_v}{(2f)^3}\,\bar{q}\boldsymbol{\gamma}\gamma_5\boldsymbol{\tau}q\cdot\vec{\nabla}\,\boldsymbol{\phi}\;\;\boldsymbol{\phi}\cdot\boldsymbol{\phi} \tag{4.5}$$

$$\mathcal{H}'(\boldsymbol{x}) = \frac{1}{2}\,[\bar{q}\gamma_0(\frac{\gamma_5\boldsymbol{\tau}}{(2f)} - \frac{(\boldsymbol{\tau}\times\boldsymbol{\phi})}{(2f)^2})q]^2 \tag{4.6}$$

$$\mathcal{H}_{4\pi}(\boldsymbol{x}) = \frac{1}{(2f)^2}\left(\boldsymbol{\Pi}^2 - (\vec{\nabla}\,\boldsymbol{\phi})^2 - m_\pi^2\boldsymbol{\phi}^2\right)\boldsymbol{\phi}\cdot\boldsymbol{\phi} \tag{4.7}$$

$$\mathcal{H}^t_{WT}(\boldsymbol{x}) = \frac{\theta_v}{(2f)^2}\,\bar{q}\gamma^0\boldsymbol{\tau}q\;\cdot(\boldsymbol{\phi}\times\boldsymbol{\Pi}) \tag{4.8}$$

$$\mathcal{H}^{so}_{WT}(\boldsymbol{x}) = \frac{\theta_v}{(2f)^2}\,\bar{q}\boldsymbol{\gamma}\boldsymbol{\tau}q\;\cdot(\boldsymbol{\phi}\times\vec{\nabla}\,\boldsymbol{\phi}) \tag{4.9}$$

Up to order $\frac{1}{(2f)^4}$, the diagrams shown in Figure 4.1 (from now on we will simply refer as Fig. 4.1 etc.) contribute to the potential. The diagram shown in Fig. 4.1a produces the Weinberg-Tomozawa result at threshold energy. When we take all interactions to order $\frac{1}{(2f)^4}$, Figs. 4.1b and 4.1c needed to be included in the calculation. However, since the driving potential is the sum of all irreducible diagrams,

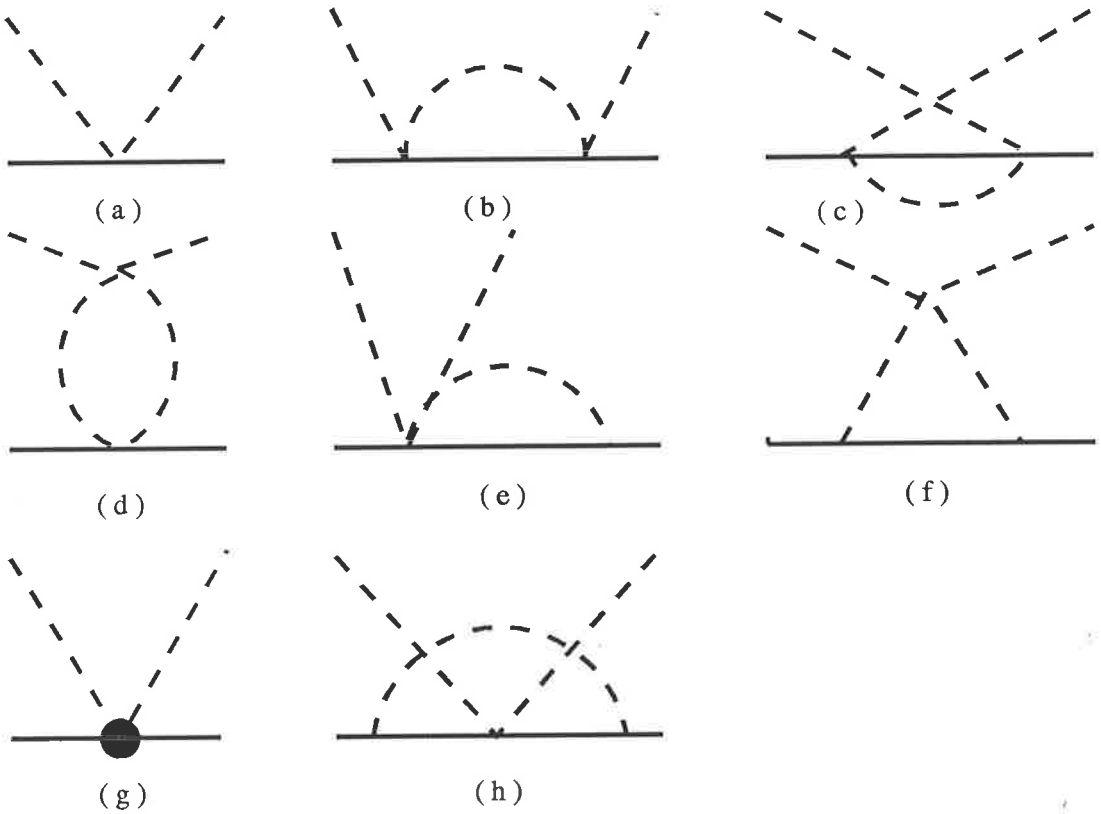

Figure 4.1: Diagrams included in this calculation

Fig. 4.1b will not be included since it is an iteration of Fig. 4.1a. We will now show how the potentials for Fig. 4.1a to Fig. 4.1h are calculated in the CBM.

4.2.1 Vertex Functions

When we use the linearized CBM Lagrangian (4.1) to describe pion-nucleon interactions we not only have the Yukawa type vertex Fig. 4.2a, but also the three pion vertex Fig. 4.2b . The vertices of Fig. 4.2a and 4.2b are generated by $\mathcal{H}_1(\boldsymbol{x})$ and $\mathcal{H}_3(\boldsymbol{x})$ respectively. Figures 4.2a and 4.2b are needed when we calculate higher order diagrams shown in Fig. 4.1e and Fig. 4.1f. The dependence on the momentum of the third meson in Fig. 4.2b when we consider the S-wave isoscalar interaction in Fig. 4.1e is the same as the dependence on the meson momentum in Fig. 4.2a (pseudovector coupling) because the isoscalar pair in $\mathcal{H}_3(\boldsymbol{x})$ will interact with ingoing and

Figure 4.2: One pion and 3-pion vertices

outgoing mesons.

The calculation for the process shown in Fig. 4.2a : $B' \rightarrow B + \pi$ is given in [Tho+83, Tho+80] for the pseudoscalar coupling. For pseudovector coupling the same form factor as for the pseudoscalar case is obtained after integration by parts [Tho+86]. Here, we calculate the pseudovector form factor in a straight forward manner.

In order to clarify the presentation later in this thesis where several interactions occur, we shall formally retain the coordinate at which the interaction occurs(even though it is integrated). Thus the interaction Hamiltonian for the diagram shown in Fig. 4.2a will be written as:

$$\begin{aligned} H_1(\boldsymbol{x}) &= \int d^3x\ \mathcal{H}_1(\boldsymbol{x}) \\ &= -\frac{\theta_v(x)}{(2f)} \int d^3x\ \bar{q}(\boldsymbol{x})\gamma\gamma_5\tau q(\boldsymbol{x}) \cdot \vec{\nabla}\ \phi(\boldsymbol{x}) \ . \end{aligned} \tag{4.10}$$

The transition from the initial state

$$|i\ \rangle = |S_B m_B, I_B i_B\rangle \tag{4.11}$$

to the final state

$$|f\rangle = |S_{B'} m_{B'}, I_{B'} i_{B'}; \boldsymbol{k}, i_{M'}\rangle \tag{4.12}$$

can be described by the matrix element of interaction Hamiltonian $H_1(\boldsymbol{x})$:

$$\begin{aligned}\langle f|H_1(\boldsymbol{x})|i\rangle &= \langle f|PH_1(\boldsymbol{x})P|i\rangle \\ &= \langle f|\alpha^\dagger\langle\alpha|H_1(\boldsymbol{x})|\beta\rangle\beta|i\rangle \end{aligned} \tag{4.13}$$

where the kets $|\alpha\rangle$and $|\beta\rangle$ are colourless baryonic bag states which have the same quantum numbers as baryons and α ($\alpha^\dagger$) are annihilation (creation) operators for a real nucleon. Therefore the projection operator $P = \sum_\alpha |\alpha\rangle\langle\alpha|$ projects the pion-quark Hamiltonian $H_1(\boldsymbol{x})$ onto baryon space. Now

$$\langle\alpha|H_1(\boldsymbol{x})|\beta\rangle = (2\pi)^{-\frac{3}{2}}\int d^3q \sum_j [\ \hat{V}_j^{\alpha\beta}(\boldsymbol{q})a_j(\boldsymbol{q}) + \hat{V}_j^{\alpha\beta\dagger}(\boldsymbol{q})a_j^\dagger(\boldsymbol{q})] \tag{4.14}$$

where the interaction matrix element is

$$\begin{aligned}\hat{V}_j^{\alpha\beta}(\boldsymbol{q}) &= -\frac{i}{(2f)}\theta_v(x)\int d^3x\ \langle\alpha|\bar{q}(x)\boldsymbol{\gamma}\cdot\boldsymbol{q}\gamma_5\tau_j q(x)|\beta\rangle\frac{e^{i\mathbf{q}\cdot\mathbf{x}}}{\sqrt{2\omega_\mathbf{q}}} \\ &= -\frac{i}{(2f)}\ \frac{N_s^2}{(4\pi)}\int_0^R dx\ x^2\int d\hat{x}\ {}_{sf}\langle\alpha|\sum_{a=1}^{3}[(j_0^2(\frac{\Omega x}{R}) - j_1^2(\frac{\Omega x}{R}))\boldsymbol{\sigma}^{(a)}\cdot\boldsymbol{q}\tau_j^{(a)} \\ &\qquad + 2j_1^2(\frac{\Omega x}{R})\ \boldsymbol{\sigma}^{(a)}\cdot\hat{x}\ \boldsymbol{q}\cdot\hat{x}\ \tau_j^{(a)}]|\beta\rangle_{sf}\frac{e^{i\mathbf{q}\cdot\mathbf{x}}}{\sqrt{2\omega_\mathbf{q}}}\ . \end{aligned} \tag{4.15}$$

In eqn (4.15), the kets $|\alpha\rangle_{sf}$ denote the spin-flavour wave function for the baryon bag state $|\alpha\rangle$ and the operators $\sigma^{(a)}$ and $\tau^{(a)}$ are the spin and isospin operators for quark a. It is useful to write the interaction matrix element as

$$\hat{V}_j^{\alpha\beta}(\boldsymbol{q}) = -\frac{i}{(2f)}\ \frac{N_s^2}{(4\pi)}\int_0^R dx x^2\int d\hat{x}\ \boldsymbol{\Sigma}_j^{\alpha\beta}\cdot\boldsymbol{q}\ \frac{e^{i\mathbf{q}\cdot\mathbf{x}}}{\sqrt{2\omega_\mathbf{q}}}, \tag{4.16}$$

where the symbol $\boldsymbol{\Sigma}_j^{\alpha\beta}$ represents

$$\boldsymbol{\Sigma}_j^{\alpha\beta} = {}_{sf}\langle\alpha|\sum_{a=1}^{3}\left[(j_0^2(\frac{\Omega x}{R}) - j_1^2(\frac{\Omega x}{R}))\boldsymbol{\sigma}^{(a)}\tau_j^{(a)} + 2j_1^2(\frac{\Omega x}{R})\boldsymbol{\sigma}^{(a)}\cdot\hat{x}\ \hat{x}\tau_j^{(a)}\right]|\beta\rangle_{sf}. \tag{4.17}$$

Since we have (See Appendix C)

$$\int d\hat{x}\ \boldsymbol{\sigma}\cdot\boldsymbol{q}\ e^{i\mathbf{q}\cdot\mathbf{x}} = (4\pi) j_0(qx)\ \boldsymbol{\sigma}\cdot\boldsymbol{q} \tag{4.18}$$

and

$$\int d\hat{x}\ \boldsymbol{\sigma}\cdot\hat{x}\ \boldsymbol{q}\cdot\hat{x}\ e^{i\mathbf{q}\cdot\mathbf{x}} = \left(\frac{4\pi}{3}\right)\ (j_0(qx) - 2j_2(qx))\ \boldsymbol{\sigma}\cdot\boldsymbol{q} \tag{4.19}$$

the interaction matrix element (4.15) becomes

$$\hat{V}_j^{\alpha\beta}(\boldsymbol{q}) = -\frac{i}{(6f)}\ \frac{1}{\sqrt{2\omega_{\mathbf{q}}}}\ \left(\frac{\Omega}{\Omega-1}\right) U(qR)\ {}_{sf}\langle\alpha|\sum_{a=1}^{3}\boldsymbol{\sigma}^{(a)}\cdot\boldsymbol{q}\tau_j^{(a)}|\beta\rangle_{sf}. \tag{4.20}$$

In eqn (4.20) the form factor $U(qR)$ is given by

$$\begin{aligned} U(qR) &= \frac{3}{2R^3 j_0^2(\Omega)}\ \int_0^R dx x^2\ \rho_{pv}(qx) \\ &= \frac{3}{2R^3 j_0^2(\Omega)}\ \int_0^R dx x^2\ [(j_0^2(\frac{\Omega x}{R}) - \frac{1}{3}j_1^2(\frac{\Omega x}{R}))j_0(qx) - \frac{4}{3}\ j_1^2(\frac{\Omega x}{R})\ j_2(qx)]. \end{aligned} \tag{4.21}$$

The form factor $U(qR)$ has a different analytical form from previous calculations. However, it gives the same momentum cut-off as the form-factors of [Tho+83, Tho+86].

Now we are left with the task of replacing the quark spin and isospin operators with those of the appropriate baryons. In order to do this, we write the matrix element of the quark spin and isospin operators in eqn (4.20) in terms of transition spin ($\boldsymbol{S}$) and isospin ($\boldsymbol{T}$) as follows [BW 75]:

$$X^{\alpha\beta}\langle\alpha|\boldsymbol{S}\cdot\boldsymbol{q}\ \boldsymbol{T}|\beta\rangle = {}_{sf}\langle\alpha|\sum_{a=1}^{3}\boldsymbol{\sigma}^{(a)}\cdot\boldsymbol{q}\boldsymbol{\tau}^{(a)}|\beta\rangle_{sf} \tag{4.22}$$

Now, on the left hand side of (4.22), the kets $|\alpha\rangle$ and $|\beta\rangle$ are colourless baryonic bag wave functions which possesses the same spin-isospin quantum number as baryons,

i.e.

$$|\alpha\rangle = |S_\alpha m_\alpha, I_\alpha i_\alpha\rangle \tag{4.23}$$

$$|\beta\rangle = |S_\beta m_\beta, I_\beta i_\beta\rangle \tag{4.24}$$

where S_α (I_α) and m_α (i_α) are total spin(isospin) quantum numbers and their projections respectively. On the R.H.S. of (4.20), the kets $|\alpha\rangle_{sf}$ and $|\beta\rangle_{sf}$ represent explicit SU(6) spin-flavour quark wave functions [see Appendix A.3]. The operators $\boldsymbol{\sigma}^{(a)}$ and $\boldsymbol{\tau}^{(a)}$ are the spin and isospin operators for a-th quark. $X^{\alpha\beta}$ is a symmetry factor that arises when we eliminate the quark spin and isospin operators in favour of their nucleon counter parts.

The operators in (4.22) can be written in the spherical basis [See Appendix C],

$$X^{\alpha\beta}\ \langle S_\alpha m_\alpha, I_\alpha i_\alpha | S_{1m} T_{1n} | S_\beta m_\beta, I_\beta i_\beta\rangle\ \hat{\boldsymbol{s}}^*_m \cdot \boldsymbol{q}\ \hat{\boldsymbol{t}}^*_n$$
$$= {}_{sf}\langle\alpha| \sum_{a=1}^{3} \sigma^{(a)}_{1m} \tau^{(a)}_{1n} |\beta\rangle_{sf}\, \hat{\boldsymbol{s}}^*_m \cdot \boldsymbol{q}\ \hat{\boldsymbol{t}}^*_n \tag{4.25}$$

where $S_{1m}, T_{1n}, \sigma^{(a)}_{1m}$ and $\tau^{(a)}_{1n}$ denote spherical tensors of rank 1. The L.H.S. of (4.25) is, according to the Wigner-Eckart theorem [see Appendix C],

$$X^{\alpha\beta}\ \langle S_\alpha m_\alpha, I_\alpha i_\alpha | S_{1m} T_{1n} | S_\beta m_\beta, I_\beta i_\beta\rangle\ \hat{\boldsymbol{s}}^*_m \cdot \boldsymbol{q}\ \hat{\boldsymbol{t}}^*_n\ =$$
$$X^{\alpha\beta} \langle S_\alpha I_\alpha || \boldsymbol{S}^{(1)} \boldsymbol{T}^{(1)} || S_\beta I_\beta\rangle\ \frac{C^{m_\beta\ m\ m_\alpha}_{S_\beta\ 1\ S_\alpha}}{\sqrt{2S_\alpha+1}}\ \frac{C^{i_\beta\ n\ i_\alpha}_{I_\beta\ 1\ I_\alpha}}{\sqrt{2I_\alpha+1}} \hat{\boldsymbol{s}}^*_m \cdot \boldsymbol{q} \hat{\boldsymbol{t}}^*_n \tag{4.26}$$

Since we can calculate R.H.S. of (4.25) for a particular case of $m = 0, n = 0$, we have:

$$X^{\alpha\beta} = \frac{\mathcal{M}_{\alpha\beta}}{C^{m_\beta\ 0\ m_\alpha}_{S_\beta\ 1\ S_\alpha} C^{i_\beta\ 0\ i_\alpha}_{I_\beta\ 1\ I_\alpha}} \frac{\sqrt{2S_\alpha+1}\sqrt{2I_\alpha+1}}{\langle S_\alpha I_\alpha || \boldsymbol{S}^{(1)} \boldsymbol{T}^{(1)} || S_\beta I_\beta\rangle} \tag{4.27}$$

$$= \lambda^{\alpha\beta} \frac{\sqrt{2S_\alpha+1}\sqrt{2I_\alpha+1}}{\langle S_\alpha I_\alpha || \boldsymbol{S}^{(1)} \boldsymbol{T}^{(1)} || S_\beta I_\beta\rangle}\,. \tag{4.28}$$

In eqn (4.27) the matrix element $\mathcal{M}_{\alpha\beta}$ is defined (see Appendix A.3) as:

$$\mathcal{M}_{\alpha\beta} = {}_{sf}\langle\alpha|\sum_{a=1}^{3}\sigma_z^{(a)}\tau_3^{(a)}|\beta\rangle,$$

and in eqn (4.28), the constants $\lambda^{\alpha\beta}$ are defined by

$$\lambda^{\alpha\beta} = \mathcal{M}_{\alpha\beta}\left[C^{m_\beta 0 m_\alpha}_{S_\beta\ 1\ S_\alpha}\ C^{i_\beta\ 0\ i_\alpha}_{I_\beta\ 1\ I_\alpha}\right]^{-1}.$$

The constants $X^{\alpha\beta}$ and $\lambda^{\alpha\beta}$ are given in Tables 4.1 and 4.2.

$\alpha\backslash\beta$	N	Δ
N	$\frac{5}{3}$	$\frac{4\sqrt{2}}{3}$
Δ	$\frac{4\sqrt{2}}{3}$	$\frac{1}{3}$

Table 4.1: The symmetry factor $X^{\alpha\beta}$.

$\alpha\backslash\beta$	N	Δ
N	5	$4\sqrt{2}$
Δ	$2\sqrt{2}$	5

Table 4.2: The symmetry factor $\lambda^{\alpha\beta}$.

It is useful to introduce another constant $\lambda_1^{\alpha\beta}$. With the help of (4.28), the eqn (4.22) can be written as

$$\begin{aligned}
{}_{sf}\langle\alpha|\sum_{a=1}^{3}\boldsymbol{\sigma}^{(a)}\cdot\boldsymbol{q}\boldsymbol{\tau}^{(a)}|\beta\rangle_{sf} &= X^{\alpha\beta}\langle\alpha|\boldsymbol{S}\cdot\boldsymbol{q}\boldsymbol{T}|\beta\rangle \\
&= X^{\alpha\beta}\ \langle S_\alpha m_\alpha, I_\alpha i_\alpha|S_{1m}T_{1n}|S_\beta m_\beta, I_\beta i_\beta\rangle\ \hat{\boldsymbol{s}}^*_m\cdot\boldsymbol{q}\hat{\boldsymbol{t}}^*_n \\
&= \lambda^{\alpha\beta}C^{m_\beta\ m\ m_\alpha}_{S_\beta\ 1\ S_\alpha}\ C^{i_\beta\ n\ i_\alpha}_{I_\beta\ 1\ I_\alpha}\ \hat{\boldsymbol{s}}^*_m\cdot\boldsymbol{q}\ \hat{\boldsymbol{t}}^*_n \qquad (4.29) \\
&= \lambda_1^{\alpha\beta}C^{m_\beta\ m\ m_\alpha}_{S_\beta\ 1\ S_\alpha}\hat{\boldsymbol{s}}^*_m\cdot\boldsymbol{q}\ \langle I_\alpha i_\alpha|\boldsymbol{T}|I_\beta i_\beta\rangle \\
&= \lambda_1^{\alpha\beta}S_m^{\beta\alpha}\hat{\boldsymbol{s}}^*_m\cdot\boldsymbol{q}\langle I_\alpha i_\alpha|\boldsymbol{T}|I_\beta i_\beta\rangle \qquad (4.30)
\end{aligned}$$

The constants $\lambda_1^{\alpha\beta}$ differ from $\lambda^{\alpha\beta}$[Tho+83] as a consequence of how the matrix elements of the isospin operator are defined. This has certain advantages which we will explain in Section 4.3.3. Finally the symbol $S_m^{\beta\alpha}$ represents the Clebsch-Gordan coefficient $C^{m_\beta m m_\alpha}_{S_\beta\ 1\ S_\alpha}$.

We can now write (4.15) as

$$\hat{V}_j^{\alpha\beta}(\boldsymbol{q}) = -\frac{i}{(6f)}\frac{1}{\sqrt{2\omega_q}}\left(\frac{\Omega}{\Omega-1}\right) U(qR)\ \lambda_1^{\alpha\beta} S_m^{\beta\alpha}\hat{\boldsymbol{s}}_m^* \cdot \boldsymbol{q}\ \langle I_\alpha i_\alpha|T_j|I_\beta i_\beta\rangle \qquad (4.31)$$

The values of $\lambda_1^{\alpha\beta}$ are given in Table 4.3.

Table 4.3: The coupling constants $\lambda_1^{\alpha\beta}$

$\alpha\backslash\beta$	N	Δ
N	$\frac{5}{\sqrt{3}}$	$-4\sqrt{\frac{2}{3}}$
Δ	$\frac{4}{\sqrt{3}}$	$\sqrt{\frac{5}{3}}$

4.2.2 The Weinberg-Tomozawa Term

In the preceding section, we demonstrated how the process $B' \to B + \pi$ can be described in the CBM. In this section we will consider a more general process, i.e. $B + \pi \to B' + \pi'$. In Chapter 2 we have seen that the Weinberg- Tomozawa term gives the correct scattering length at threshold energy. In the following, we will discuss the Cloudy Bag Model version of the Weinberg-Tomozawa relation. We shall now derive the potential for Fig. 4.1a, i.e. the transition amplitude from the initial state

$$|i\ \rangle = |S_B m_B, I_B i_B; \boldsymbol{k}, i_M\rangle \qquad (4.32)$$

to the final state

$$|f\rangle = |S_{B'} m_{B'}, I_{B'} i_{B'}; \boldsymbol{k}', i_{M'}\rangle. \qquad (4.33)$$

This will be written as (we suppress spin-isospin indices):

$$v_a(\boldsymbol{k}', \boldsymbol{k}) \;=\; \langle i\,|H^t_{WT}(\boldsymbol{x})|f\rangle. \tag{4.34}$$

In eqn (4.34) the subscript a corresponds to Fig. 4.1a and H^t_{WT} the Hamiltonian for the time component of the Weinberg-Tomozawa interaction (4.8). In order to evaluate (4.34), we first determine the interaction matrix element

$$\hat{V}^{\alpha\beta}_a(\boldsymbol{k}', \boldsymbol{k}) = \langle \alpha; \boldsymbol{k}', i_{M'}|H^t_{WT}(\boldsymbol{x})|\beta; \boldsymbol{k}, i_M\rangle \tag{4.35}$$

The kets $|\alpha\rangle$ and $|\beta\rangle$ are non-exotic, baryonic SU(6) wave functions and $\alpha^\dagger\beta\hat{V}^{\alpha\beta}_a(\boldsymbol{k}', \boldsymbol{k})$ is an operator in real baryon space, i.e.

$$\langle f|H^t_{WT}(\boldsymbol{x})|i\rangle \;=\; \sum_{\alpha\beta}\langle S_{B'}m_{B'}, I_{B'}i_{B'}|\alpha^\dagger\beta\;\hat{V}^{\alpha\beta}_a(\boldsymbol{k}', \boldsymbol{k})|S_Bm_B, I_Bi_B\rangle, \tag{4.36}$$

where the operators $\alpha^\dagger$ (α) create (destroy) the real baryon. Now, the interaction matrix element,

$$\begin{aligned}\hat{V}^{\alpha\beta}_a(\boldsymbol{k}', \boldsymbol{k}) \;&=\; \langle \alpha; \boldsymbol{k}', i_{M'}|H^t_{WT}(\boldsymbol{x})|\beta; \boldsymbol{k}, i_M\rangle \\ &=\; \frac{\theta_v(x)}{(2f)^2}\,\frac{N_s^2}{(4\pi)}\,\frac{1}{(2\pi)^3}\,\frac{\omega_{\mathbf{k}'}+\omega_{\mathbf{k}}}{\sqrt{2\omega_{\mathbf{k}'}2\omega_{\mathbf{k}}}}\int d^3x\; e^{i\mathbf{k}\cdot\mathbf{x}}e^{-i\mathbf{k}'\cdot\mathbf{x}} \\ &\quad\; \rho_t(x)\;\;{}_{sf}\langle\alpha|\sum_{a=1}^{3}\boldsymbol{\tau}^{(a)}\cdot\boldsymbol{\theta}|\beta\rangle_{sf}\end{aligned} \tag{4.37}$$

In eqn (4.37), we write $\theta_i = -i\epsilon_{ii_{M'}i_M}$, the pion isospin matrix element and $\rho_t(x) = [j_0^2\left(\frac{\Omega x}{R}\right) + j_1^2\left(\frac{\Omega x}{R}\right)]$. Here the kets $|\alpha\rangle$ and $|\beta\rangle$ are the SU(6) wave functions in quark space which are combined to give the bag state. In order to project (4.37) onto nucleon space, we may write the spin-isospin part of eqn (4.37) as follows,

$$A^{\alpha\beta}\langle\alpha|\boldsymbol{T}\cdot\boldsymbol{\theta}|\beta\rangle = {}_{sf}\langle\alpha|\sum_{a=1}^{3}\boldsymbol{\tau}^{(a)}\cdot\boldsymbol{\theta}|\beta\rangle_{sf} \tag{4.38}$$

On the left hand side, the kets $|\alpha\rangle, |\beta\rangle$ are baryonic bag wave functions which have the same quantum numbers as the physical baryons. The isospin operator $\boldsymbol{T}$ operates on the baryonic wave function, therefore it is the same operator in nucleon space. On the right hand side the kets $|\alpha\rangle_{sf}, |\beta\rangle_{sf}$ are explicit spin-flavour wave functions of the quarks (see Appendix C). The operator $\boldsymbol{\tau}^{(a)}$ is the isospin operator for the a-th quark. In order to determine the symmetry factor in this case, we write the operators $\boldsymbol{T}, \boldsymbol{\tau}^{(a)}$ in spherical tensor notation

$$A^{\alpha\beta}\langle I_\alpha i_\alpha|T_{1m}|I_\beta i_\beta\rangle \hat{\boldsymbol{t}}^*_m \cdot \boldsymbol{\theta} = {}_{sf}\langle\alpha|\sum_{a=1}^{3}\tau^{(a)}_{1m}|\beta\rangle_{sf}\,\hat{\boldsymbol{t}}^*_m \cdot \boldsymbol{\theta} \tag{4.39}$$

By the Wigner-Eckart theorem we can rewrite the L.H.S. of (4.39) in terms of irreducible tensors and Clebsch-Gordan coefficients:

$$A^{\alpha\beta}\langle I_\alpha i_\alpha|T^{(1)}_m|I_\beta i_\beta\rangle = A^{\alpha\beta}\langle I_\alpha||\boldsymbol{T}^{(1)}||I_\beta\rangle \frac{C^{i_\beta\, m\, i_\alpha}_{I_\beta\, 1\, I_\alpha}}{\sqrt{2I_\alpha+1}} \tag{4.40}$$

Combining(4.39) and (4.40), for $m = 0$ we find:

$$\begin{aligned} A^{\alpha\beta} &= \frac{\sqrt{2I_\alpha+1}}{C^{i_\beta\, 0\, i_\alpha}_{I_\beta\, 1\, I_\alpha}}\,\frac{{}_{sf}\langle\alpha|\sum_{a=1}^{3}\tau_3^{(a)}|\beta\rangle_{sf}}{\langle I_\alpha||\boldsymbol{T}^{(1)}||I_\beta\rangle} \\ &= \frac{\sqrt{2I_\alpha+1}}{C^{i_\beta\, 0\, i_\alpha}_{I_\beta\, 1\, I_\alpha}}\,\frac{{}_{sf}\langle\alpha|\sum_{a=1}^{3}\tau_3^{(a)}|\beta\rangle_{sf}}{\langle I_\alpha||\boldsymbol{T}^{(1)}||I_\beta\rangle} \end{aligned} \tag{4.41}$$

Now we can write the interaction matrix element as,

$$\begin{aligned} \hat{V}_a^{\alpha\beta}(\boldsymbol{k}',\boldsymbol{k}) &= A^{\alpha\beta}\,\langle\alpha|\boldsymbol{\tau}\cdot\boldsymbol{\theta}|\beta\rangle \\ &= \sum_{II_3} C^{i_\alpha i_{M'} I_3}_{I_\alpha I_{M'} I}\; C^{i_\beta i_M I_3}_{I_\beta I_M I}\;\sum_{lm} Y^*_{lm}(\hat{k}')Y_{lm}(\hat{k}) \\ &\quad \frac{\lambda^{\alpha\beta,I}_{WT}}{8\pi^2 f^2}\,\frac{\omega_{\mathbf{k}}+\omega_{\mathbf{k}'}}{\sqrt{2\omega_{\mathbf{k}}2\omega_{\mathbf{k}'}}}N_s^2\int_0^R dx x^2\,[j_0^2(\frac{\Omega x}{R})+j_1^2(\frac{\Omega x}{R})]j_l(kx)\;j_l(k'x) \end{aligned} \tag{4.42}$$

In eqn (4.42), the constants $\lambda_{WT}^{\alpha\beta,I}$ are defined as

$$\lambda_{WT}^{\alpha\beta,I} = A^{\alpha\beta}\langle(I_\alpha I_{M'})I'I'_3|\boldsymbol{T}^{(1)}\cdot\boldsymbol{\theta}^{(1)}|(I_\beta I_M)II_3\rangle$$

where we use the notation of Edmonds [Edm 57] to describe the product of two tensor operator $\boldsymbol{T}^{(1)}$ and $\boldsymbol{\theta}^{(1)}$. The values of $\lambda_{WT}^{\alpha\beta,I}$ are given in Table 4.4.

Table 4.4: Coupling constants for WT term $\lambda_{WT}^{\alpha\beta,I}$

	$I=\frac{1}{2}$		$I=\frac{3}{2}$	
$\alpha\backslash\beta$	πN	$\pi\Delta$	πN	$\pi\Delta$
πN	-2	0	1	0
$\pi\Delta$	0	-5	0	-2

4.3 Higher order graphs

In the previous Section 4.2, much effort has been invested in order to explain how the pion-quark Hamiltonian can be projected onto pion-nucleon space. In this section, we will apply those techniques to higher order diagrams shown in Figs. 4.1c-h.

4.3.1 The Cross Box Interaction

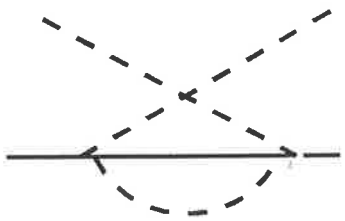

Figure 4.3: The cross box interaction

The interaction Hamiltonian for Fig. 4.3 is

$$H_c = H^t_{WT}(\boldsymbol{y})\ \frac{1}{E_i - H_0 + i\epsilon}\ H^t_{WT}(\boldsymbol{x}) \tag{4.43}$$

where $H^t_{WT}(\boldsymbol{x})$ is the time component of Weinberg-Tomozawa interaction (4.8) and the subscript c stands for Fig. 4.1c. We will first use the projection operator P to project the pion-quark Hamiltonian H_c onto pion-nucleon space by the now familiar procedure:

$$\begin{aligned} v_c(\boldsymbol{k}', \boldsymbol{k}) &= \langle f|PH_cP|i\rangle \\ &= \langle S_{B'}m_{B'}; I_{B'}i_{B'}|\alpha_3^\dagger\alpha_1 \hat{V}_c^{\alpha_3\alpha_1}(\boldsymbol{k}', \boldsymbol{k})|S_Bm_B; I_Bi_B\rangle. \end{aligned} \tag{4.44}$$

The interaction matrix element is

$$\begin{aligned} \hat{V}_c^{\alpha_3\alpha_1}(\boldsymbol{k}', \boldsymbol{k}) &= \langle \alpha_3; \boldsymbol{k}', i_{M'}|H_c|\alpha_1; \boldsymbol{k}, i_M\rangle \\ &= \int d^3x \int d^3y \langle \alpha_3|\rho_{i'}(\boldsymbol{y})\rho_i(\boldsymbol{x})|\alpha_1\rangle\ \epsilon_{i'j'k'}\epsilon_{ijk} \\ &\quad \langle \boldsymbol{k}', i_{M'}|\phi_{j'}(\boldsymbol{y})\Pi_{k'}(\boldsymbol{y})\frac{1}{E_i - H_0 + i\epsilon}\phi_j(\boldsymbol{x})\Pi_k(\boldsymbol{x})|\boldsymbol{k}, i_M\rangle, \end{aligned} \tag{4.45}$$

where ρ_i's are defined by

$$\begin{aligned} \rho_i(x) &= \frac{\theta_v(x)}{(2f)^2}\bar{q}(x)\gamma_0\tau_i q(x) \\ &= \frac{\theta_v}{(2f)^2}\ \frac{N_s^2}{(4\pi)}\rho_i(x)\sum_{a=1}^{3}\vartheta_a^\dagger\tau_i^{(a)}\vartheta_a. \end{aligned} \tag{4.46}$$

It is constructive to calculate the meson and baryon parts separately. The meson part gives

$$\epsilon_{i'j'k'}\epsilon_{ijk}\langle \boldsymbol{k}', i_{M'}|\phi_{j'}(\boldsymbol{y})\Pi_{k'}(\boldsymbol{y})\frac{1}{E_i - H_0 + i\epsilon}\phi_j(\boldsymbol{x})\Pi_k(\boldsymbol{x})|\boldsymbol{k}, i_M\rangle \tag{4.47}$$
$$= \epsilon_{i'ji_M}\epsilon_{iji_{M'}}\frac{1}{(2\pi)^6}\frac{e^{i(\mathbf{k}\cdot\mathbf{y}-\mathbf{k}'\cdot\mathbf{x})}}{\sqrt{2\omega_{\mathbf{k}}2\omega_{\mathbf{k}'}}}\int d^3q \frac{e^{i\mathbf{q}\cdot(\mathbf{y}-\mathbf{x})}}{2\omega_{\mathbf{q}}}\frac{[-\omega_{\mathbf{q}}\omega_{\mathbf{k}} + \omega_{\mathbf{q}}^2 + \omega_{\mathbf{k}}\omega_{\mathbf{k}'} - \omega_{\mathbf{k}'}\omega_{\mathbf{q}}]}{E_i - m_N - \omega_{\mathbf{k}'} - \omega_{\mathbf{k}} - \omega_{\mathbf{q}} + i\epsilon}$$

When calculating the baryon part, we will first project the quark operators $\rho_{i'}(\boldsymbol{y})$ and $\rho_i(\boldsymbol{x})$ onto baryonic bag states and then to the nucleon space as follows:

$$\sum_{\alpha_2\alpha_4}\sum_{N''}\alpha_3^\dagger\alpha_1\langle\alpha_3|\rho_{i'}(\boldsymbol{y})|\alpha_2\rangle\alpha_2|N''\rangle\langle N''|\alpha_4^\dagger\langle\alpha_4|\rho_i(\boldsymbol{x})|\alpha_1\rangle\epsilon_{i'ji_M}\epsilon_{iji_{M'}}$$
$$= \alpha_3^\dagger\alpha_1\langle I_{\alpha_3}i_{\alpha_3}; S_{\alpha_3}m_{\alpha_3}|2\delta_{i_{\alpha_1}i_{\alpha_3}}\delta_{i_Mi_{M'}} + i\,\epsilon_{ki_Mi_{M'}}\tau_k|I_{\alpha_1}i_{\alpha_1}; S_{\alpha_1}m_{\alpha_1}\rangle \tag{4.48}$$

where the kets $|N''\rangle$ represent the real baryon spin-isospin eigenstates. We also make use of the relations

$$\tau_{i'}\tau_i\epsilon_{i'ji_M}\epsilon_{iji_{M'}} = 2\delta_{i_M,i_{M'}} + i\epsilon_{ki_Mi_{M'}}\,\tau_k. \tag{4.49}$$

One may now expand the plane waves in (4.48) into spherical harmonics. For the S-wave interaction, we get:

$$v_c(\boldsymbol{k}', \boldsymbol{k}) = \frac{N_s^4}{64f^4\pi^4}\sum_I C^{i_{B'}i_{M'}I_3}_{I_{B'}I_{M'}I}\,C^{i_Bi_MI_3}_{I_BI_MI}\sum_{lm}Y_{lm}(\hat{k}')Y^*_{lm}(\hat{k})$$
$$\frac{[2\delta_{i_Bi_{B'}}\delta_{i_Mi_{M'}} + \lambda_{WT}^{B'B,I}]}{\sqrt{2\omega_{\mathbf{k}}2\omega_{\mathbf{k}'}}}\int_0^\infty dq\,\frac{q^2}{2\omega_{\mathbf{q}}}\frac{(-\omega_{\mathbf{q}}\omega_{\mathbf{k}} + \omega_{\mathbf{q}}^2 + \omega_{\mathbf{k}}\omega_{\mathbf{k}'} - \omega_{\mathbf{k}'}\omega_{\mathbf{q}})}{E_i - m_N - \omega_{\mathbf{k}'} - \omega_{\mathbf{k}} - \omega_{\mathbf{q}} + i\epsilon}$$
$$\int_0^R dx x^2\rho_t(x)j_0(qx)j_0(k'x)\int_0^R dy y^2\rho_t(y)j_0(qy)j_0(ky) \tag{4.50}$$

One problem which is encountered at high energy when we calculate diagrams to order $\frac{1}{(2f)^4}$ is that of numerical singularities. In fact the intermediate states in Figs. 4.3, 4.4, 4.5 and 4.6 contain more than one pion and should be solved as a 3-body problem. However, we are primarily interested in the low energy regime and

such 3-body problem is beyond the scope of present work. Therefore, in numerical calculations we made static approximation for the nucleon and took incoming and outgoing pions on-shell. Cooper and Jennings [CJ 86, Tho+87] also has to work within such an approximation.

4.3.2 Loop diagram

(a) (b)

Figure 4.4: Loop diagrams

The interaction Hamiltonian for Fig. 4.4 is,

$$H_d = H_{4\pi}(\boldsymbol{z})\frac{1}{E_i - H_0 + i\epsilon}H^t_{WT}(\boldsymbol{x}) + H^t_{WT}(\boldsymbol{x})\frac{1}{E_i - H_0 + i\epsilon}H_{4\pi}(\boldsymbol{z}) \qquad (4.51)$$

The projection onto the pion-nucleon space is carried out in the usual way. The interaction matrix element for Fig. 4.4b is

$$\begin{aligned}\hat{V}^{\alpha\beta}_{d(b)}(\boldsymbol{k}', \boldsymbol{k}) &= \langle \alpha; \boldsymbol{k}', i_{M'}| H^t_{WT}(\boldsymbol{x})\frac{1}{E_i - H_0 + i\epsilon}\, H_{4\pi}(\boldsymbol{z})|\beta; \boldsymbol{k}, i_M\rangle \\ &= \frac{4\theta_v}{(2f)^4}\frac{N_s^2}{(4\pi)}\int d^3x\ \rho_t(x)\ {}_{sf}\langle\alpha|\sum_{a=1}^{3}\tau_k^{(a)}|\beta\rangle_{sf}\ i\ \epsilon_{kij}\frac{e^{i(\mathbf{k}-\mathbf{k}')\cdot\mathbf{x}}}{\sqrt{2\omega_{\mathbf{k}}2\omega_{\mathbf{k}'}}} \\ &\frac{1}{4(2\pi)^6}\int d^3p\ \frac{1}{\omega_{\mathbf{p}}}\ \frac{\delta_{ii_{M'}}\delta_{ji_M}(k+k')\cdot p + \delta_{ii_M}\delta_{ji_{M'}}(k+k')\cdot(k-k'-p)}{E_i - E_N(\boldsymbol{k}') - \omega_{\mathbf{k}'} - \omega_{\mathbf{p}} - \omega_{\mathbf{k}-\mathbf{k}'-\mathbf{p}}}\end{aligned} \qquad (4.52)$$

where k, k' and p are four vectors. We will get the interaction matrix element for Fig. 4.4a by replacing $\boldsymbol{k}$ with $\boldsymbol{k}'$ and $\boldsymbol{k}'$ with $\boldsymbol{k}$ in (4.53). For the S-wave case, we

have

$$
\begin{aligned}
v_d(\boldsymbol{k}',\boldsymbol{k}) &= \sum_I C^{i_{B'} i_{M'} I_3}_{I_{B'} I_{M'} I} C^{i_B i_M I_3}_{I_B I_M I} \frac{\lambda^I}{(2f)^4} \frac{(4\pi) N_s^2}{\sqrt{2\omega_{\mathbf{k}} 2\omega_{\mathbf{k}'}}} \sum_{lm} Y_{lm}(\hat{k}') Y^*_{lm}(\hat{k}) \\
&\int_0^R dx x^2 \rho_s(x) j_0(k'x) j_0(kx)\, (2\pi)^{-6} \int d^3p\, e^{-p^2 R_\pi^2/4.0} \\
&\left[\frac{(\omega_{\mathbf{k}} + \omega_{\mathbf{k}'})(\omega_{\mathbf{p}} - \omega_{\mathbf{k}'-\mathbf{k}-\mathbf{p}} + 2(\boldsymbol{k}+\boldsymbol{k}')\cdot\boldsymbol{p} - (\boldsymbol{k}'^2 - \boldsymbol{k}^2))}{E_i - E_N(\boldsymbol{k}) - \omega_{\mathbf{k}} - \omega_{\mathbf{p}} - \omega_{\mathbf{k}'-\mathbf{k}-\mathbf{p}}} \right. \\
&\left. + \frac{(\omega_{\mathbf{k}'} + \omega_{\mathbf{k}})(\omega_{\mathbf{p}} - \omega_{\mathbf{k}-\mathbf{k}'-\mathbf{p}} + 2(\boldsymbol{k}+\boldsymbol{k}')\cdot\boldsymbol{p} - (\boldsymbol{k}^2 - \boldsymbol{k}'^2))}{E_i - E_N(\boldsymbol{k}') - \omega_{\mathbf{k}'} - \omega_{\mathbf{p}} - \omega_{\mathbf{k}-\mathbf{k}'-\mathbf{p}}} \right] \qquad (4.53)
\end{aligned}
$$

It should be noted that we treat the pion 4-point interaction as described in [Tho*86]. The exponential factor in (4.53) is the result of replacing the pion field operator $a_j(\boldsymbol{k})$ by $\tilde{a}_j(\boldsymbol{k}) e^{-k^2 R_\pi^2/12.}$ to take into account the internal structure of the pion [Tho*86]. To obtain the numerical value of the momentum integral we expand the function in terms of Legendre polynomials [see Section 4.3.4].

4.3.3 The Chiral Partner of the Sigma Diagram

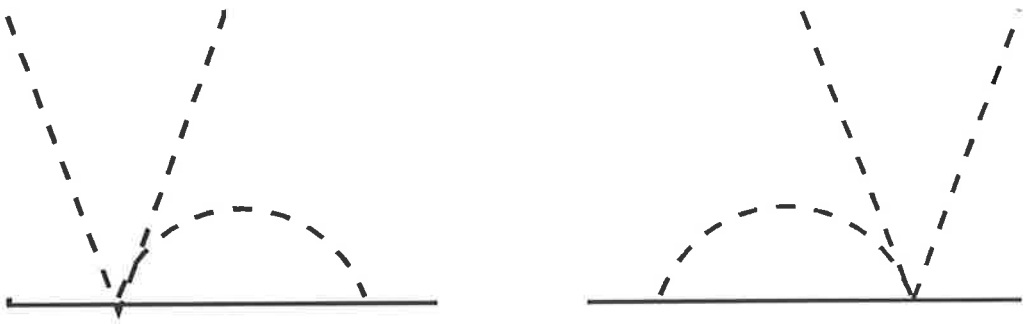

(a) (b)

Figure 4.5: The Chiral Partner of the Sigma diagram

The interaction Hamiltonian for Fig. 4.5 is

$$
H_e = H_3(\boldsymbol{y}) \frac{1}{E_i - H_0 + i\epsilon} H_1(\boldsymbol{x}) + H_1(\boldsymbol{x}) \frac{1}{E_i - H_0 + i\epsilon} H_3(\boldsymbol{y}) \qquad (4.54)
$$

We find the interaction matrix for Fig. 4.5a as follows:

$$\begin{aligned}\hat{V}_e^{\alpha_3\alpha_1}(\boldsymbol{k}',\boldsymbol{k}) &= \langle\alpha_3;\boldsymbol{k}',i_{M'}|H_3(\boldsymbol{y})\frac{1}{E_i-H_0+i\epsilon}H_1(\boldsymbol{x})|\alpha_1;\boldsymbol{k},i_M\rangle \qquad (4.55)\\ &= \frac{1}{(2f)^4}\frac{N_s^4}{(4\pi)^2}\int_0^R dx x^2\int_0^R dy y^2\int d\hat{x}\int d\hat{y}\,(2\pi)^{-3}\int d^3q_1\int d^3q\\ &\quad \sum_{\alpha_4\alpha_2}\sum_{N''}\langle\boldsymbol{k}',i'_M|\phi'_{i,q_1}(\boldsymbol{y})\,\boldsymbol{\phi}(\boldsymbol{y})\cdot\boldsymbol{\phi}(\boldsymbol{y})\boldsymbol{\Sigma}_i^{\alpha_3\alpha_4}\cdot\boldsymbol{q}_1\\ &\quad \frac{\alpha_4|N''\rangle\langle N''|\alpha_2^\dagger}{E_i-H_0-i\epsilon}\boldsymbol{\Sigma}_j^{\alpha_2\alpha_1}\cdot\boldsymbol{q}\,\phi'_{j,q}(\boldsymbol{x})|\boldsymbol{k},i_M\rangle\end{aligned}$$

where the $\boldsymbol{\Sigma}_j$'s are given by (4.17) and $\phi'_{j,q}(\boldsymbol{x})$ represents

$$\phi'_{j,q}(\boldsymbol{x})=\frac{1}{\sqrt{2\omega_{\mathbf{q}}}}(a_j(\boldsymbol{q})e^{i\mathbf{q}\cdot\mathbf{x}}-a_j^\dagger(\boldsymbol{q})e^{-i\mathbf{q}\cdot\mathbf{x}}),$$

etc. Now, as we compute the expectation value between initial and final meson states and do the integration over momentum, (4.55) becomes,

$$\begin{aligned}\hat{V}_e^{\alpha_3\alpha_1} &= -\frac{1}{(2f)^4}\frac{N_s^4}{(4\pi)^2}\frac{(2\pi)^{-6}}{\sqrt{2\omega_{\mathbf{k}}2\omega_{\mathbf{k}'}}}\int_0^R dx x^2\int_0^R dy y^2\\ &\quad \int d\hat{x}\int d\hat{y}\int d^3q\frac{1}{\omega_{\mathbf{q}}}\frac{e^{i\mathbf{q}\cdot(\mathbf{y}-\mathbf{x})}e^{i(\mathbf{k}-\mathbf{k}')\cdot\mathbf{y}}}{(E_i-m_N-\omega_{\mathbf{q}}-\omega_{\mathbf{k}}+i\epsilon)}\\ &\quad \sum_{\alpha_4\alpha_2}\sum_{N''}\delta_{\alpha_4,N''}\delta_{\alpha_2,N''}\Big\{\delta_{ji_{M'}}\delta_{ii_M}\boldsymbol{\Sigma}_i^{\alpha_3\alpha_4}\cdot\boldsymbol{k}\,\boldsymbol{\Sigma}_j^{\alpha_2\alpha_1}\cdot\boldsymbol{q} \qquad (4.56)\\ &\quad +\delta_{ij}\delta_{i_M,i_{M'}}\boldsymbol{\Sigma}_i^{\alpha_3\alpha_4}\cdot\boldsymbol{q}\,\boldsymbol{\Sigma}_j^{\alpha_2\alpha_1}\cdot\boldsymbol{q}-\delta_{ii_{M'}}\delta_{ji_M}\boldsymbol{\Sigma}_i^{\alpha_3\alpha_4}\cdot\boldsymbol{k}'\,\boldsymbol{\Sigma}_j^{\alpha_2\alpha_1}\cdot\boldsymbol{q}\Big\}\end{aligned}$$

It can be seen from (4.56) that the second term in the braces gives a purely isoscalar interaction. Let us now consider the term

$$\int d\hat{x}\int d\hat{y}\int d\hat{q}\;e^{i\mathbf{q}\cdot(\mathbf{x}-\mathbf{y})}e^{i(\mathbf{k}-\mathbf{k}')\cdot\mathbf{y}}\boldsymbol{\Sigma}_i^{\alpha_3\alpha_4}\cdot\boldsymbol{q}\boldsymbol{\Sigma}_j^{\alpha_2\alpha_1}\cdot\boldsymbol{q} \qquad (4.57)$$

First, expand $e^{i(\mathbf{k}-\mathbf{k}')\cdot\mathbf{y}}$ in spherical harmonics and set the angular momentum of the incoming and outgoing mesons to be 0. Equation (4.57) becomes

$$(4\pi)\, Y_{00}(\hat{k}')Y_{00}^{*}(\hat{k}) \int d\hat{x} \int d\hat{y} \int d\hat{q}\; e^{i\mathbf{q}\cdot(\mathbf{x}-\mathbf{y})} j_0(ky) j_0(k'y) \boldsymbol{\Sigma}_i^{\alpha_3\alpha_4} \cdot \boldsymbol{q} \boldsymbol{\Sigma}_j^{\alpha_2\alpha_1} \cdot \boldsymbol{q} \quad (4.58)$$

Since [see Section 4.2, equations (4.15)- (4.21) for comparison]

$$\begin{aligned} \int d\hat{x} \boldsymbol{\Sigma}_j^{\alpha_2\alpha_1} \cdot \boldsymbol{q} e^{-i\mathbf{q}\cdot\mathbf{x}} &= (4\pi)\rho_{pv}(qx)\; {}_{sf}\langle\alpha_2| \sum_{a=1}^{3} \boldsymbol{\sigma}^{(a)} \cdot \boldsymbol{q} \tau_j^{(a)} |\alpha_1\rangle_{sf} \\ &= (4\pi)\rho_{pv}(qx) \lambda_1^{\alpha_2\alpha_1}\; S_m^{\alpha_1\alpha_2} \hat{\boldsymbol{s}}_m^{*} \cdot \boldsymbol{q} \langle I_{\alpha_2} i_{\alpha_2} | \tau_j | I_{\alpha_1} i_{\alpha_1} \rangle, \quad (4.59) \end{aligned}$$

equation (4.58) becomes

$$\begin{aligned} &\frac{(4\pi)^4}{3} Y_{00}(\hat{k}')Y_{00}^{*}(\hat{k}) |\boldsymbol{q}|^2 \rho_{pv}(qx)\rho_{pv}(qy) j_0(ky) j_0(k'y) S_m^{\alpha_4\alpha_3} S_{m'}^{\alpha_1\alpha_2} (-)^{m'} \delta_{m,-m'} \\ &\lambda_1^{\alpha_3\alpha_4}\; \lambda_1^{\alpha_2\alpha_1}\; \langle I_{\alpha_3} i_{\alpha_3} | \tau_i | I_{\alpha_4} i_{\alpha_4} \rangle \langle I_{\alpha_2} i_{\alpha_2} | \tau_j | I_{\alpha_1} i_{\alpha_1} \rangle \delta_{ij} \delta_{i_M i_{M'}}. \quad (4.60) \end{aligned}$$

With the help of (4.60), we can now carry out the sum over α_2, α_4 in (4.56), and since N'' forms complete set of isospin states, we get

$$\begin{aligned} \sum_{\alpha_4\alpha_2} \sum_{N''} &\langle I_{\alpha_3} i_{\alpha_3} | \tau_i | I_{\alpha_4} i_{\alpha_4} \rangle \langle I_{\alpha_2} i_{\alpha_2} | \tau_j | I_{\alpha_1} i_{\alpha_1} \rangle \delta_{ij} \delta_{i_M i_{M'}} \delta_{\alpha_4, N''} \delta_{\alpha_2, N''} \\ &= \langle I_{\alpha_3} i_{\alpha_3} | \tau_i \tau_j \delta_{ij} | I_{\alpha_1} i_{\alpha_1} \rangle \delta_{i_M, i_{M'}} \\ &= 3\;\; \delta_{I_{\alpha_1} I_{\alpha_3}} \delta_{i_{\alpha_1} i_{\alpha_3}} \delta_{i_M i_{M'}}. \quad (4.61) \end{aligned}$$

Our comment after (4.30) that the advantage of writing the isospin matrix as defined in (4.30) can now be justified. When we calculate the higher order interaction matrix elements between bag and pion states, the intermediate states involved are those of baryons. In order to transform the quark spin and isospin operators into those of baryons, it is necessary to use the spherical representation. However, we have transformed the nucleon isospin operators into the orthogonal basis as in (4.30) so

that the pion field operators have simple commutation relations.

For S-wave, the potential for Fig. 4.5a-b becomes,

$$\begin{aligned} v_e(\boldsymbol{k}',\boldsymbol{k}) &= -\frac{N_s^4}{64f^4\pi^4}\frac{\lambda_1^{\alpha_3\alpha_2}\lambda_1^{\alpha_2\alpha_1}}{\sqrt{2\omega_{\mathbf{k}}2\omega_{\mathbf{k}'}}}Y_{00}(\hat{k}')Y_{00}^*(\hat{k})(-)^{S_{\alpha_2}+S_{\alpha_1}+1}\frac{\hat{S}_{\alpha_2}}{\hat{S}_{\alpha_1}}\delta_{i_M i_{M'}} \\ &\times\int_0^\infty dq\frac{q^4}{\omega_{\mathbf{q}}}\int_0^R dx x^2\int_0^R dy y^2\rho_{pv}(qx)\rho_{pv}(qy)j_0(kx)j_0(k'x) \\ &\times\left[\frac{1}{E_i-m_{\alpha_2}-\omega_{\mathbf{q}}-\omega_{\mathbf{k}}+i\epsilon}+\frac{1}{E_i-m_{\alpha_2}-\omega_{\mathbf{q}}-\omega_{\mathbf{k}'}+i\epsilon}\right] \end{aligned} \tag{4.62}$$

4.3.4 Sigma like diagrams

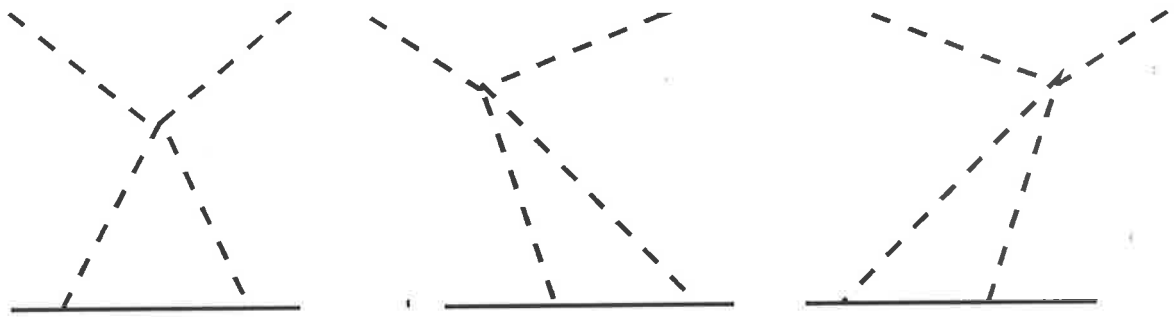

Figure 4.6: Sigma like diagrams

We can write down the interaction Hamiltonian for diagrams shown in Figs. 4.6a,b and c as follows:

$$\begin{aligned} H_{f(a)} &= H_1(\boldsymbol{y})\frac{1}{E_i-H_0+i\epsilon}H_{4\pi}(\boldsymbol{z})\frac{1}{E_i-H_0+i\epsilon}H_1(\boldsymbol{x}) \\ H_{f(b)} &= H_{4\pi}(\boldsymbol{z})\frac{1}{E_i-H_0+i\epsilon}H_1(\boldsymbol{y})\frac{1}{E_i-H_0+i\epsilon}H_1(\boldsymbol{x}) \\ H_{f(c)} &= H_1(\boldsymbol{y})\frac{1}{E_i-H_0+i\epsilon}H_1(\boldsymbol{x})\frac{1}{E_i-H_0+i\epsilon}H_{4\pi}(\boldsymbol{z}) \end{aligned} \tag{4.63}$$

Diagrams shown in Figs. 4.6a,b and c are different by the ordering of the 4-pion interaction vertex $H_{4\pi}$. We can find the interaction matrix element for Fig. 4.6a as

follows

$$\hat{V}^{\alpha_4\alpha_1}_{f(a)}(\boldsymbol{k}',\boldsymbol{k}) = \langle \alpha_4;\boldsymbol{k}',i_{M'}|H_1(\boldsymbol{y})\frac{1}{E_i-H_0+i\epsilon}H_{4\pi}(\boldsymbol{z})\frac{1}{E_i-H_0+i\epsilon}H_1(\boldsymbol{x})|\alpha_1;\boldsymbol{k},i_M\rangle \quad (4.64)$$

First we find the relevant part of the 4-pion interaction for Fig. 4.6a (which we denote by $\mathcal{Z}$)

$$\begin{aligned}\mathcal{Z} \;=\; & (2\pi)^{-3}\int d^3q_1 d^3q_2 d^3q_3 d^3q_4\;\left[2\omega_{\mathbf{q}_1}2\omega_{\mathbf{q}_2}2\omega_{\mathbf{q}_3}2\omega_{\mathbf{q}_4}\right]^{-\frac{1}{2}} \\ & \Big\{4\,\delta^3(\boldsymbol{q}_1-\boldsymbol{q}_2+\boldsymbol{q}_3-\boldsymbol{q}_4)\left(q_1\cdot q_2-m_\pi^2\right)\boldsymbol{a}(\boldsymbol{q}_1)\cdot\boldsymbol{a}^\dagger(\boldsymbol{q}_2)\;\boldsymbol{a}(\boldsymbol{q}_3)\cdot\boldsymbol{a}^\dagger(\boldsymbol{q}_4) \\ & +\delta^3(\boldsymbol{q}_1+\boldsymbol{q}_2-\boldsymbol{q}_3-\boldsymbol{q}_4)\left(-q_1\cdot q_2-m_\pi^2\right)\Big(\boldsymbol{a}^\dagger(\boldsymbol{q}_1)\cdot\boldsymbol{a}^\dagger(\boldsymbol{q}_2)\;\boldsymbol{a}(\boldsymbol{q}_3)\cdot\boldsymbol{a}(\boldsymbol{q}_4) \\ & +\boldsymbol{a}(\boldsymbol{q}_1)\cdot\boldsymbol{a}(\boldsymbol{q}_2)\;\boldsymbol{a}^\dagger(\boldsymbol{q}_3)\cdot\boldsymbol{a}^\dagger(\boldsymbol{q}_4)\Big)\Big\} \qquad (4.65)\end{aligned}$$

Now, the interaction matrix element (4.64) becomes

$$\begin{aligned}\hat{V}^{\alpha_4\alpha_1}_{f(a)}(\boldsymbol{k}',\boldsymbol{k}) \;=\; & \frac{(2\pi)^{-3}}{(2f)^2}\,\frac{N_s^4}{(4\pi)^2}\int_0^R dy y^2\int_0^R dx x^2\int d^3q\int d^3q' \\ & \sum_{\alpha_3\alpha_2}\sum_C\langle \boldsymbol{k}',i_{M'}|\int d\hat{y}\,\boldsymbol{\Sigma}_i^{\alpha_4\alpha_3}\cdot\boldsymbol{q}\;\phi'_{i,q}(\boldsymbol{y})\frac{\alpha_3|C\rangle}{E_i-H_0+i\epsilon}\mathcal{Z}\frac{\langle C|\alpha_2^\dagger}{E_i-H_0+i\epsilon} \\ & \int d\hat{x}\,\boldsymbol{\Sigma}_j^{\alpha_2\alpha_1}\cdot\boldsymbol{q}'\phi'_{j,q'}(\boldsymbol{x})|\boldsymbol{k},i_M\rangle \qquad (4.66)\end{aligned}$$

In (4.66) the intermediate state $|C\rangle$ can either be a nucleon or Δ. One can now compute the expectation value between pion eigenstates and perform the momentum integration so that we have;

$$\begin{aligned}\hat{V}^{\alpha_4\alpha_1}_{f(a)}(\boldsymbol{k}',\boldsymbol{k}) \;=\; & \frac{(2\pi)^{-6}}{(2f)^4}\,\frac{N_s^4}{(4\pi)^2}\,\frac{1}{\sqrt{2\omega_{\mathbf{k}}2\omega_{\mathbf{k}'}}}\int d\hat{x}\int d\hat{y}\sum_{\alpha_2,C}\delta_{\alpha_2,C} \qquad (4.67) \\ & \int d^3q\frac{1}{\omega_{\mathbf{q}}}\boldsymbol{\Sigma}_i^{\alpha_4\alpha_2}\cdot\boldsymbol{q}\,\boldsymbol{\Sigma}_j^{\alpha_2\alpha_1}\cdot(\boldsymbol{q}+\boldsymbol{k}'-\boldsymbol{k})\frac{e^{i\mathbf{q}\cdot(\mathbf{x}-\mathbf{y})}\;e^{-i(\mathbf{k}'-\mathbf{k})\cdot\mathbf{y}}}{(E_i-m_N-\omega_{\mathbf{k}'}-\omega_{\mathbf{q}})}\;F_{(a)\alpha}(q,k',k)\end{aligned}$$

Here, $F_{(a)\alpha}(q,k',k)$ represents

$$\begin{aligned} F_{(a)\alpha}(q,k',k) &= F_{(a)ij,i_M i_{M'}}(q,k',k) \\ &= \Big[(-k\cdot q' - k'\cdot q - m_\pi^2)\delta_{i,i_{M'}}\delta_{j,i_M} \\ &\quad + (q'\cdot k' + q\cdot k - m_\pi^2)\delta_{i,i_M}\delta_{j,i_{M'}} \\ &\quad + (q'\cdot q + k'\cdot k - m_\pi^2)\delta_{i_M,i_{M'}}\delta_{i,j}\Big] \\ &\quad \Big[\omega_{\mathbf{q+k'-k}}(E_i - m_N - \omega_{\mathbf{k}} - \omega_{\mathbf{q+k'-k}})\Big]^{-1} \end{aligned} \tag{4.68}$$

From the definition of $F_{(a)ij,i_M i_{M'}}(q,k',k)$, we can see that it is dependent on $\boldsymbol{q}, \boldsymbol{k'}$ and $\boldsymbol{k}$. Although it is possible to obtain an exact analytic expression for (4.68) at threshold for numerical computation, it is not possible for higher scattering energies. We therefore resort to some approximation methods. Since we noted that the function $F_{(a)ij,i_M i_{M'}}(q,k',k)$ depends on the magnitudes of the three momenta $|\boldsymbol{q}|, |\boldsymbol{k'}|, |\boldsymbol{k}|$ and the rotational invariant functions,z_1, z_2,where

$$\begin{aligned} z_1 &= \cos\theta_{\hat{q},\widehat{k-k'}} \\ z_2 &= \cos\theta_{\hat{k},\hat{k'}} \end{aligned}$$

We expand the function $F_{(a)ij,i_M i_{M'}}(q,k',k)$ in Legendre polynomials as follows

$$\begin{aligned} F_{(a)\alpha}(q,k',k) &= F_{(a)ij,i_M i_{M'}}(q,k',k) \\ &= \sum_{l,l'=0}^{\infty}(2l+1)(2l'+1)F_{(a)\alpha,ll'}(q,k',k)P_l(z_1)P_{l'}(z_2) \\ &= F_{(a)\alpha,00}(q,k',k)P_0(z_1)P_0(z_2) + 3F_{(a)\alpha,01}(q,k',k)P_0(z_1)P_1(z_2) \\ &\quad + 3F_{(a)\alpha,10}(q,k',k)P_1(z_1)P_0(z_2) + 9F_{(a)\alpha,11}P_1(z_1)P_1(z_2) + \end{aligned} \tag{4.69}$$

It is found that the first coefficient $F_{(a)\alpha,00}$ has the largest magnitude and the contribution from $F_{(a)\alpha,01}$ or $F_{(a)\alpha,10}$ are 10 times smaller. Therefore we approximate

$F_{(a)\alpha}(q,k',k)$ as

$$\begin{aligned} F_{(a)\alpha}(q,k',k) &\approx F_{(a)\alpha,00}(q,k',k) \\ &= \frac{1}{4}\int_{-1}^{+1} dz_1 \int_{-1}^{+1} dz_2\, F_{(a)\alpha}(q,k',k). \end{aligned} \tag{4.70}$$

Now the interaction matrix element (4.68) becomes

$$\begin{aligned} \hat{V}^{\alpha_4\alpha_1}_{f(a)}(\boldsymbol{k}',\boldsymbol{k}) &= (2\pi)^{-6}\frac{1}{(2f)^4}\frac{N_s^4}{(4\pi)^2}\frac{1}{\sqrt{2\omega_{\mathbf{k}}2\omega_{\mathbf{k}'}}}\int d\hat{x}\int d\hat{y}\int d^3q\frac{1}{\omega_{\mathbf{q}}} \\ &\boldsymbol{\Sigma}_i^{\alpha_4 C}\cdot\boldsymbol{q}\;\boldsymbol{\Sigma}_j^{C\alpha_1}\cdot(\boldsymbol{q}+\boldsymbol{k}'-\boldsymbol{k})e^{i\mathbf{q}\cdot(\mathbf{x}-\mathbf{y})}\;e^{-i(\mathbf{k}'-\mathbf{k})\cdot\mathbf{y}}\frac{F_{(a)\alpha,00}(q,k',k)}{(E_i-m_N-\omega_{\mathbf{k}'}-\omega_{\mathbf{q}})} \end{aligned} \tag{4.71}$$

One may now expand the exponential $e^{-i(\mathbf{k}'-\mathbf{k})\cdot\mathbf{y}}$ as usual. In S-wave we therefore find from (4.71),

$$\begin{aligned} &\int d\hat{x}\int d\hat{y}\int d\hat{q}\;\boldsymbol{\Sigma}_i^{\alpha_4 C}\cdot\boldsymbol{q}\;\boldsymbol{\Sigma}_j^{C\alpha_1}\cdot(\boldsymbol{q}+\boldsymbol{k}'-\boldsymbol{k})e^{i\mathbf{q}\cdot(\mathbf{x}-\mathbf{y})}\;e^{-i(\mathbf{k}'-\mathbf{k})\cdot\mathbf{y}}F_{(a)\alpha,00}(q,k',k) \\ = \;&(4\pi)Y_{00}(\hat{k}')Y^*_{00}(\hat{k})j_0(ky)j_0(k'y)\int d\hat{q}\int d\hat{y}\boldsymbol{\Sigma}_i^{\alpha_4 C}\cdot\boldsymbol{q}e^{-i\mathbf{q}\cdot\mathbf{y}} \\ &\int d\hat{x}\boldsymbol{\Sigma}_j^{C\alpha_1}\cdot(\boldsymbol{q}+\boldsymbol{k}'-\boldsymbol{k})e^{i\mathbf{q}\cdot\mathbf{x}}\;F_{(a)\alpha,00}(q,k',k) \end{aligned} \tag{4.72}$$

One may now proceed in a similar procedure as outlined from (4.58) to (4.60). Equation (4.72) becomes,

$$\begin{aligned} &\frac{(4\pi)^4}{3}Y_{00}(\hat{k}')Y^*_{00}(\hat{k})|\boldsymbol{q}|^2\rho_{pv}(qx)\rho_{pv}(qy)j_0(ky)j_0(k'y)S_m^{C\alpha_4}\;S_{m'}^{\alpha_1 C}(-)^{m'}\delta_{-m',m} \\ &\lambda_1^{\alpha_4 C}\lambda_1^{C\alpha_1}\langle I_{\alpha_4}i_{\alpha_4}|\tau_i|C\rangle\langle C|\tau_j|I_{\alpha_1}i_{\alpha_1}\rangle\;F_{(a)\alpha,00}(q,k',k). \end{aligned} \tag{4.73}$$

Since the states $|C\rangle$ form a complete set of isospin states, we have

$$
\begin{aligned}
&\langle I_{\alpha_4} i_{\alpha_4}|\tau_i\tau_j|I_{\alpha_1} i_{\alpha_1}\rangle F_{(a)\alpha,00}(q,k',k) \\
&= \frac{1}{4}\int_{-1}^{+1} dz_1 \int_{-1}^{+1} dz_2 \langle I_{\alpha_4} i_{\alpha_4}|\delta_{ij} + i\epsilon_{ijk}\tau_k|I_{\alpha_1} i_{\alpha_1}\rangle \; F_{(a)ij,i_M i_{M'}}(q,k',k) \\
&= \frac{1}{4}\int_{-1}^{+1} dz_1 \int_{-1}^{+1} dz_2 \Big\{\langle I_{\alpha_4} i_{\alpha_4}|\delta_{i_M,i_{M'}}|I_{\alpha_1} i_{\alpha_1}\rangle \; F_{(a)s}(q,k',k) \\
&\qquad\qquad + \langle I_{\alpha_4} i_{\alpha_4}|i\epsilon_{ki_{M'}i_M}\tau_k|I_{\alpha_1} i_{\alpha_1}\rangle F_{(a)v}(q,k',k)\Big\} \\
&= \delta_{i_M,i_{M'}}\delta_{I_{\alpha_4},I_{\alpha_1}}\delta_{i_{\alpha_4},i_{\alpha_1}} \; F_{(a)s,00} - C^{i_{\alpha_4} i_{M'} I_3}_{I_{\alpha_4} I_{M'} I} \; C^{i_{\alpha_1} i_M I_3}_{I_{\alpha_1} I_M I} \; \lambda^I F_{(a)v,00} \qquad (4.74)
\end{aligned}
$$

where the isoscalar and isovector contributions $F_{(a)s}$ and $F_{(a)v}$ are given by

$$
\begin{aligned}
F_{(a)s}(q,k',k) &= -\Big\{10m_\pi^2 + \omega_{\mathbf{k}'}\omega_{\mathbf{q}} - \omega_{\mathbf{q}}\omega_{\mathbf{k}} - 3\omega_{\mathbf{k}'}\omega_{\mathbf{k}} + \boldsymbol{k}\cdot\boldsymbol{k}' + |\boldsymbol{k}|^2 + |\boldsymbol{k}'|^2 \\
&\quad +3|\boldsymbol{q}|^2 + 3\boldsymbol{q}\cdot(\boldsymbol{k}'-\boldsymbol{k}) - \omega_{\mathbf{q}+\mathbf{k}'-\mathbf{k}}(-\omega_{\mathbf{k}} + \omega_{\mathbf{k}'} + 3\omega_{\mathbf{q}})\Big\} \\
&\quad \Big[\omega_{\mathbf{q}+\mathbf{k}'-\mathbf{k}}(E_i - m_C - \omega_{\mathbf{k}} - \omega_{\mathbf{q}+\mathbf{k}'-\mathbf{k}})\Big]^{-1} \qquad (4.75) \\
F_{(a)v}(q,k',k) &= -\Big\{\omega_{\mathbf{k}'}\omega_{\mathbf{q}} + \omega_{\mathbf{q}}\omega_{\mathbf{k}} - 2\boldsymbol{k}'\cdot\boldsymbol{q} - 2\boldsymbol{k}\cdot\boldsymbol{q} + |\boldsymbol{k}|^2 - |\boldsymbol{k}'|^2 \qquad (4.76) \\
&\quad +\omega_{\mathbf{q}+\mathbf{k}'-\mathbf{k}}(\omega_{\mathbf{k}} + \omega_{\mathbf{k}'})\Big\}\Big[\omega_{\mathbf{q}+\mathbf{k}'-\mathbf{k}}(E_i - m_C - \omega_{\mathbf{k}} - \omega_{\mathbf{q}+\mathbf{k}'-\mathbf{k}})\Big]^{-1}
\end{aligned}
$$

After putting everything together finally we get for the S-wave interaction

$$
\begin{aligned}
v_{f(a)}(\boldsymbol{k}',\boldsymbol{k}) &= \frac{1}{(2f)^4}\frac{N_s^4}{(4\pi)^2}\frac{\lambda_1^{\alpha_3 C}\lambda_1^{C\alpha_1}}{2\sqrt{\omega_{\mathbf{k}}\omega_{\mathbf{k}'}}}\frac{(4\pi)^4}{3}\frac{\hat{S}_C}{\hat{S}_{\alpha_1}}(-)^{1+S_C+S_{\alpha_1}}(2\pi)^{-6}Y_{00}(\hat{k}')Y_{00}^*(\hat{k}) \qquad (4.77) \\
&\int_0^\infty dq\frac{q^4}{\omega_{\mathbf{q}}}\frac{e^{-R_\pi^2 q^2/6.}}{(E_i - m_C - \omega_{\mathbf{k}'} - \omega_{\mathbf{q}})}\int_0^R dx x^2\int_0^R dy y^2\rho_{pv}(qx)\rho_{pv}(qy)j_0(k'y)j_0(ky) \\
&[\langle I_{\alpha_3} i_{\alpha_3}|\delta_{i_{M'}i_M}|I_{\alpha_1} i_{\alpha_1}\rangle F_{(a)s,00}(q,k',k) + \langle I_{\alpha_3} i_{\alpha_3}|i\epsilon_{ijk}\tau_k|I_{\alpha_1} i_{\alpha_1}\rangle\delta_{i,i_{M'}}\delta_{j,i_M}F_{(a)v,00}(q,k',k)]
\end{aligned}
$$

Similarly for Fig. 4.6b we have,

$$
\begin{aligned}
v_{f(b)}(\boldsymbol{k}',\boldsymbol{k}) &= \frac{1}{(2f)^4}\frac{N_s^4}{(4\pi)^2}\frac{\lambda_1^{\alpha_3 C}\lambda_1^{C\alpha_1}}{2\sqrt{\omega_{\mathbf{k}}\omega_{\mathbf{k}'}}}\frac{(4\pi)^4}{3}\frac{\hat{S}_C}{\hat{S}_{\alpha_1}}(-)^{1+S_C+S_{\alpha_1}}(2\pi)^{-6}Y_{00}(\hat{k}')Y_{00}^*(\hat{k}) \\
&\quad \int_0^\infty dq\frac{q^4}{\omega_{\mathbf{q}}}\, e^{-R_\pi^2 q^2/4}\int_0^R dx x^2\int_0^R dy y^2\rho_{pv}(qx)\rho_{pv}(qy)j_0(k'x)j_0(kx) \\
&\quad [\langle I_{\alpha_3}i_{\alpha_3}|\delta_{i_{M'}i_M}|I_{\alpha_1}i_{\alpha_1}\rangle F_{(b)s,00} + \langle I_{\alpha_3}i_{\alpha_3}|i\epsilon_{i_{M'}i_M k}\tau_k|I_{\alpha_1}i_{\alpha_1}\rangle\, F_{(b)v,00}] \qquad (4.78)
\end{aligned}
$$

Where $F_{(b),s}$ and $F_{(b)v}$ are given by

$$
\begin{aligned}
F_{(b)s} &= \{-\omega_{\mathbf{k}}\omega_{\mathbf{q}'} + \omega_{\mathbf{q}}\omega_{\mathbf{k}'} - \omega_{\mathbf{k}}\omega_{\mathbf{q}} + \omega_{\mathbf{q}'}\omega_{\mathbf{k}'} - 3\omega_{\mathbf{q}}\omega_{\mathbf{q}'} + 3\omega_{\mathbf{k}}\omega_{\mathbf{k}'} \\
&\quad -10m_\pi^2 - |\boldsymbol{k}|^2 - |\boldsymbol{k}'|^2 - \boldsymbol{k}\cdot\boldsymbol{k}' + 3\boldsymbol{q}\cdot(\boldsymbol{k}'-\boldsymbol{k}) - 3\boldsymbol{q}^2\} \\
&\quad [\omega_{\mathbf{k}'-\mathbf{k}-\mathbf{q}}(E_i - m_C - \omega_{\mathbf{q}} - \omega_{\mathbf{k}'-\mathbf{k}-\mathbf{q}} - \omega_{\mathbf{k}})(E_i - m_C - \omega_{\mathbf{k}'-\mathbf{k}-\mathbf{q}} - \omega_{\mathbf{k}})]^{-1} \\
F_{(b)v} &= \{-\omega_{\mathbf{k}}\omega_{\mathbf{q}'} + \omega_{\mathbf{q}}\omega_{\mathbf{k}'} + \omega_{\mathbf{k}}\omega_{\mathbf{q}} - \omega_{\mathbf{q}'}\omega_{\mathbf{k}'} - |\boldsymbol{k}|^2 + |\boldsymbol{k}'|^2 - 2\boldsymbol{q}\cdot(\boldsymbol{k}'+\boldsymbol{k})\} \\
&\quad [\omega_{\mathbf{k}'-\mathbf{k}-\mathbf{q}}(E_i - m_C - \omega_{\mathbf{q}} - \omega_{\mathbf{k}'-\mathbf{k}-\mathbf{q}} - \omega_{\mathbf{k}})(E_i - m_C - \omega_{\mathbf{k}'-\mathbf{k}-\mathbf{q}} - \omega_{\mathbf{k}})]^{-1}
\end{aligned}
$$

4.3.5 The Contact Interaction

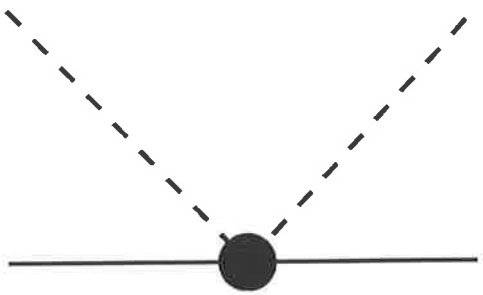

Figure 4.7: Contact interaction

The interaction Hamiltonian for this diagram can be written as

$$
H_g(\boldsymbol{x}) = \frac{1}{2}\theta_v\int d^3x\left[\bar{q}\gamma_0\left(\frac{\gamma_5\boldsymbol{\tau}}{(2f)} - \frac{\boldsymbol{\tau}\times\boldsymbol{\phi}}{(2f)^2}\right)q\right]^2 \qquad (4.79)
$$

The interaction matrix element for this is

$$\begin{aligned}\hat{V}_g^{\alpha\beta}(\boldsymbol{k}',\boldsymbol{k}) &= \langle\alpha;\boldsymbol{k}',i_{M'}|H_g(\boldsymbol{x})|\beta;\boldsymbol{k},i_M\rangle \\ &= \frac{\theta_v}{(2f)^4}\frac{N_s^4}{(4\pi)^2}\frac{1}{(2\pi)^3}\int d^3x\rho_t^2(x)\frac{e^{i(\mathbf{k}-\mathbf{k}')\cdot\mathbf{x}}}{\sqrt{2\omega_{\mathbf{k}}2\omega_{\mathbf{k}'}}} \\ &\quad {}_{sf}\langle\alpha|\sum_{a=1}^{3}\tau_i^{(a)}\tau_j^{(a)}|\beta\rangle_{sf}(\epsilon_{kii_M}\epsilon_{kji_{M'}}+\epsilon_{kji_{M'}}\epsilon_{kii_M})\end{aligned} \tag{4.80}$$

For S-wave we found that,

$$\begin{aligned}v_g(\boldsymbol{k}',\boldsymbol{k}) &= \delta_{i_Bi_{B'}}\delta_{i_Mi_{M'}}\frac{1}{(2f)^4}\frac{N_s^4}{(2\pi)^3}\frac{1}{\sqrt{\omega_{\mathbf{k}}\omega_{\mathbf{k}'}}}Y_{00}(\hat{k}')Y_{00}^*(\hat{k}) \\ &\quad \int_0^R dxx^2\rho_t^2(x)j_0(kx)j_0(k'x)\end{aligned} \tag{4.81}$$

4.3.6 The Interaction for Diagram h

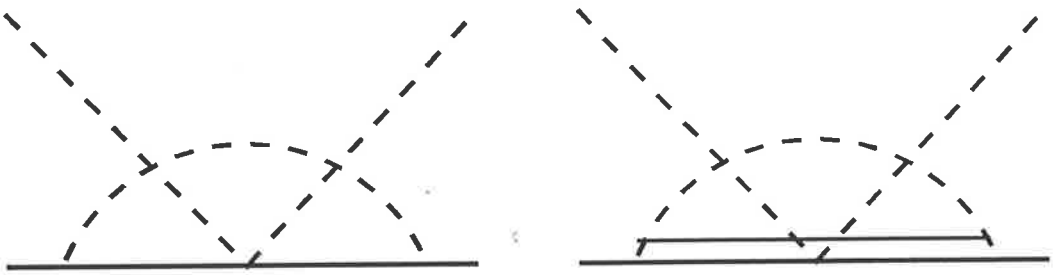

Figure 4.8: The interaction for Diagram h

The interaction Hamiltonian for this diagram is

$$H_h = H_1(\boldsymbol{y})\frac{1}{E_i-H_0+i\epsilon}H_{WT}^t(\boldsymbol{z})\frac{1}{E_i-H_0+i\epsilon}H_1(\boldsymbol{x}) \tag{4.82}$$

We may project this Hamiltonian into baryon space in usual way. The interaction matrix element is

$$\begin{aligned}&\hat{V}_h^{\alpha_4\alpha_1}(\boldsymbol{k}',\boldsymbol{k}) = \\ &\sum_{\alpha_3\alpha_2}\langle\alpha_4;\boldsymbol{k}',i_{M'}|H_1(\boldsymbol{y})\frac{|\alpha_3\rangle\langle\alpha_3|}{E_i-H_0+i\epsilon}H_{WT}^t(\boldsymbol{z})\frac{|\alpha_2\rangle\langle\alpha_2|}{E_i-H_0+i\epsilon}H_1(\boldsymbol{x})|\alpha_1;\boldsymbol{k},i_M\rangle\end{aligned} \tag{4.83}$$

Since the incoming and outgoing mesons interact at the contact point z we can write this as

$$\hat{V}_h^{\alpha_4\alpha_1}(\boldsymbol{k}',\boldsymbol{k}) = \sum_{\alpha_3\alpha_2}\langle\alpha_4|H_1(\boldsymbol{y})|\alpha_3\rangle\frac{1}{E_i-H_0+i\epsilon}\langle\alpha_3;\boldsymbol{k}',i_{M'}|H_{WT}^t(\boldsymbol{z})|\alpha_2;\boldsymbol{k},i_M\rangle \frac{1}{E_i-H_0+i\epsilon}H_1(\boldsymbol{x})|\alpha_1;\boldsymbol{k},i_M\rangle \quad (4.84)$$

By recalling from eqns (4.20),(4.21) and (4.29), the interaction matrix element for Yukawa vertex is

$$\hat{V}^{\alpha\beta}(\boldsymbol{q}) = \frac{-i}{(2f)}\frac{N_s^2}{\sqrt{2\omega_{\mathbf{q}}}}\int_0^R dr\; r^2\rho_{pv}(qr)\lambda^{\alpha\beta}C^{m_\beta m m_\alpha}_{S_\beta\,1\;S_\alpha}C^{i_\beta n i_\alpha}_{I_\beta 1 I_\alpha}\hat{\boldsymbol{s}}_m^*\cdot\boldsymbol{q}\;\hat{\boldsymbol{t}}_n^*. \quad (4.85)$$

We also noted from the eqn (4.37) that the interaction at the contact point, z, is

$$\langle\alpha_3;\boldsymbol{k}',i_{M'}|H_{WT}^t(\boldsymbol{z})|\alpha_2;\boldsymbol{k},i_M\rangle = \frac{1}{(2f)^2}\frac{N_s^2}{(4\pi)}\frac{\omega_{\mathbf{k}'}+\omega_{\mathbf{k}}}{\sqrt{2\omega_{\mathbf{k}'}2\omega_{\mathbf{k}}}}\int_0^R dz z^2\rho_t(z)\int d\hat{z}\frac{e^{i(\mathbf{k}-\mathbf{k}')\cdot\mathbf{z}}}{(2\pi)^3} \delta_{S_{\alpha_3}S_{\alpha_2}}\delta_{m_{\alpha_3}m_{\alpha_2}}\langle I_{\alpha_3}i_{\alpha_3};I_{M'}i_{M'}|\boldsymbol{\tau}\cdot\boldsymbol{\theta}|I_{\alpha_2}i_{\alpha_2};I_M i_M\rangle \quad (4.86)$$

With the help of eqn (4.85) and (4.86), the interaction matrix element for eqn (4.83) becomes,

$$\begin{aligned}\hat{V}_h^{\alpha_4\alpha_1}(\boldsymbol{k}',\boldsymbol{k}) = {}& \frac{1}{(2f)^4}\frac{N_s^6}{(4\pi)}\frac{(2\pi)^{-3}}{(2\pi)^3}\frac{\omega_{\mathbf{k}'}+\omega_{\mathbf{k}}}{\sqrt{2\omega_{\mathbf{k}'}2\omega_{\mathbf{k}}}}\int d^3q_1\int d^3q_2\frac{1}{\sqrt{2\omega_{\mathbf{q}_1}2\omega_{\mathbf{q}_2}}}\\ &\lambda^{\alpha_4\alpha_3}\lambda^{\alpha_2\alpha_1}\int_0^R dy y^2\rho_{pv}(q_1y)\int_0^R dx x^2\rho_{pv}(q_2x)\int_0^R dz z^2\rho_t(z)\int d\hat{z}e^{i(\mathbf{k}-\mathbf{k}')\cdot\mathbf{z}}\\ &C^{m_{\alpha_3}m'm_{\alpha_4}}_{S_{\alpha_3}\,1\,S_{\alpha_4}}C^{i_{\alpha_3}n'i_{\alpha_4}}_{I_{\alpha_3}1\,I_{\alpha_4}}\hat{\boldsymbol{s}}_{m'}^*\cdot\boldsymbol{q}_1\frac{1}{E_i-m_{\alpha_3}-\omega_{\mathbf{q}_1}-\omega_{\mathbf{k}'}}\delta_{S_{\alpha_3}S_{\alpha_2}}\delta_{m_{\alpha_3}m_{\alpha_2}}\\ &\langle 0|\hat{\boldsymbol{t}}_{n'}^*\cdot\boldsymbol{a}(\boldsymbol{q}_1)\hat{\boldsymbol{t}}_n^*\cdot\boldsymbol{a}^\dagger(\boldsymbol{q}_2)|0\rangle\langle I_{\alpha_3}i_{\alpha_3};I_{M'}i_{M'}|\boldsymbol{\tau}\cdot\boldsymbol{\theta}|I_{\alpha_2}i_{\alpha_2};I_Mi_M\rangle\\ &\frac{1}{E_i-m_{\alpha_2}-\omega_{\mathbf{q}_2}-\omega_{\mathbf{k}}}C^{m_{\alpha_1}mm_{\alpha_2}}_{S_{\alpha_1}\,1\,S_{\alpha_2}}C^{i_{\alpha_1}n\,i_{\alpha_2}}_{I_{\alpha_1}1\,I_{\alpha_2}}\hat{\boldsymbol{s}}_m^*\cdot\boldsymbol{q}_2. \end{aligned} \quad (4.87)$$

Since we have

$$\langle 0|\hat{\boldsymbol{t}}^*_{n'}\cdot\boldsymbol{a}(\boldsymbol{q}_1)\,\hat{\boldsymbol{t}}^*_n\cdot\boldsymbol{a}^\dagger(\boldsymbol{q}_2)|0\rangle = \delta^3(\boldsymbol{q}_1-\boldsymbol{q}_2)(-)^n\delta_{n,-n'}, \tag{4.88}$$

the momentum integral over $\boldsymbol{q}_2$ can be done. Therefore the spin part of eqn (4.87) is

$$\begin{aligned}
&\sum_{S_{\alpha_3}m_{\alpha_3}}\sum_{S_{\alpha_2}m_{\alpha_2}}\sum_{m,m'} C^{m_{\alpha_3}m'm_{\alpha_4}}_{S_{\alpha_3}\,1\,S_{\alpha_4}} C^{m_{\alpha_1}mm_{\alpha_2}}_{S_{\alpha_1}\,1\,S_{\alpha_2}} \int d\hat{q}_1\hat{\boldsymbol{s}}^*_{m'}\cdot\boldsymbol{q}_1\hat{\boldsymbol{s}}^*_m\cdot\boldsymbol{q}_1\;\delta_{S_{\alpha_3},S_{\alpha_2}}\;\delta_{m_{\alpha_3},m_{\alpha_2}} \\
&= \sum_{S_{\alpha_2}m_{\alpha_2}}\sum_{m,m'} C^{m_{\alpha_2}m'm_{\alpha_4}}_{S_{\alpha_2}\,1\,S_{\alpha_4}} C^{m_{\alpha_1}mm_{\alpha_2}}_{S_{\alpha_1}\,1\,S_{\alpha_2}} |\boldsymbol{q}|^2\left(\frac{4\pi}{3}\right)(-)^m\delta_{m',-m} \\
&= |\boldsymbol{q}|^2\left(\frac{4\pi}{3}\right)\delta_{S_{\alpha_4}S_{\alpha_1}}\;\delta_{m_{\alpha_4}m_{\alpha_1}}(-)^{S_{\alpha_3}+S_{\alpha_1}+1}\left[\frac{2S_{\alpha_3}+1}{2S_{\alpha_1}+1}\right]^{\frac{1}{2}}
\end{aligned} \tag{4.89}$$

The isospin part of eqn (4.87) becomes [see Appendix C]

$$\begin{aligned}
&\sum_{i_M,i_{M'}}\sum_n(-)^n\,C^{i_{\alpha_4}i_{M'}I_3}_{I_{\alpha_4}I_{M'}I}C^{i_{\alpha_3}-n\;i_{\alpha_4}}_{I_{\alpha_3}\;1\;I_{\alpha_4}} \\
&\qquad\qquad \langle I_{\alpha_3}i_{\alpha_3};I_{M'}i_{M'}|\boldsymbol{\tau}\cdot\boldsymbol{\theta}|I_{\alpha_2}i_{\alpha_2};I_Mi_M\rangle C^{i_{\alpha_1}n\;i_{\alpha_2}}_{I_{\alpha_1}1\;I_{\alpha_2}}C^{i_{\alpha_1}i_MI_3}_{I_{\alpha_1}I_MI} \\
&= (-)^{I+I_{\alpha_1}+1}\;[(2I_{\alpha_4}+1)(2I_{\alpha_2}+1)]^{\frac{1}{2}} \\
&\qquad\qquad \langle I_{\alpha_3}||\boldsymbol{\tau}^{(1)}||I_{\alpha_2}\rangle\langle I_{M'}||\boldsymbol{\theta}^{(1)}||I_M\rangle\begin{Bmatrix} I_{\alpha_1} & I_M & I \\ I_{M'} & I_{\alpha_4} & 1\end{Bmatrix}\begin{Bmatrix} I_{\alpha_1} & 1 & I_{\alpha_4} \\ I_{\alpha_3} & 1 & I_{\alpha_2}\end{Bmatrix}
\end{aligned} \tag{4.90}$$

By noting

$$\begin{aligned}
SI_\alpha &= \lambda^{\alpha_4\alpha_3}\lambda^{\alpha_2\alpha_1}\frac{\hat{S}_{\alpha_3}}{\hat{S}_{\alpha_1}}\,\hat{I}_{\alpha_4}\hat{I}_{\alpha_2}\begin{Bmatrix} I_{\alpha_1} & I_{\alpha_4} & l_2 \\ I_{M'} & I_M & I\end{Bmatrix}\begin{Bmatrix} I_{\alpha_1} & I_{\alpha_4} & l_2 \\ I_{\alpha_3} & I_{\alpha_2} & l_1\end{Bmatrix} \\
&\qquad (-)^{S_{\alpha_3}+S_{\alpha_1}+1+I+I_{\alpha_1}+1}\langle I_{\alpha_3}||\boldsymbol{T}^{(1)}||I_{\alpha_2}\rangle\langle I_{M'}||\boldsymbol{\theta}^{(1)}||I_M\rangle\;,
\end{aligned} \tag{4.91}$$

we can write the interaction for Fig. 4.2h as

$$v_h(\boldsymbol{k}',\boldsymbol{k}) = \frac{N_s^6}{384 f^4 \pi^4} \frac{\omega_{\mathbf{k}'}+\omega_{\mathbf{k}}}{\sqrt{2\omega_{\mathbf{k}} 2\omega_{\mathbf{k}'}}} \int_0^\infty dq \frac{q^4}{\omega_{\mathbf{q}}} \int_0^R dy y^2 \rho_{pv}(qy) \int_0^R dx x^2 \rho_{pv}(qx)\, SI_\alpha$$
$$\int_0^R dz z^2 \rho_t(z) j_0(kz) j_0(k'z) \frac{1}{(E_i - m_{\alpha_3} - \omega_{\mathbf{q}} - \omega_{\mathbf{k}'})} \frac{1}{(E_i - m_{\alpha_2} - \omega_{\mathbf{q}} - \omega_{\mathbf{k}})} \quad (4.92)$$

The Spin-Isospin constant SI_α are given in Table 4.5.

Table 4.5: Spin-Isospin factors arise from diagram (h).

α	*Total Isospin*	*State*$(\alpha_4,\alpha_3,\alpha_2,\alpha_1)$	SI_α
1	1/2	(N,N,N,N)	-50/3
2	3/2	(N,N,N,N)	+25/3
3	1/2	(N,Δ,Δ,N)	+320/3
4	3/2	(N,Δ,Δ,N)	-160/3

4.4 Summary

In this chapter we presented the derivation of potential for S-wave πN interactions. Kalbermann and Eisenberg's variant of the non-linear CBM Lagrangian was used to derive diagrams to order $\frac{1}{(2f)^4}$. We firstly gave examples in the CBM formalism to transform the interaction of pion and quarks to those of pion and nucleons. We then calculated higher order diagrams to order $\frac{1}{(2f)^4}$. These interactions will be used as driving potential to calculate phase shifts and scattering lengths in Chapter 7.

Chapter 5

P Wave Scattering

5.1 Introduction

In Chapter 4, we calculated the S-wave interaction to order $\frac{1}{(2f)^4}$ within the context of the Cloudy Bag Model. In this chapter we will calculate the P-wave interaction to order $\frac{1}{(2f)^2}$ using the same technique.

The CBM has been very successful in describing P-wave pion nucleon scattering [Tho+80, Tho+86, PA 86, PA 89]. Our purpose in rederiving the P-wave interaction is to provide a complete formulation of the πN system in this work. This P-wave interaction will also be used in testing various propagators in Chapter 7.

5.2 P-wave interactions

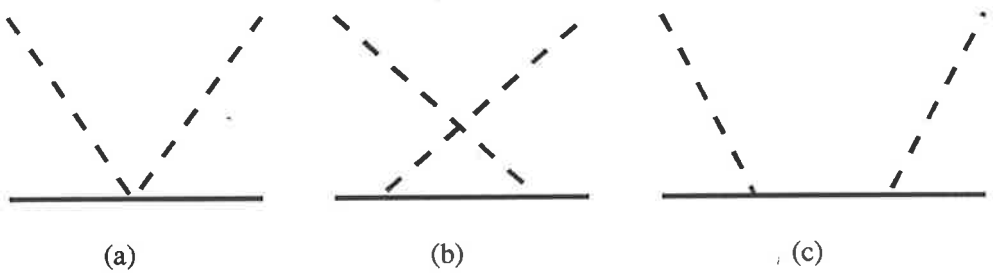

Figure 5.1: Diagrams contributing to the P-wave interaction

5.2.1 Contact Interaction

The contact interaction diagram shown in Fig. 5.1a is generated by the time piece (4.8) as well as spatial piece (4.9) of the Weinberg-Tomozawa (WT) interaction:

$$\hat{H}^{t}_{WT}(x) = \frac{\theta_v}{(2f)^2}\int d^3x\bar{q}\gamma_0\boldsymbol{\tau}q\cdot(\boldsymbol{\phi}\times\boldsymbol{\Pi}) \ , \tag{5.1}$$

$$\hat{H}^{so}_{WT}(x) = \frac{\theta_v}{(2f)^2}\int d^3x\bar{q}\boldsymbol{\gamma}\boldsymbol{\tau}q\cdot(\boldsymbol{\phi}\times\vec{\nabla}\,\boldsymbol{\phi}) \ . \tag{5.2}$$

For the time piece of WT interaction, the amplitude between the final state $|f\rangle$ and initial state $|i\rangle$ is given by,

$$\begin{aligned} v^{a(t)}_{Bi_M;B'i_{M'}}(\boldsymbol{k},\boldsymbol{k}') &= \langle f|\hat{H}^{t}_{WT}(x)|i\rangle \\ &= \langle S_Bm_B,I_Bi_B;\boldsymbol{k},I_Mi_M|\hat{H}^{t}_{WT}(x)|S_{B'}m_{B'},I_{B'}i_{B'};\boldsymbol{k}',I_{M'}i_{M'}\rangle \\ &= \langle S_Bm_B;lm|v^{BB'}_{a}(\boldsymbol{k},\boldsymbol{k}')|S_{B'}m_{B'};lm\rangle, \end{aligned} \tag{5.3}$$

where in eqn (5.3), the interaction matrix elements $v^{BB'}_{a}(\boldsymbol{k},\boldsymbol{k}')$ are those of (4.42) with the primed and unprimed labels interchanged. The matrix element (5.3) can be transformed to yield the scattering of total isospin I and spin J as

$$\begin{aligned} v^{a(t)}_{IJ}(\boldsymbol{k},\boldsymbol{k}') &= \sum_{i_Bi_{B'}}\sum_{i_Mi_{M'}} C^{i_Bi_MI_3}_{I_BI_MI}C^{i_{B'}i_{M'}I_3}_{I_{B'}I_{M'}I}\sum_{m_Bm_{B'}}\sum_{mm'} C^{m_Bm_Mm}_{S_B\ l\ J}C^{m_{B'}m'M}_{S_{B'}\ l'\ J}v^{a(t)}_{Bi_M;B'i_{M'}}(\boldsymbol{k},\boldsymbol{k}') \\ v^{a(t)}_{IJ}(\boldsymbol{k},\boldsymbol{k}') &= \frac{\lambda^{BB',I}_{WT}}{8\pi^2f^2}\frac{\omega_{\mathbf{k}}+\omega_{\mathbf{k}'}}{\sqrt{2\omega_{\mathbf{k}}2\omega_{\mathbf{k}'}}}N_s^2\int_0^R dxx^2\rho_t(x)j_1(kx)j_1(k'x)Y_{1m}(\hat{k})Y^*_{1m}(\hat{k}') \end{aligned} \tag{5.4}$$

For the spatial piece of WT term, we first calculate the amplitude between the final state $|f\rangle$ and initial state $|i\rangle$(please note the change of the label in this chapter);

$$\begin{aligned} v^{a}_{Bi_M;B'i_{M'}}(\boldsymbol{k},\boldsymbol{k}') &= \langle f|\hat{H}^{so}_{WT}(x)|i\rangle \\ &= \langle S_Bm_B,I_Bi_B;\boldsymbol{k},I_Mi_M|\hat{H}^{so}_{WT}(x)|S_{B'}m_{B'},I_{B'}i_{B'};\boldsymbol{k}',I_{M'}i_{M'}\rangle \end{aligned}$$

$$v^a_{Bi_M;B'i_{M'}}(\boldsymbol{k},\boldsymbol{k}') = \sum_{\alpha\beta}\langle B|\alpha^\dagger\beta\hat{V}^a_{\alpha i_M;\beta i_{M'}}(\boldsymbol{k},\boldsymbol{k}')|B'\rangle \tag{5.5}$$

The interaction matrix element between SU(6) bag states is

$$\begin{aligned}\hat{V}^a_{\alpha i_M;\beta i_{M'}}(\boldsymbol{k},\boldsymbol{k}') &= \langle\alpha;\boldsymbol{k},i_M|\hat{H}^{so}_{WT}(x)|\beta;\boldsymbol{k}',i_{M'}\rangle \\ &= \frac{\theta_v}{(2f)^2}\int d^3x\langle\alpha|\bar{q}\boldsymbol{\gamma}\tau_i q|\beta\rangle\langle\boldsymbol{k},i_M|(\boldsymbol{\phi}\times\vec{\nabla}\,\boldsymbol{\phi})_i|\boldsymbol{k}',i_{M'}\rangle. \end{aligned}\tag{5.6}$$

The meson part in eqn (5.6) is gives

$$\langle\boldsymbol{k},i_M|(\boldsymbol{\phi}\times\vec{\nabla}\,\boldsymbol{\phi})_i|\boldsymbol{k}',i_{M'}\rangle = -i\epsilon_{ijk}\delta_{ki_M}\delta_{ji_{M'}}(\boldsymbol{k}'+\boldsymbol{k})\frac{1}{(2\pi)^3}\frac{e^{-i(\mathbf{k}-\mathbf{k}')\cdot\mathbf{x}}}{\sqrt{2\omega_{\mathbf{k}}2\omega_{\mathbf{k}'}}}. \tag{5.7}$$

The baryon part for eqn (5.6) is given by

$$\langle\alpha|\bar{q}\boldsymbol{\gamma}\tau_i q|\beta\rangle = i\frac{N_s^2}{(4\pi)}j_0(\omega_s x)j_1(\omega_s x)\,{}_{sf}\langle\alpha|\sum_{a=1}^{3}\{\boldsymbol{\sigma}^{(a)}\boldsymbol{\sigma}^{(a)}\cdot\hat{r}-\boldsymbol{\sigma}^{(a)}\cdot\hat{r}\boldsymbol{\sigma}^{(a)}\}\tau_i^{(a)}|\beta\rangle_{sf} \tag{5.8}$$

Equations (5.7) and (5.8) put into (5.6) yield:

$$\begin{aligned}\hat{V}^{so}_{\alpha i_M;\beta i_{M'}}(\boldsymbol{k},\boldsymbol{k}') &= i\frac{\theta_v}{(2f)^2}\frac{N_s^2}{(4\pi)}\frac{1}{(2\pi)^3\sqrt{2\omega_{\mathbf{k}}2\omega_{\mathbf{k}'}}}\int d^3x j_0(\omega_s x)j_1(\omega_s x) \\ &\quad {}_{sf}\langle\alpha;i_M|\sum_{a=1}^{3}\{\boldsymbol{\sigma}^{(a)}\boldsymbol{\sigma}^{(a)}\cdot\hat{r}-\boldsymbol{\sigma}^{(a)}\cdot\hat{r}\boldsymbol{\sigma}^{(a)}\}(-\boldsymbol{\tau}^{(a)}\cdot\boldsymbol{\theta})|\beta;i_{M'}\rangle_{sf}(\boldsymbol{k}'+\boldsymbol{k})e^{-i(\mathbf{k}-\mathbf{k}')\cdot\mathbf{x}}\end{aligned}\tag{5.9}$$

where in (5.9) we used the notation

$$-\theta_i = -i\epsilon_{ijk}\delta_{ki_M}\delta_{ji_{M'}}.$$

Since we can prove that (see Appendix C)

$$\begin{aligned}&\int d\hat{x}(\boldsymbol{\sigma}\boldsymbol{\sigma}\cdot\hat{r}-\boldsymbol{\sigma}\cdot\hat{r}\boldsymbol{\sigma})\cdot(\boldsymbol{k}'+\boldsymbol{k})e^{-i(\mathbf{k}-\mathbf{k}')\cdot\mathbf{x}} \\ &= \frac{-4}{|x|}(4\pi)^2\sum_l j_l(k'x)j_l(kx)Y^*_{lm'}(\hat{k}')Y_{lm}(\hat{k})\sqrt{l(l+1)}\sum_{mm'm_2}\sigma_{1m_2}C^{mm_2m'}_{l\ 1\ l}\end{aligned}\tag{5.10}$$

we write eqn (5.9) as

$$\hat{V}^{so}_{\alpha i_M;\beta i_{M'}}(\boldsymbol{k},\boldsymbol{k}') = \frac{+i}{2\pi^2 f^2}\frac{1}{\sqrt{2\omega_{\mathrm{k}}2\omega_{\mathrm{k}'}}}N_s^2\int_0^R dx\frac{x^2}{|x|}j_0(\omega_s x)j_1(\omega_s x)\sum_l j_l(k'x)j_l(kx)$$
$$\sqrt{l(l+1)}\sum_{mm'm_2}{}_{sf}\langle\alpha;i_M|\sum_{a=1}^{3}\sigma^{(a)}_{m_2}\boldsymbol{\tau}^{(a)}\cdot\boldsymbol{\theta}|\beta;i'_M\rangle_{sf}C^{mm_2m'}_{l\ 1\ l}Y^*_{lm'}(\hat{k}')Y_{lm}(\hat{k}) \quad (5.11)$$

In order to project the interaction between quarks, (5.11), onto nucleons we will first define the symmetry factor $X^{BB'}$ such that

$${}_{sf}\langle\alpha|\sum_{a=1}^{3}\sigma^{(a)}_{m_2}\tau^{(a)}_q|\beta\rangle_{sf} = X^{\alpha\beta}\langle\alpha|\sigma_{m_2}\tau_q|\beta\rangle. \quad (5.12)$$

On the L.H.S. of (5.12) the eigenstates $|\alpha\rangle_{sf}$ and $|\beta\rangle_{sf}$ are explicit SU(6) spin-flavour wave functions and on the R.H.S. the nucleon bag wave functions (c.f. Section 4.2.1). The symmetry factor $X^{\alpha\beta}$ in (5.12) is given by

$$X^{\alpha\beta} = \lambda^{\alpha\beta}\frac{\sqrt{2S_\alpha+1}}{\langle S_\alpha||\boldsymbol{S}^{(1)}||S_\beta\rangle}\frac{\sqrt{2I_\alpha+1}}{\langle I_\alpha||\boldsymbol{T}^{(1)}||I_\beta\rangle} \quad (5.13)$$

The value for $X^{\alpha\beta}$ is given in Table 4.1. Using (5.13) we can write eqn (5.11) as

$$v^a_{Bi_M;B'i_{M'}}(\boldsymbol{k},\boldsymbol{k}') = \frac{+i}{2\pi^2 f^2}\frac{N_s^2}{\sqrt{2\omega_{\mathrm{k}}2\omega_{\mathrm{k}'}}}\int_0^R dx\frac{x^2}{|x|}j_0(\omega_s x)j_1(\omega_s x)\sum_l j_l(k'x)j_l(kx) \quad (5.14)$$
$$Y^*_{lm'}(\hat{k}')Y_{lm}(\hat{k})\sqrt{l(l+1)}\ X^{BB'}\sum_{mm'm_2q}(-)^q\langle B|\sigma_{1m_2}\tau_{1q}|B'\rangle\langle I_M i_M|\theta_{1,-q}|I_{M'}i_{M'}\rangle C^{mm_2m'}_{l\ 1\ l}$$

The interaction (5.14) represent the transition from initial state with spin and isospin

$$|i\rangle = |S_{B'}m_{B'}, I_{B'}i_{B'};\boldsymbol{k}', I_{M'}, i_{M'}\rangle$$

to the final state with spin and isospin

$$|f\rangle = |S_B m_B, I_B i_B;\boldsymbol{k}, I_M i_M\rangle.$$

Now we will transform (5.14) to get the interaction for total spin (J) and total isospin (I). We can transform (5.14) as

$$v^a_{IJ}(\boldsymbol{k},\boldsymbol{k'}) = \sum_{m_B m_{B'}} C^{m_B m M}_{S_B\ l\ J} C^{m_{B'} m' M}_{S_{B'}\ l'\ J} \sum_{i_B, i_{B'}} \sum_{i_M i_{M'}} C^{i_B i_M I_3}_{I_B I_M I} C^{i_{B'} i_{M'} I_3}_{I_{B'} I_{M'} I} v^a_{B i_M; B' i_{M'}}(\boldsymbol{k},\boldsymbol{k'}) \quad (5.15)$$

Since we can prove that

$$\begin{aligned} &\frac{1}{(2J+1)} \sum_{m_B m_{B'}} \sum_{M m\ m' m_2} C^{m_B m M}_{S_B\ l\ J} C^{m_{B'} m' M}_{S_{B'}\ l'\ J} \langle S_B m_B | \sigma_{1 m_2} | S_{B'} m_{B'} \rangle C^{m m_2 m'}_{l\ 1\ l} \\ &= (-)^{J+l+S_B} \sqrt{2l+1} \langle S_B || \boldsymbol{S}^{(1)} || S_{B'} \rangle \begin{Bmatrix} S_B & S_{B'} & 1 \\ l & l' & J \end{Bmatrix} , \end{aligned} \quad (5.16)$$

and

$$\begin{aligned} &\frac{1}{(2I+1)} \sum_{i_B i_{B'}} \sum_{q I_3} \sum_{i_M i_{M'}} C^{i_B i_M I_3}_{I_B I_M I} C^{i_{B'} i_{M'} I_3}_{I_{B'} I_{M'} I} (-)^q \langle I_B i_B | \tau_{1q} | I_{B'} i_{B'} \rangle \langle I_M i_M | \theta_{1,-q} | I_{M'} i_{M'} \rangle \\ &= (-)^{I+I_M+I_{B'}} \langle I_B || \boldsymbol{T}^{(1)} || I_{B'} \rangle \langle I_M || \boldsymbol{\theta}^{(1)} || I_{M'} \rangle \begin{Bmatrix} I_{M'} & I & I_{B'} \\ I_B & 1 & I_M \end{Bmatrix} , \end{aligned} \quad (5.17)$$

we can write eqn (5.15) as

$$\begin{aligned} v^a_{IJ}(\boldsymbol{k},\boldsymbol{k'}) &= \sum_I \frac{\lambda^{so,I}_{BB'}}{2f^2} \frac{1}{2\pi^2 \sqrt{2\omega_{\mathrm{k}} 2\omega_{\mathrm{k'}}}} (-2) \sqrt{6l(l+1)} \sqrt{2l+1} Y^*_{lm'}(\hat{k'}) Y_{lm}(\hat{k}) \quad (5.18) \\ &(-)^{J+l+\frac{1}{2}} \begin{Bmatrix} S_B & S_{B'} & 1 \\ l & l & J \end{Bmatrix} \int_0^R dx x^2 [2N_s^2 \frac{1}{|x|} j_0(\omega_s x) j_1(\omega_s x) j_l(kx) j_{l'}(k'x)] \end{aligned}$$

where $\lambda^{so,I}_{BB'}$ in equation (5.18) are defined as

$$\begin{aligned} \lambda^{so,I}_{BB'} = \frac{X^{BB'}}{(-2\sqrt{6})} &\langle S_B || \boldsymbol{S}^{(1)} || S_{B'} \rangle \langle I_B || \boldsymbol{T}^{(1)} || I_{B'} \rangle \langle I_M || \boldsymbol{\theta}^{(1)} || I_{M'} \rangle \quad (5.19) \\ &(-)^{I+I_M+I_{B'}} \begin{Bmatrix} I_{M'} & I & I_{B'} \\ I_B & 1 & I_M \end{Bmatrix} \end{aligned}$$

The values for $\lambda^{so,I}_{BB'}$ are given in Table 5.1.

Table 5.1: The coupling constants for the contact term, $\lambda^{so,I}_{BB'}$.

$B\backslash B'$	$I=1/2$		$I=3/2$	
	N	Δ	N	Δ
N	$\frac{5}{3}$	$\frac{-2\sqrt{2}}{3}$	$\frac{-5}{6}$	$\frac{-2\sqrt{5}}{3}$
Δ	$\frac{2\sqrt{2}}{3}$	$\frac{5\sqrt{10}}{3}$	$\frac{2\sqrt{5}}{3}$	$\frac{\sqrt{10}}{3}$

5.2.2 Crossed Born Term

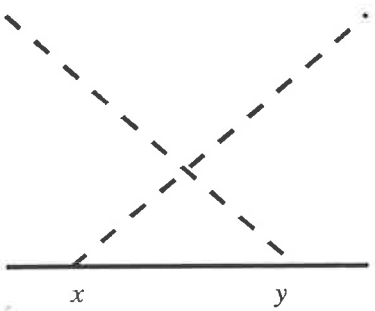

Figure 5.2: Crossed Born term.

The crossed Born diagram shown in Fig. 5.2 is generated by the Yukawa interactions. The interaction Hamiltonian for Fig. 5.2 is given by

$$H_b = H_1(\boldsymbol{x})\frac{1}{E_i - H_0 + i\epsilon}H_1(\boldsymbol{y}) \tag{5.20}$$

We will first calculate the interaction matrix element between two SU(6) eigenstates

$$v^b_{\beta i_M;\alpha i_{M'}}(\boldsymbol{k},\boldsymbol{k}') = \langle\beta;\boldsymbol{k}i_M|H_1(\boldsymbol{x})\frac{1}{E_i - H_0 + i\epsilon}H_1(\boldsymbol{y})|\alpha;\boldsymbol{k}',i_{M'}\rangle \tag{5.21}$$

Recalling eqn (4.14), the Yukawa interaction is given by

$$H_1(\boldsymbol{x}) = (2\pi)^{-\frac{3}{2}} \int d^3k \sum_{\alpha\beta} \sum_i \{\hat{V}_i^{\beta\alpha}(\boldsymbol{k}) a_i(\boldsymbol{k}) + \hat{V}_i^{\beta\alpha\dagger}(\boldsymbol{k}) a_i^\dagger(\boldsymbol{k})\} \beta^\dagger \alpha \tag{5.22}$$

$$= (2\pi)^{-\frac{3}{2}} \int d^3k \sum_{\alpha\beta} \sum_n \{\hat{V}_n^{\beta\alpha}(\boldsymbol{k}) a_n(\boldsymbol{k}) + (-)^n \hat{V}_n^{\beta\alpha\dagger}(\boldsymbol{k}) a_{-n}^\dagger(\boldsymbol{k})\} \beta^\dagger \alpha \tag{5.23}$$

where in eqn (5.23), $\hat{V}_n^{\beta\alpha}(\boldsymbol{k})$ is given by

$$\hat{V}_n^{\beta\alpha}(\boldsymbol{k}) = \frac{-i}{(6f)} \frac{\lambda^{\beta\alpha}}{\sqrt{2\omega_{\mathbf{k}}}} \left(\frac{\Omega}{\Omega - 1}\right) U(kR) C^{m_\alpha m m_\beta}_{S_\alpha\ 1\ S_\beta} (\hat{\boldsymbol{s}}^*_m \cdot \boldsymbol{k}) C^{i_\alpha n i_\beta}_{I_\alpha 1 I_\beta}. \tag{5.24}$$

It must be noted that in (5.22) the indices $i = 1, 2, 3$ are written in a Cartesian basis while in (5.23) $n = \pm 1, 0$ are written in a spherical basis for the pion field.

Now by using (5.23) the interaction matrix element for (5.21) is

$$v^b_{\beta i_M; \alpha i_{M'}}(\boldsymbol{k}, \boldsymbol{k}') = (2\pi)^{-3} \sum_C \sum_{\alpha'\alpha''} \int d^3q_1 d^3q_2 \langle \boldsymbol{k}, i_M | \{\hat{V}_n^{\beta\alpha''}(\boldsymbol{q}_1) a_n(\boldsymbol{q}_1)$$
$$\frac{\alpha'' |C\rangle\langle C| \alpha'^\dagger}{E_i - H_0 + i\epsilon} (-)^{n'} \hat{V}_{n'}^{\alpha'\alpha}(\boldsymbol{q}_2) a^\dagger_{-n'}(\boldsymbol{q}_2) | \boldsymbol{k}', i_{M'} \rangle \tag{5.25}$$
$$= (2\pi)^{-3} \sum_C \sum_{\alpha'\alpha''} \hat{V}^{\beta\alpha''}_{i_{M'}}(\boldsymbol{k}')\ \hat{V}^{\alpha'\alpha}_{-i_M}(\boldsymbol{k}) \frac{(-)^{i_M} \delta_{\alpha'',C} \delta_{\alpha',C}}{E_i - m_C - \omega_{\mathbf{k}} - \omega_{\mathbf{q}_1}}$$

We will now calculate the transition from state $|B'; \boldsymbol{k}', i_{M'}\rangle$ to $|B; \boldsymbol{k}, i_M\rangle$ as

$$v^b_{B i_M; B' i_{M'}}(\boldsymbol{k}, \boldsymbol{k}') = \sum_{\beta\alpha} \langle B | \beta^\dagger \alpha v^b_{\beta i_M; \alpha i_{M'}}(\boldsymbol{k}, \boldsymbol{k}') | B' \rangle$$
$$= (2\pi)^{-3} \frac{1}{(2f)^2} \frac{\lambda^{BC} \lambda^{CB'}}{\sqrt{2\omega_{\mathbf{k}} 2\omega_{\mathbf{k}'}}} \left(\frac{\Omega}{\Omega - 1}\right)^2 \frac{U(k'R) U(kR)}{E_i - m_C - \omega_{\mathbf{k}} - \omega_{\mathbf{q}_1}}$$
$$C^{m_C m m_B}_{S_C\ 1\ S_B} (\hat{\boldsymbol{s}}^*_{m'} \cdot \boldsymbol{k}') C^{i_C i_{M'} i_B}_{I_C\ 1\ I_B} C^{m_{B'} m m_C}_{S_{B'}\ 1\ S_C} (\hat{\boldsymbol{s}}^*_m \cdot \boldsymbol{k}) C^{i_{B'} - i_M i_C}_{I_{B'}\ 1\ I_C} (-)^{i_M} \tag{5.26}$$

Since we can write

$$\hat{\boldsymbol{s}}^*_{m'} \cdot \boldsymbol{k}'\ \ C^{m_C m' m_B}_{S_C\ 1\ S_B} = |\boldsymbol{k}'| \sqrt{\frac{4\pi}{3}} (-)^{m'} Y^*_{1m'}(\hat{k}') C^{m_C m' m_B}_{S_C\ 1\ S_B}$$

we rewrite eqn (5.26) as

$$v^b_{Bi_M;B'i_{M'}}(\boldsymbol{k},\boldsymbol{k}') = (2\pi)^{-3}\frac{1}{(2f)^2}\frac{\lambda^{BC}\lambda^{CB'}}{\sqrt{2\omega_{\mathbf{k}}2\omega_{\mathbf{k}'}}}\left(\frac{\Omega}{\Omega-1}\right)^2\frac{U(k'R)U(kR)|\boldsymbol{k}||\boldsymbol{k}'|}{E_i-m_C-\omega_{\mathbf{k}}-\omega_{\mathbf{q}_1}} \quad (5.27)$$
$$\left(\frac{4\pi}{3}\right)Y^*_{1m'}(\hat{k}')Y_{1m}(\hat{k})C^{m_Cm'm_B}_{S_C\ 1\ S_B}C^{m_{B'}mm_C}_{S_{B'}\ 1\ S_C}(-)^{m'}C^{i_Ci_{M'}i_B}_{I_C\ 1\ I_B}C^{i_{B'}-i_Mi_C}_{I_{B'}\ 1\ I_C}(-)^{i_M}$$

In order to get the interaction for total spin (J) and isospin (I), we carried out a similar transformation to that used in (5.15). We can prove that

$$\frac{1}{(2J+1)}\sum_{m_Bm_{B'}}\sum_{M,-m}\sum_{-m',m_C}C^{m_B-mM}_{S_B\ l\ J}C^{m_{B'}-m'M}_{S_{B'}\ l'\ J}C^{m_Cm'm_B}_{S_C\ 1\ S_B}C^{m_{B'}mm_C}_{S_{B'}\ 1\ S_C}(-)^{m'}$$
$$= \hat{S}_B\hat{S}_c(-)^{S_B+S_C}\begin{Bmatrix} S_B & l & J \\ S_{B'} & l' & S_C\end{Bmatrix}. \quad (5.28)$$

A similar summation over isospin indices can be carried out. By denoting

$$f(k) = \left(\frac{\Omega}{\Omega-1}\right)\frac{j_1(kR)}{R}$$

the interaction with total isospin (I) and total spin (J) for the crossed box diagram 5.2 becomes

$$v^b_{IJ}(\boldsymbol{k},\boldsymbol{k}') = \frac{1}{3}\frac{\lambda^{BC}}{2f}\frac{\lambda^{CB'}}{2f}\frac{1}{2\pi^2\sqrt{2\omega_{\mathbf{k}}2\omega_{\mathbf{k}'}}}Y^*_{1m'}(\hat{k}')Y_{1m}(\hat{k})(-)^{S_B+S_C+I_B+I_C}\hat{S}_B\hat{S}_C\hat{I}_B\hat{I}_C$$
$$\begin{Bmatrix} S_B & l & J \\ S_{B'} & l' & S_C\end{Bmatrix}\begin{Bmatrix} I_B & I_M & I \\ I_{B'} & I_{M'} & I_C\end{Bmatrix}\frac{f(k')f(k)}{E_i-m_C-\omega_{\mathbf{k}}-\omega_{\mathbf{k}'}} \quad (5.29)$$

5.2.3 The P_{33} Resonance

The CBM had its first success in explaining P_{33} resonance [Tho+80]. In the context of Gellmann and Ne'eman's quark model, the P_{33} resonance is a stable particle consisting of three quarks. There have been calculations of πN scattering in the so-called Δ-isobar model, which treats the Δ as a stable particle. In the CBM, the

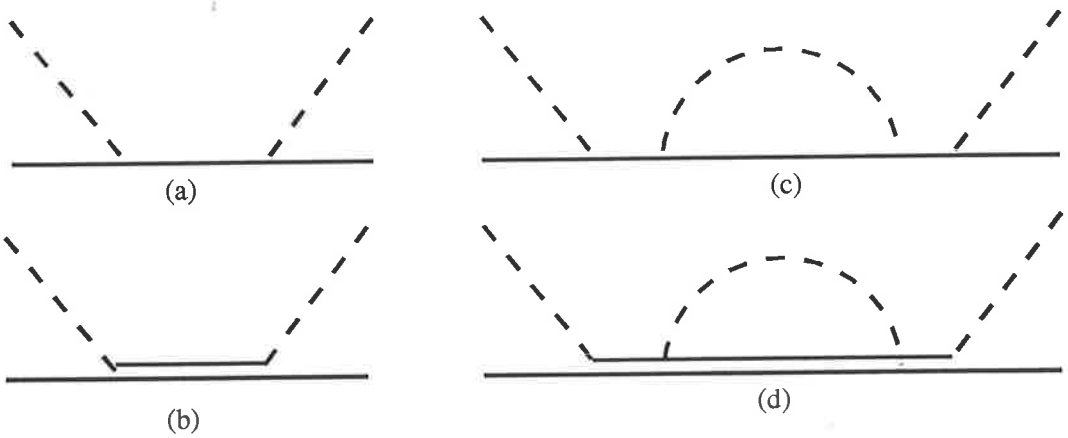

Figure 5.3: Direct channel contributing only P_{11} and P_{33}:(a) The direct channel with intermediate state nucleon; (b) with delta ; (c) the intermediate nucleon is renormalised; (d) intermediate delta is renormalised.

direct term appears in Fig. 5.3. The matrix element for the direct term can be calculated in the following manner. The interaction matrix element is

$$\begin{aligned}\hat{V}^{c}_{\beta i_M;\alpha i_{M'}}(\boldsymbol{k},\boldsymbol{k}') &= \langle\beta;\boldsymbol{k},i_M|H_1(\boldsymbol{y})\frac{1}{(E_i-H_0+i\epsilon)}H_1(\boldsymbol{x})|\alpha;\boldsymbol{k}',i_{M'}\rangle \qquad (5.30)\\ &= (2\pi)^{-3}\sum_C\sum_{\alpha'\alpha''}\hat{V}^{\beta\alpha''\dagger}_{i_M}(\boldsymbol{k})\hat{V}^{\alpha'\alpha}_{i_{M'}}(\boldsymbol{k}')\frac{\alpha''|C\rangle\langle C|\alpha'^{\dagger}}{E_i-H_0+i\epsilon}(-)^{i_M}\end{aligned}$$

The propagator $(E_i - H_0 + i\epsilon)^{-1}$ in eqn (5.30) needs to be treated as outlined in [Tho+80]. The intermediate states $|C\rangle$ involve the self energy graphs shown in Fig. 5.3 which can be a nucleon or Δ. When the intermediate state is a nucleon we will approximate the propagator as

$$S_N(E_i) = (E_i - m_N - \Sigma_{N\pi}(E_i) - \Sigma_{\Delta\pi}(E_i) - \Sigma_{HO}(E_i))^{-1}. \qquad (5.31)$$

On the other hand, $|C\rangle$ is a Δ state, we need to include Δ self energy shift in the propagator as

$$S_\Delta(E_i) = (E_i - m_\Delta - \Sigma_{\Delta\pi}(E_i))^{-1}. \qquad (5.32)$$

After the self energy graphs are included in the propagators, it is straightforward to calculate the potential for the direct term as

$$
\begin{aligned}
v^c_{IJ}(\boldsymbol{k},\boldsymbol{k}') &= \sum_{m_B m_{B'}} \sum_{m m'} \sum_{i_B i_{B'}} \sum_{i_M i_{M'}} C^{m_B m M}_{S_B\ l\ J} C^{m_{B'} m' M'}_{S_{B'}\ l'\ J'} C^{i_B i_M I_3}_{I_B I_M I} C^{i_{B'} i_{M'} I_3}_{I_{B'} I_{M'} I} \\
&\qquad \sum_{\beta\alpha} \langle B|\beta^\dagger \alpha v_{\beta i_M;\alpha i_{M'}}(\boldsymbol{k},\boldsymbol{k}')|B'\rangle \\
&= \frac{(2\pi)^3}{(6f)^2} \frac{\lambda^{BC}\lambda^{CB'}}{\sqrt{2\omega_{\mathrm{k}} 2\omega_{\mathrm{k}'}}} \left(\frac{\Omega}{\Omega-1}\right)^2 |\boldsymbol{k}||\boldsymbol{k}'| U(kR)U(k'R) \\
&\qquad \frac{(4\pi)}{3} Y_{1m}(\hat{k}) Y^*_{1m'}(\hat{k}') S_C(E_i - m_C) \frac{\hat{S}_B}{\hat{J}} \frac{\hat{S}_C}{\hat{J}} \frac{\hat{I}_B}{\hat{I}} \frac{\hat{I}_C}{\hat{I}}
\end{aligned} \tag{5.33}
$$

5.3 Summary

In this chapter, we explained how the πN P-wave interaction is described in the CBM to order $\frac{1}{(2f)^2}$. These P-wave interactions will also be used to calculate phase shifts and scattering lengths using different propagators in Chapter 7.

Chapter 6

Renormalization

6.1 Introduction

So far we have described the πN interaction in terms of a bare three-quark bag (MIT) and pions. In QED the physical electron is described by a bare electron surrounded by a cloud of photons. In the case of the strong interaction, the bare nucleon, which is described by a three-quark bag, is surrounded by a cloud of pions. As a result, the strength of the coupling constant and, hence, the interaction itself has changed. This is known as the renormalization effect. In this chapter we will examine the renormalization effects on πN interactions. In Section 6.2, we give an outline of how the various quantities of interest, such as baryon self-energy, the bare bag probability and the renormalized vertex functions are calculated. In Section 6.3, we calculate the baryon self-energy in detail. In Section 6.4, we study the bare bag probability. In Sections 6.5.1 and 6.5.2 we calculate the renormalizations for the Yukawa vertex and contact, or Weinberg-Tomozawa, terms.

6.2 The Physical Baryon Expansion

We describe the physical baryon state $|A\rangle$ as a combination of the bare baryon, $|A_0\rangle$; bare baryon and one pion, $|A_0; \boldsymbol{q}_1, i\rangle$; a bare baryon and two pions, $|A_0; \boldsymbol{q}_1, i; \boldsymbol{q}_2, j\rangle$ ... etc. The physical state, $|A\rangle$, and the bare eigenstate, $|A_0\rangle$, possess the same quantum numbers (T, T_3, J, J_z). We can write $|A\rangle$ as,

$$|A\rangle = \sqrt{Z_2^A}|A_0\rangle + \Lambda|A\rangle \tag{6.1}$$

where Z_2^A is a bare bag probability and the operator Λ projects all components of $|A\rangle$ that have at least one pion. The physical state ,$|A\rangle$, satisfies

$$H|A\rangle = m_A|A\rangle \tag{6.2}$$

where H is the total Hamiltonian and m_A is the physical mass of the nucleon. The bare nucleon state $|A_0\rangle$ and bare mass m_{0A} satisfy a similar equation

$$H_0|A_0\rangle = m_{0A}|A_0\rangle. \tag{6.3}$$

From (6.2) and (6.3) it is clear that in the presence of a pion field, the free Hamiltonian, H_0, will become the total Hamiltonian, $H = H_0 + H_{int}$, where H_{int} is interaction Hamiltonian.

Following [Wick55, Tho+81, Tho+83, Tho+80], the physical wave function $|A\rangle$ can be described in terms of the bare bag probability Z_2^A and bare bag wave function $|A_0\rangle$ as follows

$$\begin{aligned} |A\rangle &= \sqrt{Z_2^A}\{1 + (m_A - H_0 - \Lambda H_{int}\Lambda)^{-1} H_{int}\}|A_0\rangle \\ &= \sqrt{Z_2^A}\{1 + (m_A - \tilde{H}_0)^{-1} H_{int}\}|A_0\rangle \end{aligned} \tag{6.4}$$

where $\tilde{H}_0$ is defined as

$$\tilde{H}_0 = \sum_A A_0^\dagger A_0 m_{0A} + \sum_j \int d^3k\ \omega_{\rm k}\ a_j^\dagger(\boldsymbol{k}) a_j(\boldsymbol{k}). \tag{6.5}$$

The mass shift or self energy of the baryon can be defined [Wick55, Tho+81, Tho+83, Tho+80] by

$$\Sigma^A(m_A) = \langle A_0 | H_{int}(m_A - \tilde{H}_0)^{-1} H_{int} | A_0 \rangle \tag{6.6}$$

The bare bag probability Z_2^A can be derived [Wick55, Tho+81, Tho+83, Tho+80] from the normalization condition of the physical state

$$Z_2^A(m_A) = \left[1 - \frac{\partial}{\partial E}\Sigma^A(E)\right]^{-1}_{E=m_A} \tag{6.7}$$

In the renormalization procedure, the interaction matrix elements are the matrix elements between physical baryon states. In general, the relation between the bare matrix element, M_0^{AB}, and physical one, M^{AB}, is given by [Wick55, Tho+81, Tho+83, Tho+80],

$$\begin{aligned} M^{AB} &= \langle A | \hat{M} | B \rangle \\ &= \frac{\sqrt{Z_2^A}\sqrt{Z_2^B}}{Z_1^{AB}}\, M_0^{AB} \end{aligned} \tag{6.8}$$

where Z_1^{AB} is another renormalization constant defined via

$$Z_1^{AB} = [1 + \xi_1^{AB}]^{-1} \tag{6.9}$$

and ξ_1^{AB} is defined through:

$$M_0^{AB}\xi_1^{AB} = \langle A_0 | H_{int}(m_A - \tilde{H}_0)^{-1} \hat{M} (m_B - \tilde{H}_0)^{-1} H_{int} | B_0 \rangle. \tag{6.10}$$

6.3 Baryon Self Energy

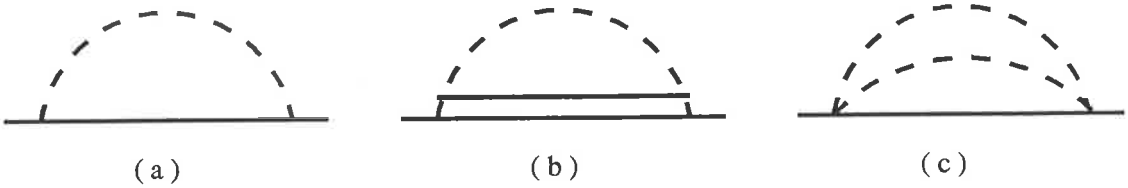

Figure 6.1: Diagrams contributing to the baryon self energy

When we tried to extend the calculation to higher order, as we did in Chapter 4, we saw that in eqn (4.1) the interaction Hamiltonian contains not only the Yukawa term, $\mathcal{H}_1(\boldsymbol{x})$, which is linear in the pion field, but also other terms non-linear in the pion field. Yet, when we calculate the self energy for baryons, (6.6), only the Yukawa term will be taken into account. For the CBM Lagrangian the contribution from multi-pion states is rather small in comparison to that from one pion. Thomas etal. [Tho+81] have rigorously shown that the probability for one pion field surrounding nucleon is large compared to two or three pions. We will assume that is also true for our volume coupling type Lagrangian, Kalbermann and Eisenberg's version of CBM (See Appendix A.2). The baryon self energy is represented graphically in Fig. 6.1. Figures 6.1a and 6.1b, which contribute to the nucleon self energy are generated by the Yukawa interaction. For our non-linear version of the CBM there is an additional contribution for the self energy which is generated by the Weinberg-Tomozawa interaction Fig. 6.1c. We shall assume this contribution from Fig. 6.1c is small and can be ignored in our calculations. Therefore, we will simply replace $\mathcal{H}_{int}$ in eqn (6.6) by H_1. Then the self-energy for the baryon is given by

$$\begin{aligned} \Sigma^A(m_A) &\approx \langle A_0|H_1(m_A - \tilde{H}_0)^{-1}H_1|A_0\rangle \\ &= \sum_{B,C}\langle A_0|H_1|B\rangle\langle B|(m_A - \tilde{H}_0)^{-1}|C\rangle\langle C|H_1|A_0\rangle \end{aligned} \tag{6.11}$$

The intermediate states, $|B\rangle$, are taken as a baryon with one pion. i.e.

$$\sum_B |B\rangle\langle B| = \sum_{B_0}\sum_i \int d^3q |B_0;\boldsymbol{q},i\rangle\langle B_0;\boldsymbol{q},i|. \tag{6.12}$$

where i is the isospin index of the pion. We recall eqn (4.14),

$$\begin{aligned} H_1 &= \sum_j \int d^3k \{\hat{V}_{0j}(\boldsymbol{k})a_j(\boldsymbol{k}) + \hat{V}^\dagger_{0j}(\boldsymbol{k})a^\dagger_j(\boldsymbol{k})\}, \\ &= \sum_{A_0,B_0} A^\dagger_0 B_0 \int d^3k \{v^{AB}_{0n}(\boldsymbol{k})\hat{\boldsymbol{t}}^*_n \cdot \boldsymbol{a}(\boldsymbol{k}) + v^{AB\dagger}_{0n}(\boldsymbol{k})\hat{\boldsymbol{t}}^*_n \cdot \boldsymbol{a}^\dagger(\boldsymbol{k})\} \end{aligned} \tag{6.13}$$

where $v^{AB}_{0n}(\boldsymbol{k})$ is given by

$$v^{AB}_{0n}(\boldsymbol{k}) = \left(\frac{if^{AB}_0}{m_\pi}\right)\frac{U(kR)}{\sqrt{2\omega_{\mathrm{k}}(2\pi)^3}} C^{m_B m m_A}_{S_B\ 1\ S_A}(\hat{\boldsymbol{s}}^*_m \cdot \boldsymbol{k})\ C^{i_B\ n\ i_A}_{I_B\ 1\ I_A}. \tag{6.14}$$

The subscript 0 in (6.13) and (6.14) is to symbolise that these matrix elements are bare matrix elements. The form factor $U(kR)$ in (6.14) is the same as in eqn (4.21) and the λ^{AB} are given in Table 4.2. The constants f^{AB}_0 are given by

$$\left(\frac{f^{AB}_0}{m_\pi}\right) = \frac{\lambda^{AB}}{(6f_{0\pi})}\left(\frac{\Omega}{\Omega-1}\right)$$

where $f_{0\pi}$ is the pion decay constant and $\Omega = 2.04$ is the eigen frequency for quarks in S-state. Since $\langle 0|\hat{\boldsymbol{t}}^*_n \cdot \boldsymbol{a}(\boldsymbol{k})\hat{\boldsymbol{t}}^*_{n'} \cdot \boldsymbol{a}^\dagger(\boldsymbol{k}')|0\rangle = \langle 0|(-)^{n'}a_n(\boldsymbol{k})a^\dagger_{-n'}(\boldsymbol{k}')|0\rangle$, eqn (6.11) becomes

$$\begin{aligned} \Sigma^A(m_A) &= \sum_{B_0}\int d^3k\ d^3k' v^{AB}_{0n}(\boldsymbol{k})v^{BA}_{0n'}(\boldsymbol{k}')\delta(\boldsymbol{k}'-\boldsymbol{k})\delta_{n,-n'}(-)^{n'} \\ &= \sum_{B_0}\left(\frac{f^{AB}_0 f^{BA}_0}{m^2_\pi}\right)\int_0^\infty dk \frac{k^4 U(kR)}{\sqrt{2\omega_{\mathrm{k}}(2\pi)^3}}\frac{1}{(m_A - m_B - \omega_{\mathrm{k}})} \\ &\quad \int d\hat{k} C^{m_B m m_A}_{S_B\ 1\ S_A} C^{m_A m' m_B}_{S_A\ 1\ S_B}(\hat{\boldsymbol{s}}^*_m \cdot \hat{k})(\hat{\boldsymbol{s}}^*_{m'} \cdot \hat{k}) \sum_{n,n'} C^{i_B n i_A}_{I_B 1 I_A} C^{i_A n' i_B}_{I_A 1\ I_B}\delta_{n,-n'}(-)^{n'} \end{aligned} \tag{6.15}$$

The sum over charge index n, n' and the angular integration can be done easily. Noting that $f_0^{AB} f_0^{BA} (\hat{S}_B \hat{I}_B)/(\hat{S}_A \hat{I}_A) = (f_0^{AB})^2$, the self energy of the baryon $\Sigma^A(m_A)$ becomes

$$\Sigma^A(m_A) = \sum_{B_0} (-)^{S_A+S_B+I_A+I_B} \frac{1}{12\pi^2} \left(\frac{f_0^{AB}}{m_\pi}\right)^2 \int_0^\infty dk \frac{k^4 U^2(kR)}{\omega_{\mathbf{k}}(m_A - m_B - \omega_{\mathbf{k}})} \quad (6.16)$$

6.4 Bare Bag Probability

The bare bag probability is defined by eqn (6.7). In the Cloudy Bag Model this can described in term of the bag radius. Here we plot the bare bag probability.

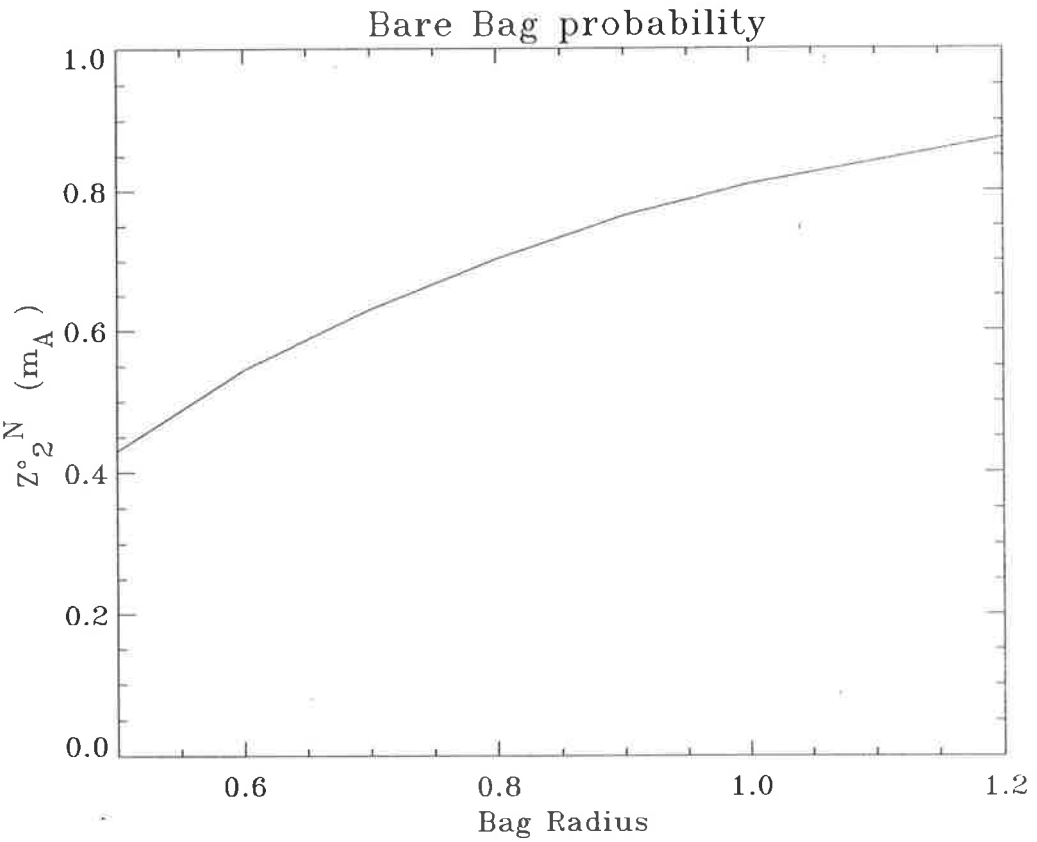

Figure 6.2: The Bare bag probability

6.5 Vertex Renormalization

6.5.1 Yukawa Interaction

(a) (b)

Figure 6.3: Yukawa vertex (a) and Renormalised vertex (b)

As we have stated in Section 6.2 in renormalization procedure we calculate interaction matrix element between two real nucleon states. To do this, it is important to find the function ξ_1^{AB}, such that,

$$v_{0n}^{AB}(\boldsymbol{k})\xi_1^{AB} = \langle A_0|H_1(m_A - \tilde{H}_0)^{-1}\hat{V}_{0n}(\boldsymbol{k})(m_B - \tilde{H}_0)^{-1}H_1|B_0\rangle \tag{6.17}$$

where v_{0n}^{AB} is given by (6.14). Let us first calculate the right hand side of eqn (6.17). By denoting

$$D^{-1}(m_A, m_C, \omega_{\mathbf{q}_1}) = (m_A - m_C - \omega_{\mathbf{q}_1})^{-1},$$

we have:

$$\begin{aligned}
&\langle A_0|H_1(m_A - \tilde{H}_0)^{-1}\hat{V}_{0n}(\boldsymbol{k})(m_B - \tilde{H}_0)^{-1}H_1|B_0\rangle \\
&= \sum_{C_0,D_0}\sum_{i,i'}\int d^3q_1\, d^3q_2\langle A_0|H_1|C_0;\boldsymbol{q}_1,i\rangle\delta_{i,i'}\delta(\boldsymbol{q}_1-\boldsymbol{q}_2)\langle C_0|\hat{V}_{0n}(\boldsymbol{k})|D_0\rangle \\
&\qquad \langle D_0;\boldsymbol{q}_2,i'|H_1|B_0\rangle\; D^{-1}(m_A,m_B,\omega_{\mathbf{q}_1})D^{-1}(m_B,m_D,\omega_{\mathbf{q}_2}) \\
&= \sum_{C_0,D_0}\sum_{i}\int d^3q_1 v_{0n'}^{AC}(\boldsymbol{q}_1)v_{0n}^{CD}(\boldsymbol{k})v_{0n''}^{DB\dagger}(\boldsymbol{q}_1)(-)^{n''}\delta_{n'',-i}\delta_{n',i} \\
&\qquad D^{-1}(m_A,m_C,\omega_{\mathbf{q}_1})D^{-1}(m_B,m_D,\omega_{\mathbf{q}_1})
\end{aligned}$$

$$= \sum_{C_0,D_0}\sum_i \int d^3q_1(-i)\left(\frac{f_0^{AC}f_0^{CD}f_0^{DB}}{m_\pi^3}\right)\frac{U^2(q_1R)}{2\omega_{\mathbf{q}_1}}\frac{U(qR)}{\sqrt{2\omega_{\mathbf{k}}(2\pi)^3}}$$
$$D^{-1}(m_A,m_C,\omega_{\mathbf{q}_1})D^{-1}(m_B,m_D,\omega_{\mathbf{q}_1})C^{m_Cm'm_A}_{S_C\ 1\ S_A}C^{m_Dmm_C}_{S_D\ 1\ S_C}C^{m_Bm''m_D}_{S_B\ 1\ S_D}$$
$$\hat{\boldsymbol{s}}^*_{m'}\cdot\boldsymbol{q}_1\hat{\boldsymbol{s}}^*_m\cdot\boldsymbol{k}\hat{\boldsymbol{s}}^*_{m''}\cdot\boldsymbol{q}_1 C^{i_Cn'i_A}_{I_C\ 1\ I_A}C^{i_Dni_C}_{I_D1I_C}C^{i_Bn''i_D}_{I_B1\ I_D}\delta_{n',i}\delta_{n'',-i}(-)^{n''}\hat{\boldsymbol{t}}^*_n \qquad (6.18)$$

By noting that $\int d\hat{q}_1\hat{\boldsymbol{s}}^*_{m'}\cdot\boldsymbol{q}_1\hat{\boldsymbol{s}}^*_{m''}\cdot\boldsymbol{q}_1 = |\boldsymbol{q}_1|^2(\frac{4\pi}{3})(-)^{m'}\delta_{m',-m''}$, we can simplify the sum over spin indices. Consider the spin part of eqn (6.18). The Clebsch-Gordan coefficients can be summed over m_A, m_B as follows:

$$\sum_{m_A,m_B}C^{m_Bmm_A}_{S_B\ 1\ S_A}\left\{C^{m_Bm_1m_A}_{S_B\ 1\ S_A}\hat{\boldsymbol{s}}^*_{m_1}\cdot\boldsymbol{k} \Longleftrightarrow C^{m_cm'm_A}_{S_C\ 1\ S_A}C^{m_D-m_2m_C}_{S_D\ 1\ S_C}C^{m_B-m'm_D}_{S_B\ 1\ S_D}(-)^{m'}\hat{\boldsymbol{s}}^*_{m_2}\cdot\boldsymbol{k}\right\} \qquad (6.19)$$

where our notation in eqn (6.19) implied: the spin part of L.H.S(R.H.S) of (6.17) being written on the L.H.S(R.H.S) of double arrows respectively. Then we applied the summation $C^{m_Am_Bm}_{S_A\ 1\ S_B}$ on both sides. The result is

$$\hat{\boldsymbol{s}}^*_m\cdot\boldsymbol{k} \Longleftrightarrow (-)^{S_C+S_D}\ [(2I_C+1)(2I_B+1)]^{\frac{1}{2}}\left\{\begin{array}{ccc} S_A & 1 & S_B \\ S_D & 1 & S_C \end{array}\right\}\hat{\boldsymbol{s}}^*_m\cdot\boldsymbol{k} \qquad (6.20)$$

A similar procedure is carried out for the isospin part. The result is

$$\hat{\boldsymbol{t}}^*_n \Longleftrightarrow (-)^{I_C+I_D}\ [(2I_C+1)(2I_D+1)]^{\frac{1}{2}}\left\{\begin{array}{ccc} I_A & 1 & I_B \\ I_D & 1 & I_C \end{array}\right\}\hat{\boldsymbol{t}}^*_n \qquad (6.21)$$

By combining the equations (6.17),(6.19) and (6.21), we finally have;

$$\xi_1^{AB} = (-)\sum_{C_0,D_0}\left(\frac{f_0^{AC}f_0^{CD}f_0^{DB}}{f_0^{AB}m_\pi^2}\right)U^{AB}_{CD}$$
$$(12\pi^2)^{-1}\int_0^\infty dq\frac{q^4U^2(qR)}{\omega_{\mathbf{q}}}D^{-1}(m_A,m_C,\omega_{\mathbf{q}})D^{-1}(m_B,m_D,\omega_{\mathbf{q}}) \qquad (6.22)$$

where

$$U_{CD}^{AB} = (-)^{S_C+S_D+I_C+I_D}[(2S_C+1)(2S_D+1)(2I_C+1)(2I_D+1)]^{\frac{1}{2}} \begin{Bmatrix} S_A & 1 & S_B \\ S_D & 1 & S_C \end{Bmatrix} \begin{Bmatrix} I_A & 1 & I_B \\ I_D & 1 & I_C \end{Bmatrix} \tag{6.23}$$

From eqn (6.8), the ratio between physical and bare matrix element is

$$\begin{aligned} \frac{M^{AB}}{M_0^{AB}} &= \frac{\sqrt{Z_2^A}\sqrt{Z_2^B}}{Z_1^{AB}} \\ &= \sqrt{Z_2^A Z_2^B}[1+\xi_1^{AB}] \end{aligned} \tag{6.24}$$

In CBM, Z_2^N and ξ_1^{AB} are both functions of the bag radius R. In Fig. 6.4 we show (M^{AB}/M_0^{AB}) as a function of R.

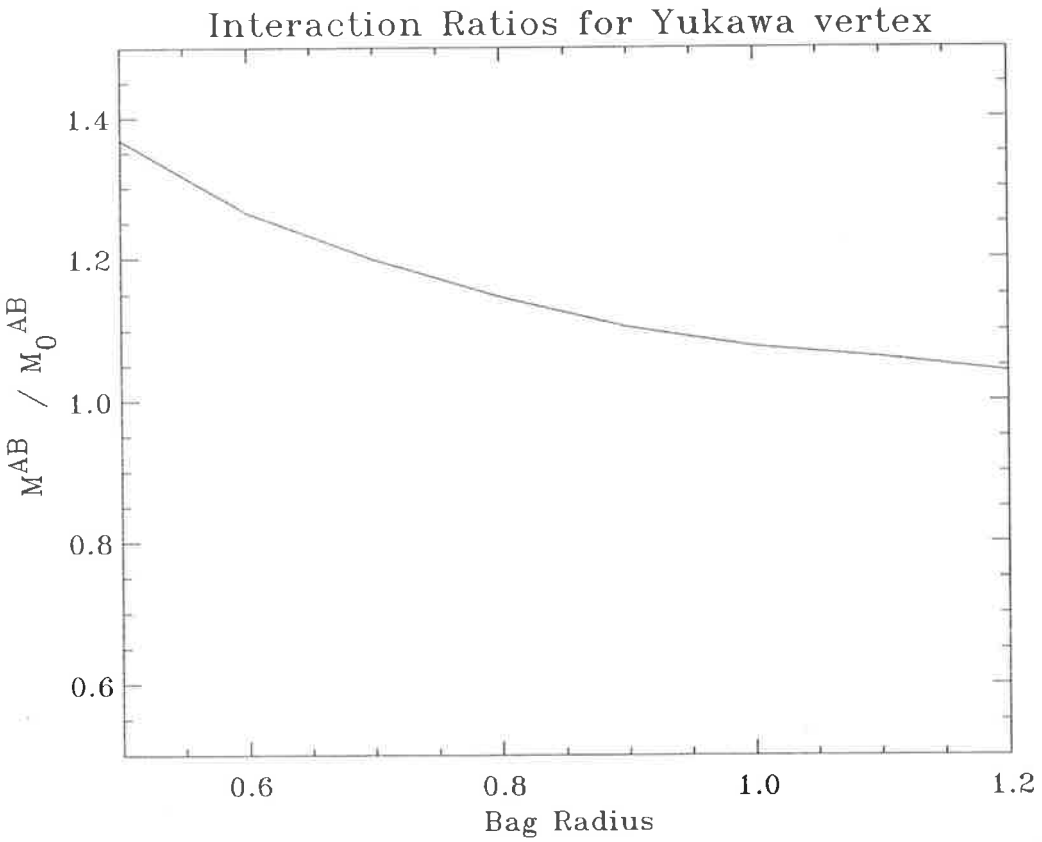

Figure 6.4: Ratios of unrenormalised and renormalised interactions

6.5.2 Weinberg-Tomozawa Interaction

(a) (b)

Figure 6.5: Unrenormalised Weinberg-Tomozawa interaction (a) and renormalised interaction (b)

In Section 6.5.1, we obtained the renormalized version of the Yukawa interaction. In this section we repeat the same procedure on the Weinberg-Tomozawa interaction. To do this we need to find the expression for ξ^{AB}_{WT} which satisfies

$$v^{AB}_{0i_{M'}i_M}(\boldsymbol{k}',\boldsymbol{k})\xi^{AB}_{WT} = \langle A_0|H_1(m_A-\tilde{H}_0)^{-1}\hat{V}_{0i_{M'}i_M}(\boldsymbol{k}',\boldsymbol{k})(m_B-\tilde{H}_0)^{-1}H_1|B_0\rangle \quad (6.25)$$

By recalling eqn (4.37), the L.H.S. of eqn (6.25) is,

$$\begin{aligned}
& \xi^{AB}_{WT}\langle A_0|\hat{V}_{0i_{M'}i_M}(\boldsymbol{k}',\boldsymbol{k})|B_0\rangle \\
= \;& \xi^{AB}_{WT}\langle A_0;\boldsymbol{k}',i_{M'}|H^t_{WT}(\boldsymbol{x})|B_0;\boldsymbol{k},i_M\rangle \qquad (6.26)\\
= \;& \xi^{AB}_{WT}\frac{1}{(2f)^2}\frac{N_s^2}{(4\pi)}\frac{\omega_{\mathrm{k}'}+\omega_{\mathrm{k}}}{\sqrt{2\omega_{\mathrm{k}'}2\omega_{\mathrm{k}}}}\int_0^R dz z^2\rho_t(z)\int d\hat{z}\frac{e^{i(\boldsymbol{k}-\boldsymbol{k}')\cdot\boldsymbol{z}}}{(2\pi)^3}\langle A_0;i_{M'}|\boldsymbol{\tau}\cdot\boldsymbol{\theta}|B_0;i_M\rangle \\
= \;& \xi^{AB}_{WT}\sum_{II_3}C^{i_Ai_{M'}I_3}_{I_AI_{M'}I}C^{i_Bi_MI_3}_{I_BI_MI}\frac{\lambda^{AB,I}_{WT}}{(2f)^2}\frac{N_s^2}{4\pi}\frac{\omega_{\mathrm{k}'}+\omega_{\mathrm{k}}}{\sqrt{2\omega_{\mathrm{k}'}2\omega_{\mathrm{k}}}}\int_0^R dz z^2\rho_t(z)\int d\hat{z}\frac{e^{i(\boldsymbol{k}-\boldsymbol{k}')\cdot\boldsymbol{z}}}{(2\pi)^3}
\end{aligned}$$

On the other hand, the R.H.S. of (6.25) is written as

$$\begin{aligned}
& \langle A_0|H_1(m_A-\tilde{H}_0)^{-1}\hat{V}_{0i_{M'}i_M}(\boldsymbol{k}',\boldsymbol{k})(m_B-\tilde{H}_0)^{-1}H_1|B_0\rangle \\
= \;& \sum_{C_0,D_0}\sum_{i,i'}\int d^3q_1\, d^3q_2\langle A_0|H_1|C_0;\boldsymbol{q}_1,i'\rangle\langle C_0;\boldsymbol{q}_1,i'|\hat{V}_{0i_{M'}i_M}(\boldsymbol{k}',\boldsymbol{k})|D_0;\boldsymbol{q}_2,i\rangle \\
& \qquad \langle D_0;\boldsymbol{q}_2,i|H_1|B_0\rangle D^{-1}(m_A,m_C,\omega_{\mathrm{q}_1})D^{-1}(m_B,m_D,\omega_{\mathrm{q}_2})
\end{aligned}$$

$$
\begin{aligned}
&= \sum_{C_0,D_0}\sum_{i,i'}\int d^3q \langle A_0|\hat{V}_{0n'}(\boldsymbol{k}_1)a_{n'}(\boldsymbol{k}_1)|C_0;\boldsymbol{q},i\rangle\langle C_0;i'|\hat{V}_{0i_{M'}i_M}(\boldsymbol{k}',\boldsymbol{k})|D_0;i\rangle \\
&\quad \langle D_0;\boldsymbol{q},i|\hat{V}^{\dagger}_{0,-n''}(\boldsymbol{k}_2)a^{\dagger}_{n''}(\boldsymbol{k}_2)(-)^{n''}|B_0\rangle D^{-1}(m_A,m_C,\omega_{\mathbf{q}})D^{-1}(m_B,m_D,\omega_{\mathbf{q}}) \\
&= (2\pi)^{-3}\sum_{C_0,D_0}\left(\frac{f_0^{AC}f_0^{DB}}{m_\pi^2}\right)\int_0^\infty dq\; q^2\frac{U^2(qR)}{2\omega_{\mathbf{q}}}D^{-1}(m_A,m_C,\omega_{\mathbf{q}})D^{-1}(m_B,m_D,\omega_{\mathbf{q}}) \\
&\quad \frac{1}{(2f)^2}\frac{N_s^2}{(4\pi)}\frac{\omega_{\mathbf{k}'}+\omega_{\mathbf{k}}}{\sqrt{2\omega_{\mathbf{k}'}2\omega_{\mathbf{k}}}}\int_0^R dz z^2\rho_t(z)\int d\hat{z}\frac{e^{i(\boldsymbol{k}-\boldsymbol{k}')\cdot\boldsymbol{z}}}{(2\pi)^3} \qquad (6.27)\\
&\quad \int d\hat{q}C^{m_C m' m_A}_{S_C\ 1\ S_A}C^{m_B m'' m_D}_{S_B\ 1\ S_D}\hat{\boldsymbol{s}}^*_{m'}\cdot\boldsymbol{q}\hat{\boldsymbol{s}}^*_{m''}\cdot\boldsymbol{q}C^{i_C n i_A}_{I_C 1 I_A}C^{i_B -n i_D}_{I_B\ 1\ I_D}(-)^n\langle C_0;i_{M'}|\boldsymbol{\tau}\cdot\boldsymbol{\theta}|D_0;i_M\rangle
\end{aligned}
$$

As in Section 6.5.1, we shall sum over Clebsch-Gordan coefficients. We first write isospin part of eqn (6.25) as,

$$
\begin{aligned}
\sum_{II_3}\lambda^{AB,I}_{WT}C^{i_A i_{M'} I_3}_{I_A I_{M'} I}C^{i_B i_M I_3}_{I_B I_M I} &\iff (-)^n C^{i_C n i_A}_{I_C 1 I_A}C^{i_B -n i_D}_{I_B\ 1\ I_D}\langle I_C i_C;I_{M'}i_{M'}|\boldsymbol{\tau}\cdot\boldsymbol{\theta}|I_D i_D;I_M i_M\rangle \\
&\iff (-)^{n+q}C^{i_C n i_A}_{I_C 1 I_A}C^{i_B -n i_D}_{I_B\ 1\ I_D}C^{i_D q\ i_C}_{I_D l_2 I_C}C^{i_M -q\ i_{M'}}_{I_M\ l_2\ I_{M'}} \\
&\quad \frac{\langle I_c||\boldsymbol{\tau}^{(1)}||I_D\rangle}{\sqrt{2I_c+1}}\frac{\langle I_{M'}||\boldsymbol{\theta}^{(1)}||I_M\rangle}{\sqrt{2I_M+1}} \qquad (6.28)
\end{aligned}
$$

Applying

$$
\sum_{i_A,i_B}\sum_{i_{M'},i_M}C^{i_A i_{M'} I'_3}_{I_A I_{M'} I'}C^{i_B i_M I'_3}_{I_B I_M I'},
$$

to both L.H.S and R.H.S of (6.28) we get (a similar procedure is carried out in obtaining equation (4.90));

$$
\begin{aligned}
\lambda^{AB,I}_{WT} \iff (-)^{I+I_B+1}\hat{I}_A\hat{I}_D & \qquad (6.29)\\
\langle I_C||\boldsymbol{T}^{(1)}||I_D\rangle\langle I_{M'}||\boldsymbol{\theta}^{(1)}||I_M\rangle & \begin{Bmatrix} l_2 & I_A & I_B \\ I & I_M & I_{M'} \end{Bmatrix}\begin{Bmatrix} l_2 & I_A & I_B \\ l_1 & I_D & I_C \end{Bmatrix}
\end{aligned}
$$

Finally, by combining eqns (6.25)-(6.29), we have:

$$\xi_{WT}^{AB} = \sum_{C_0,D_0} \left(\frac{f_0^{AC} f_0^{DB}}{\lambda_{WT}^{AB,I} m_\pi^2} \right) \frac{1}{12\pi^2} \int_0^\infty dq \frac{q^4 U^2(qR)}{2\omega_{\mathbf{q}}} D^{-1}(m_A, m_C, \omega_{\mathbf{q}}) D^{-1}(m_B, m_D, \omega_{\mathbf{q}})$$
$$\langle I_C || \boldsymbol{T}^{(1)} || I_D \rangle \langle I_{M'} || \boldsymbol{\theta}^{(1)} || I_M \rangle \hat{I}_A \hat{I}_D \hat{S}_C \hat{S}_A^{-1}$$
$$(-)^{I+S_C+1} \left\{ \begin{array}{ccc} l_2 & I_A & I_B \\ I & I_M & I_{M'} \end{array} \right\} \left\{ \begin{array}{ccc} l_2 & I_A & I_B \\ l_1 & I_D & I_C \end{array} \right\} \quad (6.30)$$

The R dependence of the ratio of renormalised to unrenormalised strength for the Weinberg-Tomozawa interaction is given in Fig. 6.6.

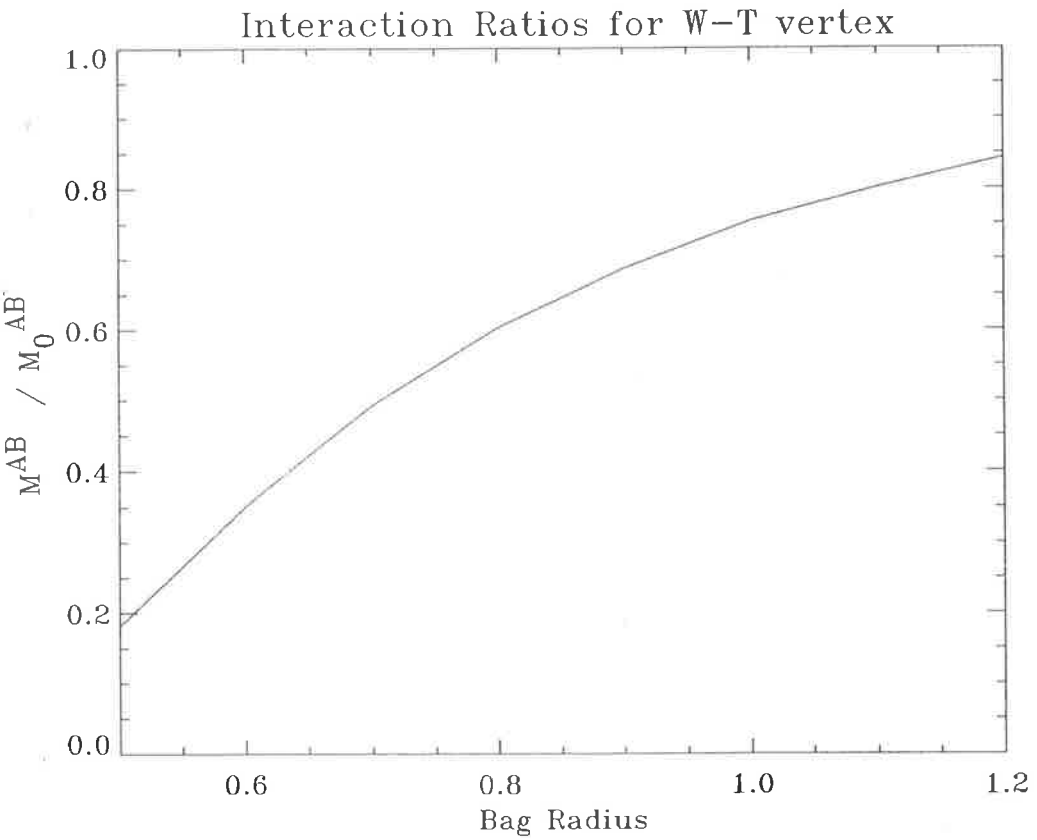

Figure 6.6: Renormalised to unrenormalised ratios of Weinberg-Tomozawa term

6.6 Summary

In this chapter we presented the renormalization procedure for the CBM. We first outlined how the bare bag probability, self energy and vertex renormalization are obtained. Firstly, we calculated the baryon self energy and bare bag probability. We then calculated the vertex renormalization for the Yukawa interaction and the Weinberg-Tomozawa interaction. The effect of renormalization on S-wave in πN scattering will be studied in Chapter 7.

Chapter 7

Numerical Results

In this Chapter, we present the results for the S-wave and P-wave πN phase shifts and scattering lengths and compare the use of different propagators. In Section 7.2.1 we show how the scattering length and phase shift for S-wave πN data is reproduced phenomenologically. We also compare the scattering lengths and phase shift for different propagators using phenomenological potentials. In Section 7.2.2 we study the threshold behaviour of the S-wave potentials which we derived in Chapter 4 . In Section 7.2.3 the S-wave scattering lengths and phase shifts for different propagators with CBM potentials are presented. In Section 7.2.4 we discuss the effects of renormalization on the S-wave results.

In Section 7.3.1 the phenomenological approach to πN P-wave scattering with a comparison of different propagators is presented. In Section 7.3.2 we present the theoretical results for P-wave scattering using the CBM potentials derived in Chapter 5. The comparison with different propagators has also been made.

7.1 Experimental Data for πN S and P-waves

There are accurate πN scattering data up to a c.m. energy of 1.7 GeV. The experimental phase shifts for both S-and P-wave in this work are from R.A.Arndt and L.D.Roper, Scattering analysis dial in(SAID programme). The experimental scattering lengths and volumes are given in Table 7.1 and Table 7.2(see also Ref. [Kol 69]).

Table 7.1: The Experimental S-wave scattering lengths (m_π^{-1})

a_1	a_3	*References*
0.182 ± 0.006	-0.103 ± 0.006	[Fis 59, Bie 62]
0.17	-0.10	[McK 63]
0.171 ± 0.005	-0.088 ± 0.004	[Ham 63]
0.183 ± 0.016	-0.109 ± 0.016	[Wool65]
0.179 ± 0.019	-0.013 ± 0.019	[Don 66]
0.206 ± 0.007	-0.099 ± 0.007	[AZR 80]
0.170	-0.099	[Stah]

Table 7.2: The Experimental P-wave scattering volumes (m_π^{-3})

a_{11}	a_{13}	a_{31}	a_{33}	Reference
-0.015	-0.0035	-0.13	0.243	[McK 63]a
-0.016	-0.13	-0.13	0.201	[McK 63]b
-0.101$\pm$ 0.007	-0.029 $\pm$ 0.005	-0.038 $\pm$ 0.005	0.215 $\pm$ 0.005	[Ham 63]

7.2 The S-wave Scattering Lengths and Phase Shifts

7.2.1 Phenomenological Results

There have been many calculations for S-wave πN scattering using separable, phenomenological potentials [Tho 76]. In his work, Thomas used a separable potential

of the form

$$v(k', k) = \lambda g(k')g(k),$$

where $\lambda = (\pm 1)$ is repulsive(attractive) and the form factor $g(k)$ is given by

$$g(k) = S_1/(\alpha_1^2 + k^2) + S_2/(\alpha_2^2 + k^2)\,. \tag{7.1}$$

The nucleon is treated as static and the pion relativistic, while the R-matrix approach was used to solve the scattering equation. The parameters $S_1, S_2, \alpha_1, \alpha_2$ are given in Table 7.3. We repeated this calculation using fully relativistic kinematics for both the pion and nucleon. The results from matrix inversion method of Haftel and Tabakin [HT 70] using various relativistic equations are given in Table 7.4 and Figure 7.1. There has also been a calculation for the comparison among relativistic propagators by Pearce and Jennings [PJ 90]. In their work, Pearce and Jennings used a Lagrangian that treated the nucleon and Δ as elementary particles and therefore were able to describe the interaction in a covariant fashion. They found that there are no significant difference in phase shifts in using the Smooth (CJ) and Blankenbecler-Sugar (BbS) propagators. In our work the CBM Lagrangian is used and therefore interactions are calculated in non-covariant fashion. We therefore include not only relativistic propagators but also Lippmann-Schwinger (LS) propagators in our calculations. In this work we find a significance difference in the scattering lengths and phase shifts between Lippmann-Schwinger (LS) and relativistic propagators while very close results are produced by CJ and BbS propagators as can be seen from Table 7.4 and Fig. 7.1.

7.2.2 The Threshold Behaviour

It is well known that at threshold, the Weinberg-Tomozawa(WT) term reproduces the isovector scattering lengths [Tho 81]. For our calculation with the CBM, we must

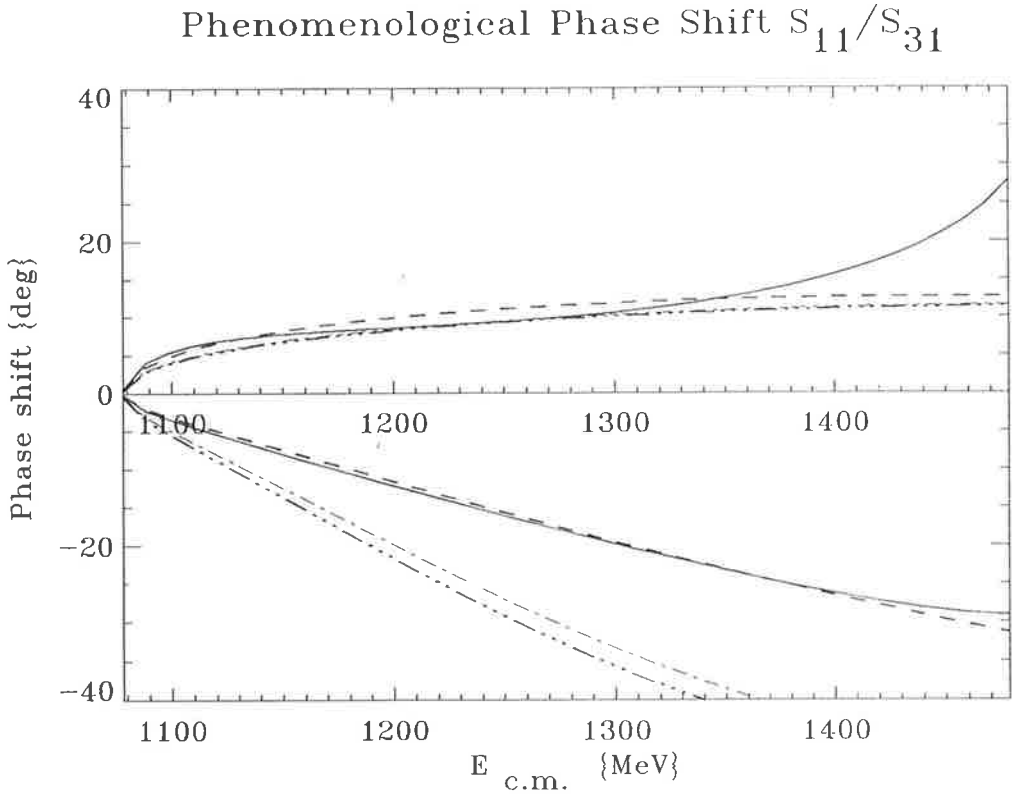

Figure 7.1: The S-wave phase shifts using phenomenological potentials. The solid line experimental data. The dashed line Lippmann Schwinger(LS) propagator. The dash-dotted line Smooth(CJ) propagator. The dash-3 dot Blankenbecler-Sugar(BbS) propagators.

Table 7.3: The parameters used in the form factor (7.1) and the corresponding scattering lengths

Channel	S_1	α_1	S_2	α_2	*Scattg : Length*
S_{11}	1.7826	3.188	0.894	0.8255	$+0.171\ m_\pi^{-1}$
S_{31}	6.078	3.382	-0.1661	1.107	$-0.091\ m_\pi^{-1}$

Table 7.4: Phenomenological scattering lengths (m_π^{-1})

Propagator	a_1	a_3
LS	0.1756	-0.0894
CJ	0.1477	-0.1358
BbS	0.1441	-0.1538

compare with the phase shifts as well as the scattering lengths. When we iterate the LS equation using the WT term as the driving potential we observe a large discrepancy in scattering lengths as well as in the S_{11} phase shifts. This discrepancy is known to arise from not preserving chiral symmetry when we iterate the WT term in a LS equation [Tho+87]. Attempts have been made to overcome this difficulty by including the diagrams to order $\frac{1}{(2f)^4}$ in driving potential. In the work of Thomas *et al.* [Tho+87, CJ 86] experimental isovector form factors were used and only the isoscalar interaction for Fig. 4.1e and Fig. 4.1f was calculated in the model. In this work we calculated both the isovector and isoscalar contributions from the CBM Lagrangian. Within the isoscalar interaction for v_e and v_f, the essential difference between our work and that of Cooper and Jennings is the treatment of the pion-pion scattering. Cooper and Jennings did not wish to introduce an extra parameter (pion radius) in their formulation and sidesteped this difficulty by transforming the interaction to coordinate space. They also approximated the nucleon and Δ as having the same mass. In our work, the pion form factor was introduced and formulated in momentum space.

We will firstly look at the behaviour of transition amplitude as we extend the

calculation to order $\frac{1}{(2f)^4}$. As we can see from Table 7.6, WT term in the Born approximation, which is a transition amplitude of order $\frac{1}{(2f)^2}$ obeys the Adler consistency condition $a_1 + 2a_3 = 0$. This condition is badly violated when we include potentials to order $\frac{1}{(2f)^4}$ in Born Approximation. It is found that the scattering length a_3 is then changed by 100 per cent (see Table 7.6).

We also study the behaviour of transition amplitude in the soft pion limits. It is how each potential v_a to v_h behaves when the incident pion energy becomes zero. In the following we list the analytic form of the potentials which were derived in Chapter 4 at threshold. These can be obtained by setting ingoing and outgoing pion energies are the same, i.e. $\omega_{\mathbf{k}} = \omega_{\mathbf{k}'}$, and the incident energy being taken as $E_i = m_N + \omega_{\mathbf{k}}$.

$$v_a = \frac{\lambda^I_{WT}}{8f^2\pi^2} N_s^2 \int_0^R dx x^2 \rho_t(x) \tag{7.2}$$

$$v_b = \frac{N_s^4}{64f^4\pi^4}\frac{1}{4\omega_{\mathbf{k}}}\int_0^\infty dq \frac{q^2}{\omega_{\mathbf{q}}}\frac{(\omega_{\mathbf{k}}+\omega_{\mathbf{q}})^2}{(\omega_{\mathbf{k}}-\omega_{\mathbf{q}})}\left[\int_0^R dx x^2 \rho_t(x) j_0(qx)\right]^2 (2\delta_{i_M,i_{M'}} - \lambda^I_{WT}) \tag{7.3}$$

$$v_c = \frac{N_s^4}{64f^4\pi^4}\frac{1}{4\omega_{\mathbf{k}}}\int_0^\infty dq \frac{q^2}{\omega_{\mathbf{q}}}\frac{(\omega_{\mathbf{k}}-\omega_{\mathbf{q}})^2}{(\omega_{\mathbf{k}}+\omega_{\mathbf{q}})}\left[\int_0^R dx x^2 \rho_t(x) j_0(qx)\right]^2 (-2\delta_{i_M i_{M'}} - \lambda^I_{WT}) \tag{7.4}$$

$$v_e = -\frac{\delta_{i_M i_{M'}}}{64f^4\pi^4}\frac{N_s^4}{\omega_{\mathbf{k}}}\int_0^\infty dq \frac{q^4}{\omega_{\mathbf{q}}}\left(\frac{25}{3}\frac{1}{-\omega_{\mathbf{q}}}\right)\left[\int_0^R dx x^2 \rho_{pv}(qx)\right]^2 \tag{7.5}$$

$$v_e(\Delta) = -\frac{\delta_{i_M i_{M'}}}{64f^4\pi^4}\frac{N_s^4}{\omega_{\mathbf{k}}}\int_0^\infty dq \frac{q^4}{\omega_{\mathbf{q}}}\left(\frac{32}{3}\frac{1}{m_N - m_\Delta - \omega_{\mathbf{q}}}\right)\left[\int_0^R dx x^2 \rho_{pv}(qx)\right]^2 \tag{7.6}$$

$$v_{f(a)} = \frac{N_s^4}{64f^4\pi^4}\frac{25}{9}\frac{1}{2\omega_{\mathbf{k}}}\int_0^\infty dq \frac{q^4}{\omega_{\mathbf{q}}^4} e^{-R_\pi^2 q^2/6.}\left[\int_0^R dx x^2 \rho_{pv}(qx)\right]^2 \left\{\delta_{i_M,i_{M'}}\left(-10m_\pi^2 + 3\omega_{\mathbf{k}}^2 + 3(\omega_{\mathbf{q}}^2 - |\boldsymbol{q}|^2)\right) + 4\lambda^I_{WT}\omega_{\mathbf{k}}\omega_{\mathbf{q}}\right\} \tag{7.7}$$

$$v_{f(b)} = -\frac{N_s^4}{64f^4\pi^4}\frac{25}{9}\frac{1}{4\omega_{\mathbf{k}}}\int_0^\infty dq \frac{q^4}{\omega_{\mathbf{q}}^4} e^{-R_\pi^2 q^2/4.}\left[\int_0^R dx x^2 \rho_{pv}(qx)\right]^2 \delta_{i_M i_{M'}}\left(-10m_\pi^2 + 3\omega_{\mathbf{k}}^2 - 3(\omega_{\mathbf{q}}^2 + |\boldsymbol{q}|^2)\right) \tag{7.8}$$

$$v_{f(a)}(\Delta) = \frac{N_s^4}{64f^4\pi^4}\frac{32}{9}\frac{1}{2\omega_{\mathbf{k}}}\int_0^\infty dq \frac{q^4}{\omega_{\mathbf{q}}^2}\frac{e^{-R_\pi^2 q^2/6.}}{(m_\Delta - m_N + \omega_{\mathbf{q}})^2}\left[\int_0^R dx x^2 \rho_{pv}(qx)\right]^2 \left\{\delta_{i_M i_{M'}}\left(-10m_\pi^2 + 3\omega_{\mathbf{k}}^2 - 3(\omega_{\mathbf{q}}^2 + |\boldsymbol{q}|^2)\right) + 4\lambda^I_{WT}\omega_{\mathbf{k}}\omega_{\mathbf{q}}\right\} \tag{7.9}$$

$$v_{f(b)}(\Delta) = \frac{N_s^4}{64f^4\pi^4}\frac{32}{9}\frac{1}{2\omega_{\mathbf{k}}}\int_0^\infty dq\frac{q^4}{\omega_{\mathbf{q}}^2}\frac{e^{-R_\pi^2 q^2/4}\cdot[\int_0^R dx x^2\rho_{pv}(qx)]^2}{(m_\Delta - m_N + 2\omega_{\mathbf{q}})(m_\Delta - m_N + \omega_{\mathbf{q}})}$$
$$\delta_{i_M i_{M'}}\left(-10m_\pi^2 + 3\omega_{\mathbf{k}}^2 - 3(\omega_{\mathbf{q}}^2 + |\boldsymbol{q}|^2)\right) \quad (7.10)$$

$$V_g = -\frac{\delta_{i_M i_{M'}}}{64f^4\pi^4}\frac{N_s^4}{2\omega_{\mathbf{k}}}\int_0^R dx x^2\rho_t^2(x)\,\pi \quad (7.11)$$

$$V_h = \frac{N_s^6}{384\pi^4 f^4}\int_0^R dz\, z^2\rho_t(z)$$
$$\int_0^\infty dq\frac{q^4}{\omega_{\mathbf{q}}}\frac{[\int_0^R dx x^2\rho_{pv}(qx)]^2}{(m_N - m_{\alpha_2} - \omega_{\mathbf{q}})\,(m_N - m_{\alpha_3} - \omega_{\mathbf{q}})}SI_\alpha \quad (7.12)$$

Here, the numerical factors SI_α in eqn (7.12) are those of the spin-isospin factors given in Table 4.5. In Table 7.5, we give numerical values of the potentials at threshold energy.

One can now divide the potential into three different categories, depending on the behaviour of vanishing external pion energy limit $\omega_{\mathbf{k}} \approx 0$. i.e.

(i) Independent of this limit

(ii) goes to zero in that limit

(iii) Becomes infinite in that limit.

In order to see the dependence of the external pion energy, lets rewrite v_a to v_f tabulated in eqns (7.2-7.12) as follows:

$$v_a = \frac{N_s^2}{8\pi^2 f^2}\mathcal{I}_t(x)\lambda_{WT}^I \quad (7.13)$$

$$v_b = \frac{N_s^4}{64f^4\pi^4}\frac{1}{4}\left(\frac{1}{\omega_{\mathbf{k}}}\mathcal{I}_0 - \mathcal{I}_1 - 4\mathcal{I}_2^{(b)}\right)[-2\delta_{i_M,i_{M'}} + \lambda_{WT}^I] \quad (7.14)$$

$$v_c = \frac{N_s^4}{64f^4\pi^4}\frac{1}{4}\left(\frac{1}{\omega_{\mathbf{k}}}\mathcal{I}_0 + \mathcal{I}_1 - 4\mathcal{I}_2^{(c)}\right)[-\delta_{i_M,i_{M'}} - \lambda_{WT}^I] \quad (7.15)$$

$$v_e = \frac{N_s^4}{64f^4\pi^4}\frac{25}{3}\frac{1}{\omega_{\mathbf{k}}}\mathcal{I}_e^{(N)}\;\delta_{i_M,i_{M'}} \quad (7.16)$$

$$v_e(\Delta) = \frac{N_s^4}{64f^4\pi^4}\frac{32}{3}\frac{1}{\omega_{\mathbf{k}}}\mathcal{I}_e^{(\Delta)}\;\delta_{i_M,i_{M'}} \quad (7.17)$$

$$v_{f(a)} = \frac{N_s^4}{64f^4\pi^4}\frac{25}{18}\Big[\,4\,\lambda_{WT}^I\,\mathcal{F}_{3a}^{(N)}+ \left\{-10\frac{m_\pi^2}{\omega_{\mathbf{k}}}\mathcal{F}_{1a}^{(N)}+3\omega_{\mathbf{k}}\mathcal{F}_{1a}^{(N)}+\frac{3}{\omega_{\mathbf{k}}}\mathcal{F}_{2a}^{(N)}\right\}\delta_{i_M,i_{M'}}\Big] \quad (7.18)$$

$$v_{f(a)}(\Delta) = \frac{N_s^4}{64f^4\pi^4}\frac{32}{18}\Big[\,4\,\lambda_{WT}^I\mathcal{F}_{3a}^{(\Delta)}+ \left\{-10\frac{m_\pi^2}{\omega_{\mathbf{k}}}\mathcal{F}_{1a}^{(\Delta)}+3\omega_{\mathbf{k}}\mathcal{F}_{1a}^{(\Delta)}+\frac{3}{\omega_{\mathbf{k}}}\mathcal{F}_{2a}^{(\Delta)}\right\}\delta_{i_M,i_{M'}}\Big] \quad (7.19)$$

$$v_{f((b)+(c))} = \frac{N_s^4}{64f^4\pi^4}\frac{25}{18}\left\{-10\frac{m_\pi^2}{\omega_{\mathbf{k}}}\mathcal{F}_{1b}^{(N)}+3\omega_{\mathbf{k}}\mathcal{F}_{1b}^{(N)}-\frac{3}{\omega_{\mathbf{k}}}\mathcal{F}_{2b}^{(N)}\right\}\delta_{i_M,i_M} \quad (7.20)$$

$$v_{f((b)+(c))}(\Delta) = \frac{N_s^4}{64f^4\pi^4}\frac{32}{9}\left\{-10\frac{m_\pi^2}{\omega_{\mathbf{k}}}\mathcal{F}_{1b}^{(\Delta)}+3\omega_{\mathbf{k}}\mathcal{F}_{1b}^{(\Delta)}-\frac{3}{\omega_{\mathbf{k}}}\mathcal{F}_{2b}^{(\Delta)}\right\}\delta_{i_M,i_M} \quad (7.21)$$

$$v_g = \frac{N_s^4}{64f^4\pi^4}\frac{\pi}{2}\frac{1}{\omega_{\mathbf{k}}}\mathcal{I}_g(x)\delta_{i_M,i_{M'}} \quad (7.22)$$

$$v_h = \frac{N_s^4}{64f^4\pi^4}\frac{N_s^2}{6}\mathcal{I}_t(z)\mathcal{I}_h^{(N)}(x)SI_\alpha \quad (7.23)$$

$$v_h(\Delta) = \frac{N_s^4}{64f^4\pi^4}\frac{N_s^2}{6}\mathcal{I}_t(z)\mathcal{I}_h^{(\Delta)}(x)SI_\alpha \quad (7.24)$$

The integrals $\mathcal{I},\mathcal{F}$ are given in Appendix A.4. It can be seen that the Weinberg-Tomozawa term v_a and v_h are independent of this $m_\pi^2 \approx 0$ (i.e. $\omega_{\mathbf{k}} \approx 0$) limit. The troublesome terms that are infinite in the soft-pion limit $m_\pi^2 \approx 0$ come from v_b, v_c, v_e, v_f and v_g. Numerically, The sum of troublesome terms from v_b and v_c cancel with v_g since

$$\mathcal{I}_3 \approx \frac{\pi}{2}\mathcal{I}_g(x).$$

This is not surprising since the contact term v_g is designed to cancel the terms that are infinite in the soft pion limit arising from iteration of v_a, i.e. v_b and v_c [Gui 85]. However, as shown below, the troublesome term from v_e does not cancel with that of v_f. Therefore, in contrast to the transition amplitude for the Weinberg-Tomozawa term, which is independent of the soft-pion limit, the transition amplitude of order

$\frac{1}{(2f)^4}$ is sensitive to the soft pion limit.

$$\begin{aligned}
&\frac{N_s^4}{64f^4\pi^4}\frac{1}{\omega_{\mathbf{k}}}\Big\{-\mathcal{I}_0+\frac{\pi}{2}\mathcal{I}_g(x)+\frac{25}{3}(\mathcal{I}_e^{(N)}+\frac{1}{2}\mathcal{F}_{2a}^{(N)}-\frac{1}{2}\mathcal{F}_{2b}^{(N)})+\\
&\qquad\qquad\frac{32}{3}(\mathcal{I}_e^{(\Delta)}+\frac{1}{2}\mathcal{F}_{2a}^{(\Delta)}-\frac{1}{2}\mathcal{F}_{2a}^{(\Delta)})\Big\}\\
=\;&\frac{0.08558}{m_\pi}\{-0.0033+0.2658+0.4070\}\\
=\;&0.08104
\end{aligned}$$

Table 7.5: The potential strength at threshold energy. The Δ in brackets denotes for inclusion of the Δ intermediate state in that diagram.

Diagram	*Total Isospin*		
	1/2	3/2	Iso-scalar
v_a	-0.11372	0.05686	0.00000
v_b	-0.07386	-0.01847	0.00000
v_c	0.00473	-0.00236	-0.00473
v_e	0.00000	0.00000	0.06909
$v_e(\Delta)$	0.00000	0.00000	0.05914
v_f	-0.02096	0.01048	-0.04742
$v_f(\Delta)$	-0.00894	0.00446	-0.02698
v_g	0.00000	0.00000	0.02299
v_h	0.00757	-0.00379	0.00000
$v_h(\Delta)$	0.01365	-0.00683	0.00000

Table 7.6: S-wave Scattering Lengths at Threshold in Born approximation

	a_{11}	a_{31}
WT Term (v_a) only	0.208	-0.104
Full-set (v_a to v_h)	0.219	-0.206

7.2.3 Phase shifts and scattering lengths at finite energy

We now calculate the phase shifts and scattering lengths using various propagators. The scattering lengths are given in Table 7.7. The phase shifts plotted in Figure

7.2 corresponds to using only the WT term (Fig. 4.1a) as the driving potential. For the WT term as driving potential with various propagators, it is found that the BbS propagator gives the best scattering lengths. The phase shifts plotted in Fig. 7.3 are the results from the full set of potentials derived in Chapter 4 to order $\frac{1}{(2f)^4}$, while the contributions from Δ intermediate states in Figs. 4.1e and 4.1f are omitted. In Figure 7.4, we plot the phase shifts using various propagators with the fullset of potentials including Δ contributions in Figs.4.1e and 4.1f. From Figs. 7.3 and 7.4, we see that the inclusion of the Δ in potentials has no significant effect on phase shifts however Table 7.7 shows an improvement in the scattering lengths. All of the CBM results tabulated in Table 7.7 were calculated for a bag radius $R = 1$ fm and pion coupling constant $f = 93$ MeV.

Table 7.7: Scattering lengths for CBM calculation (m_π^{-1})

	a_1	a_3	Remarks
WT term (LS)	0.3006	−0.0616	v_a only
WT term (CJ)	0.2042	−0.0683	v_a only
WT term (BbS)	0.1942	−0.0707	v_a only
Fullset-1 (LS)	0.2320	−0.0941	no Δ in v_e and v_f
Fullset-1 (CJ)	0.1532	−0.1137	no Δ in v_e and v_f
Fullset-1 (BbS)	0.1443	−0.1172	no Δ in v_e and v_f
Fullset-2 (LS)	0.1810	−0.1195	Δ in v_e and v_f
Fullset-2 (CJ)	0.1148	−0.1486	Δ in v_e and v_f
Fullset-2 (BbS)	0.1069	−0.1538	Δ in v_e and v_f

7.2.4 Renormalised S-wave scattering

We derived the renormalised Weinberg-Tomozawa term in Chapter 6. We present the renormalised scattering lengths in Table 7.8 and the phase shifts obtained for different propagators in Fig.7.5. The phase shifts for different bag radii for unrenormalised WT term and renormalised WT term are given in Figs. 7.6 and 7.7 respectively. In Fig. 7.7 it can be seen that the phase shifts are insensitive to the bag

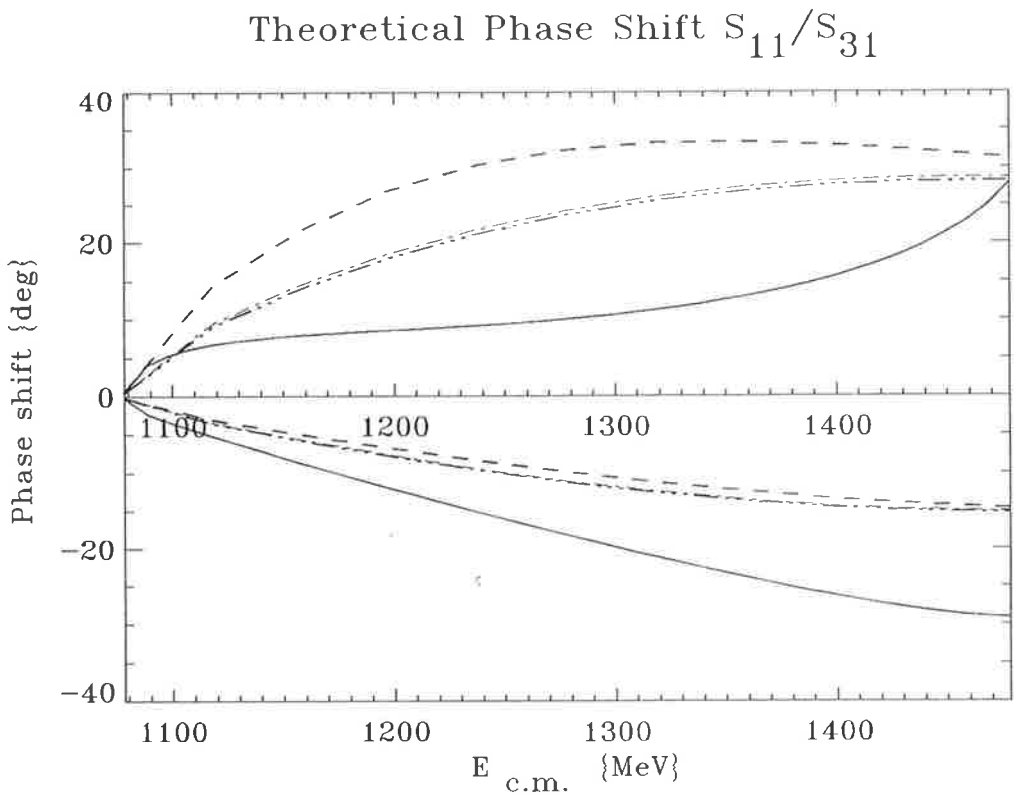

Figure 7.2: S-wave phase shifts using only the Weinberg-Tomozawa term as the driving potential; solid line experimental value; dashed line Lippmann-Schwinger(LS) propagator; dot-dash Smooth(CJ) propagator; 3-dot-dash Blankenbecler-Sugar(BbS) propagator.

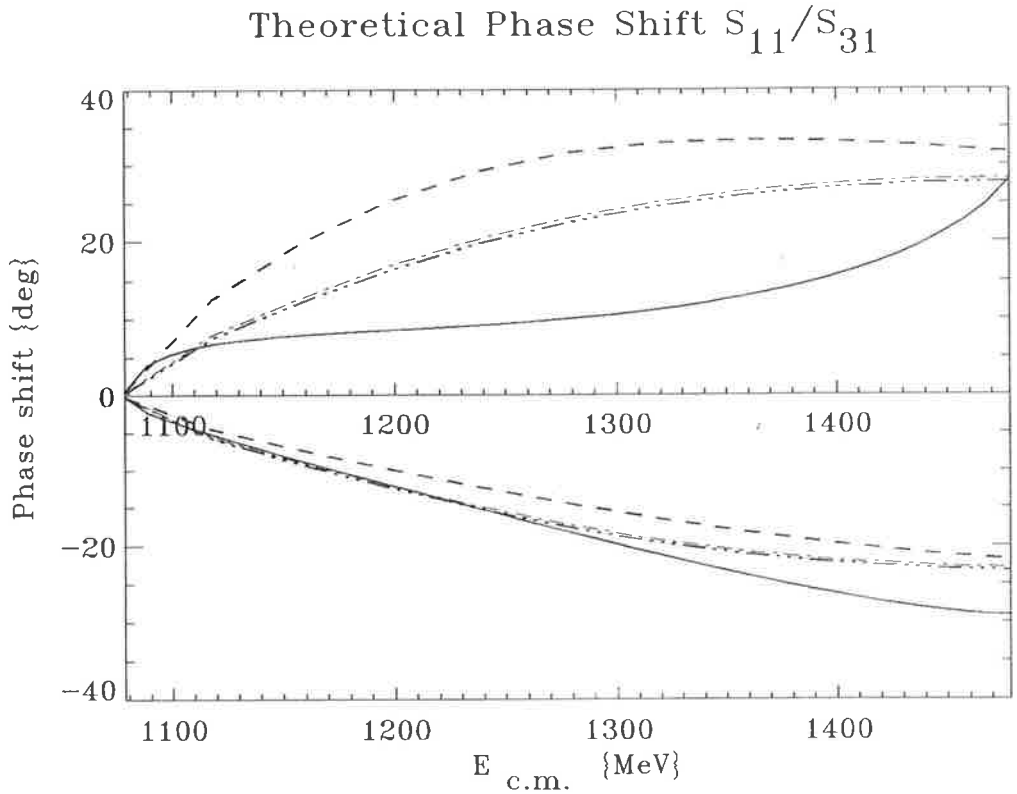

Figure 7.3: S-wave phase shifts using the full set of theoretical driving potentials; solid line experimental value; dash line Lippmann-Schwinger(LS) propagator; dot-dash, Smooth(CJ) propagator; 3-dot-dash, Blankenbecler-Sugar(BbS) propagator.

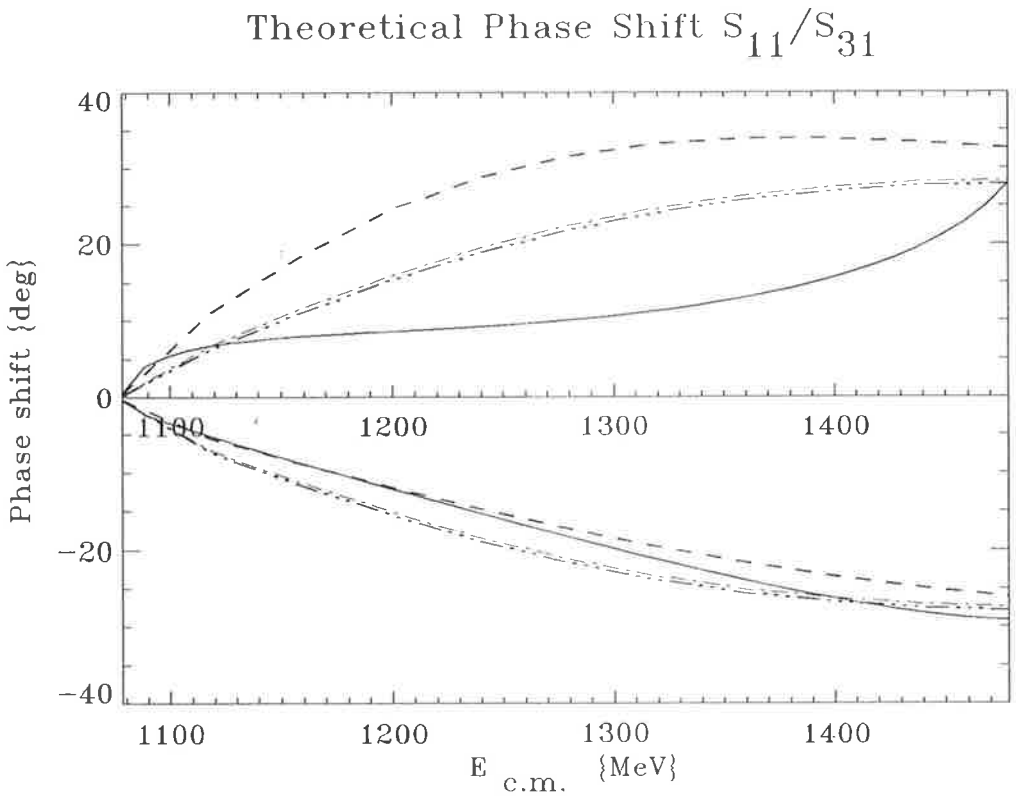

Figure 7.4: S-wave theoretical phase shifts with the full set of potentials including the Δ contributions. The same symbols are used here as in previous Figures.

radius when the WT interaction gets renormalised. This is in contrast with unrenormalised WT term in Fig. 7.6 for which the phase shifts show a strong dependence on the bag radius.

Table 7.8: S-wave renormalised scattering lengths with various propagators.

Method	a_1	a_3
LS Propagator	0.1856	−0.0490
CJ Propagator	0.1430	−0.0537
BbS Propagator	0.1380	−0.0545

Table 7.9: S-wave renormalised scattering lengths for different bag radii. The LS propagator is used.

$BagRadius(fm^{-1})$	a_1	a_3
0.7	0.1353	−0.0305
0.8	0.1613	−0.0378
0.9	0.1792	−0.0436
1.0	0.1856	−0.0490

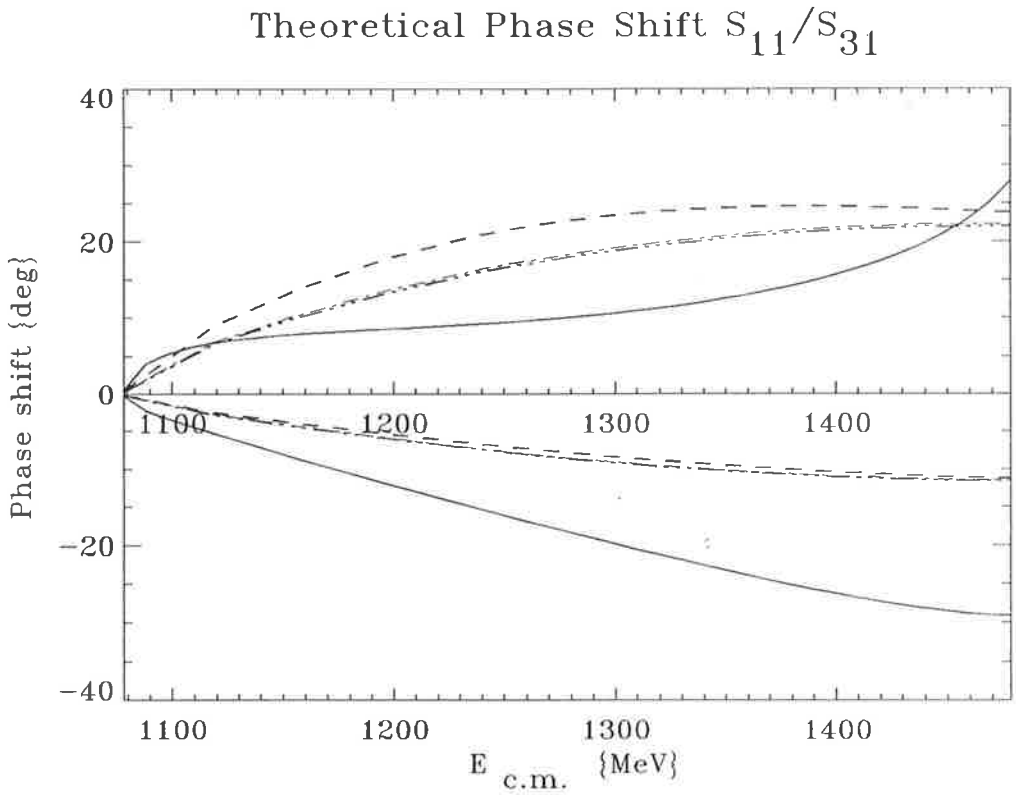

Figure 7.5: The phase shifts obtained for the renormalised Weinberg-Tomozawa term with various propagators. The notation for different propagators is as before.

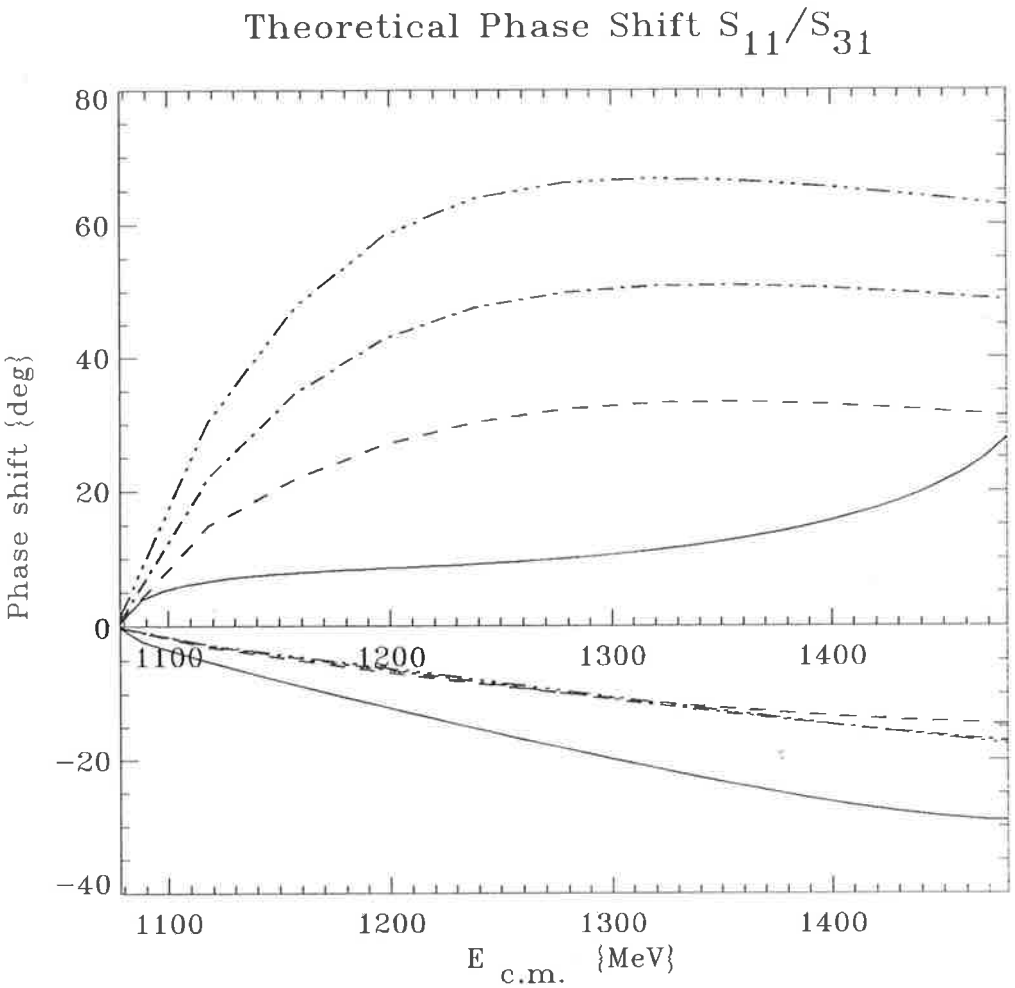

Figure 7.6: The phase shifts for different bag radii with the un-renormalised Weinberg-Tomozawa term; dash line for R=1.0; dot-dash for R=0.8 and 3-dot dash for R=0.7 fm.

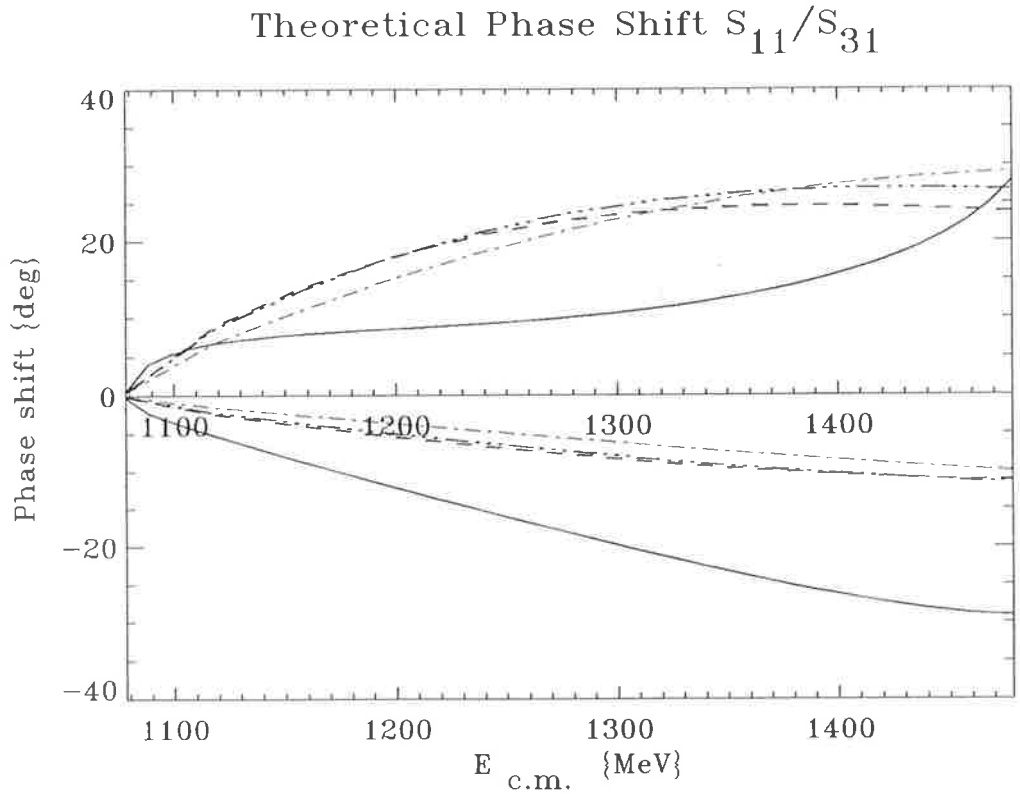

Figure 7.7: The phase shifts for different bag radii with the renormalised Weinberg-Tomozawa term; dash line for R=1.0; dot-dash for R=0.7 and 3-dot dash for R=0.9fm.

7.3 P-wave Scattering Lengths and Phase Shifts

7.3.1 Phenomenological Results

The P-wave phenomenological scattering parameters can be found in [Tho 76]. The form factors used in those potentials are:

$$g(k) = S_1 k/(\alpha_1^2 + k^2)^2 + S_2 k^3/(\alpha_2^2 + k^2)^2. \tag{7.25}$$

Table 7.10: The parameter for the P-wave scattering

Channel	S_1	α_1	S_2	α_2
P_{33}	0.5403	1.475	1.0583	3.400
P_{31}	4.290	2.059	0.0	0.0
P_{13}	1.557	1.224	3.659	1.945
P_{11}	0.3959	1.074	0.0	0.0

The parameters $S_1, \alpha_1, S_2, \alpha_2$ for eqn (7.25) are given in Table 7.10. The phenomenological potentials are used in testing various propagators. It is found that for P_{33} phase shifts are not reproduced for the CJ and BbS propagators in Fig. 7.8. These two relativistic propagators behave differently for the P_{13} and P_{31} cases as well. In Fig. 7.10 different phase shifts among propagators is observed for P_{13} channel while almost the same behaviour was shown for P_{31} in Fig. 7.11. The scattering volumes evaluated by various propagators are given in Table 7.11.

Table 7.11: Phenomenological scattering volumes (m_π^{-3}).

Propagator	a_{11}	a_{31}	a_{13}	a_{33}
Experiment	-0.101	-0.029	-0.038	0.215
LS	-0.05946	-0.4562	-0.03545	0.1853
CJ	-0.05991	-0.1645	-0.03735	-0.00474
BbS	-0.05996	-0.3798	-0.03767	-0.00389

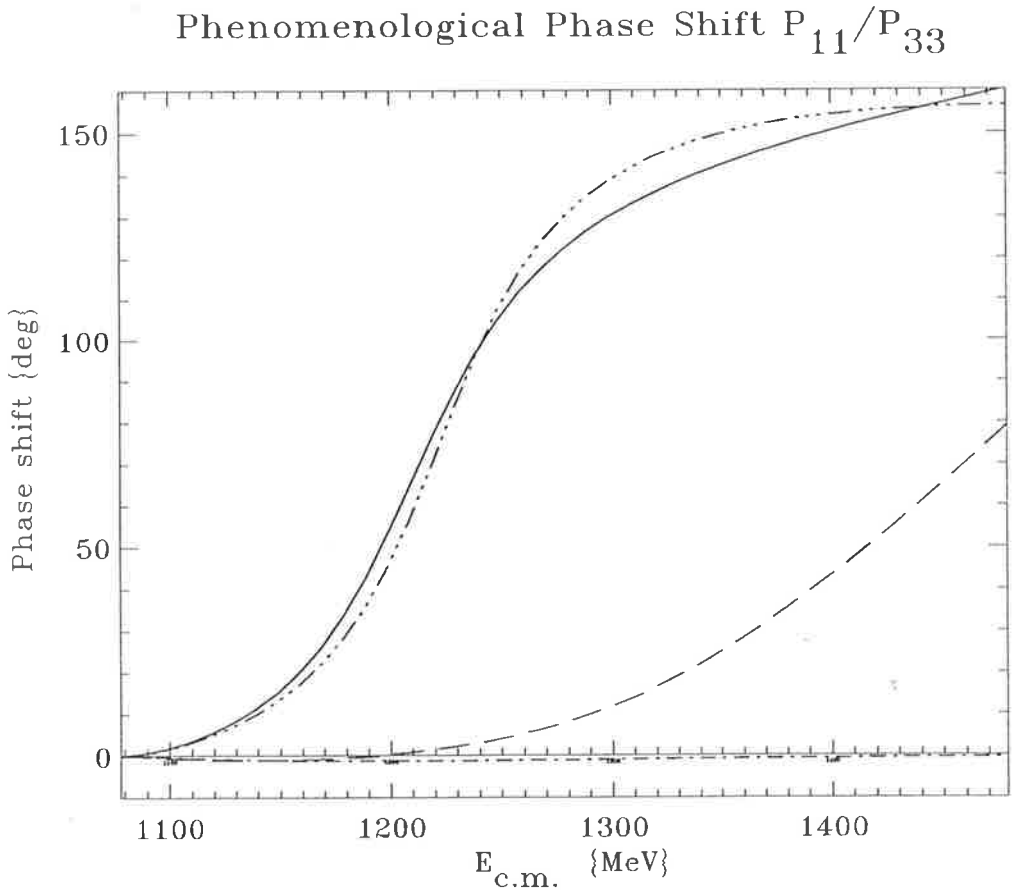

Figure 7.8: Phenomenological P_{11}/P_{33} phase shifts; solid line and long dash represents the P_{33} and P_{11} experimental phase shifts respectively; 3-dot dash and short dash represents phenomenological P_{33} and P_{11}. The LS propagator is used for the P_{33} calculation and the relativistic propagators do not produce a resonance.

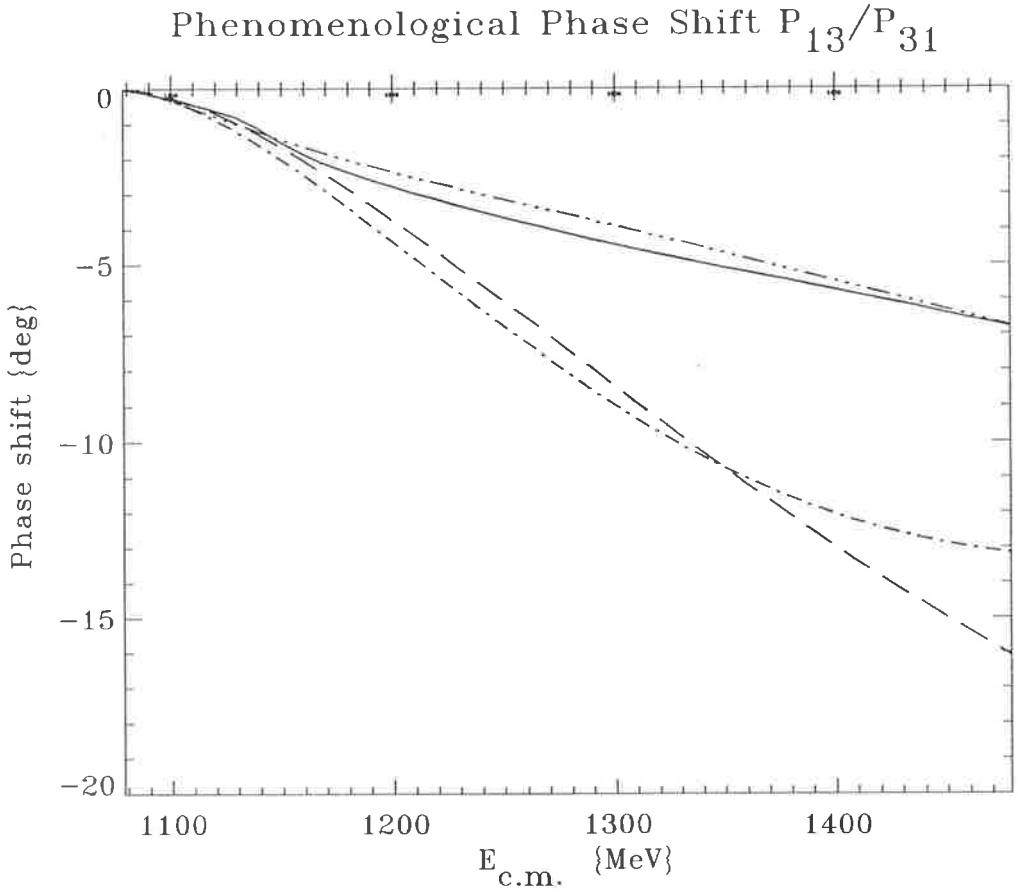

Figure 7.9: Phenomenological P_{13} and P_{31} phase shifts; solid line and long dash line represents experimental P_{13} and P_{31} phase shifts; dot dash line and 3-dot dash line represents the phenomenological P_{31} and P_{13} phase shifts respectively.

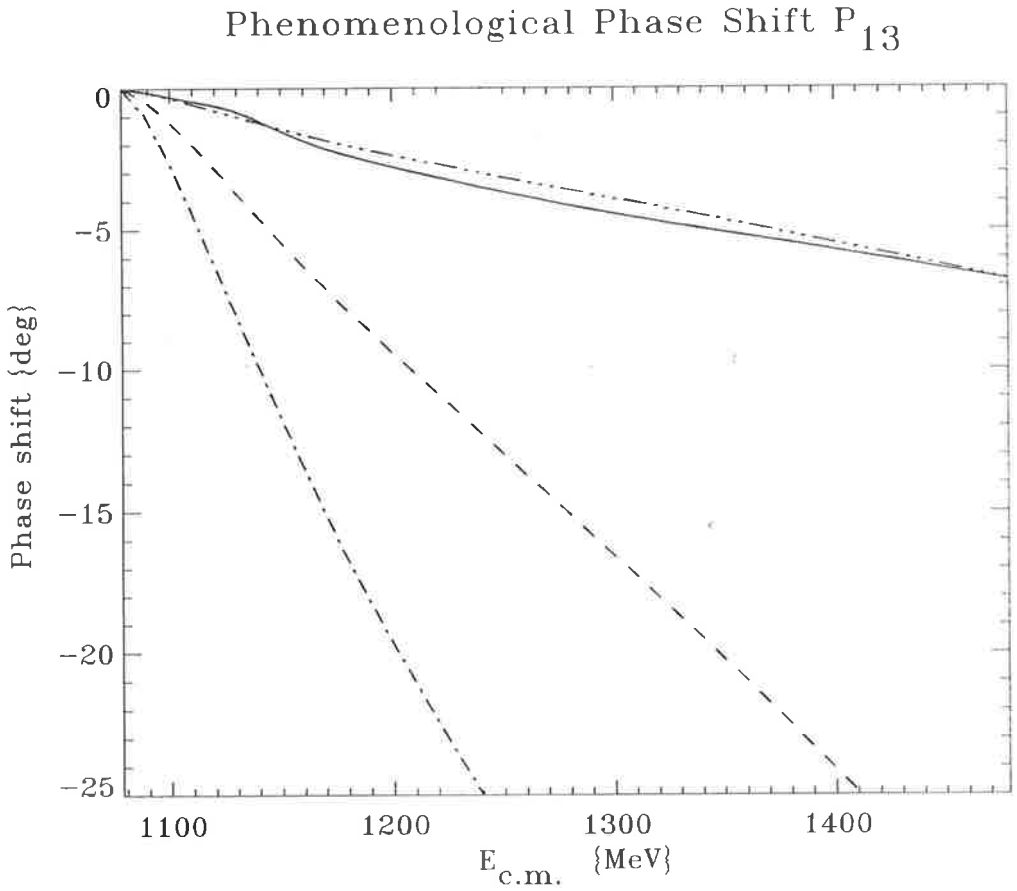

Figure 7.10: Phenomenological P_{13} phase shifts with different propagators; solid line the experimental; 3-dot dash line LS propagator; dash and dot dash lines CJ and BbS propagators respectively.

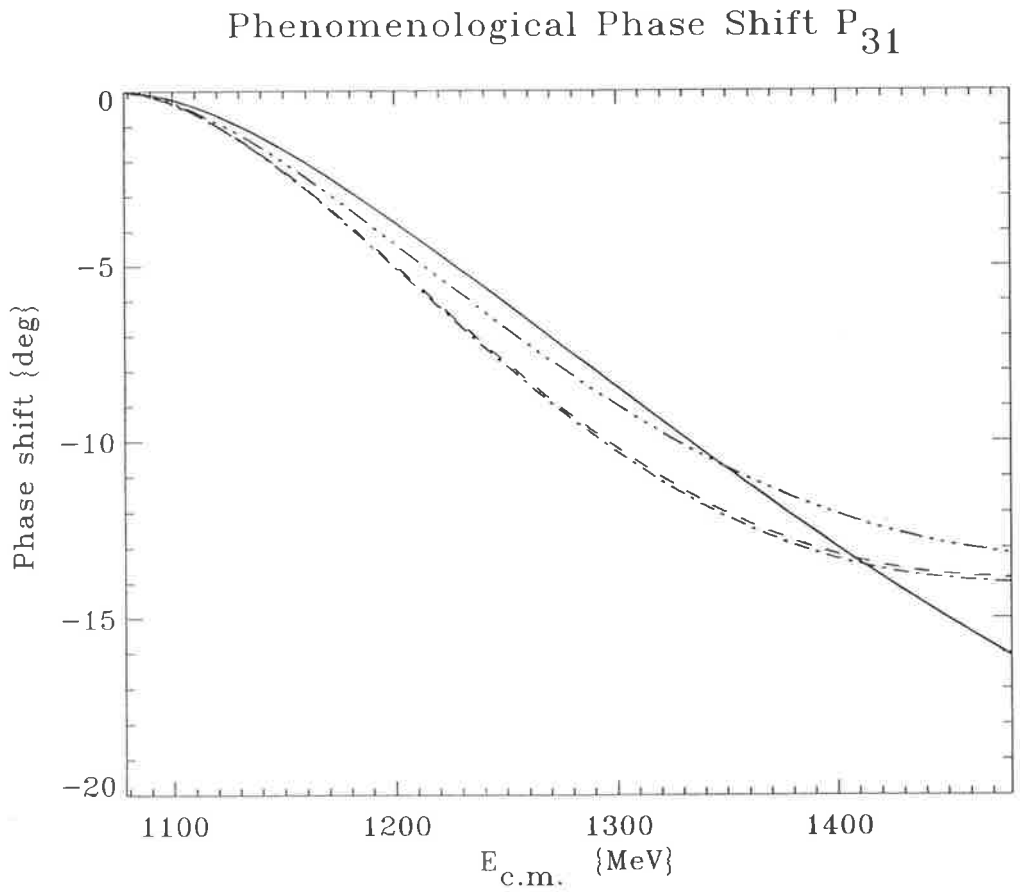

Figure 7.11: Phenomenological P_{31} phase shifts with different propagators; solid line the experimental; 3-dot dash line LS propagator; dash and dot dash lines CJ and BbS propagators respectively.

7.3.2 Theoretical P-wave results

For the theoretical P-wave calculations, we used the CBM potentials derived in Chapter 5 as the driving potential with the various propagators given in Chapter 3. The scattering volumes are given in Table 7.12. The phase shifts are plotted in Figures 7.12,7.13,7.14. In Fig. 7.12 phase shifts for P_{33} channel is given and it is found that the LS propagator as well as the relativistic propagators produce the resonance. This is in contrast with the phenomenological potential that fails to produce the resonance for the relativistic propagators in Fig. 7.8. In Fig. 7.12 we only show the phase shifts for potential with parameters (coupling constant and mass of Δ) unadjusted.

The CBM has been very successful in describing P-waves. The first calculation for P_{33} resonance using a surface coupling version of CBM was done by Thomas *et al* [Tho+80]. The calculation for the P-wave scattering using volume coupling version was done in Ref. [Tho+86]. When we use the Lagrangian of Kalbermann and Eisenberg and take the interaction to order $\frac{1}{(2f)^2}$, the potentials are the same as those of [Tho+86]. Those calculations (and ours too) give good agreement with the experimental phase shifts except for the P_{11} channel. Our point in repeating the calculation was not only to provide a comprehensive presentation but also to test the different propagators for the P-waves.

We also noticed that Pearce and Afnan [PA 86, PA 89] have made a serious investigation of the P_{11} channel. In their work, they demand that the renormalization procedure should be consistent with the LS equation and used modified version of LS equation. A reasonable agreement was found for the P_{11} channel for $T_\pi < 400$ MeV.

For the P-wave scattering volumes, it is well known that Born approximation to order $\frac{1}{(2f)^2}$ produces a good result in usual covariant calculations [EW 88]. Our experience in S-wave tell us that the scattering volume produced by LS equation will

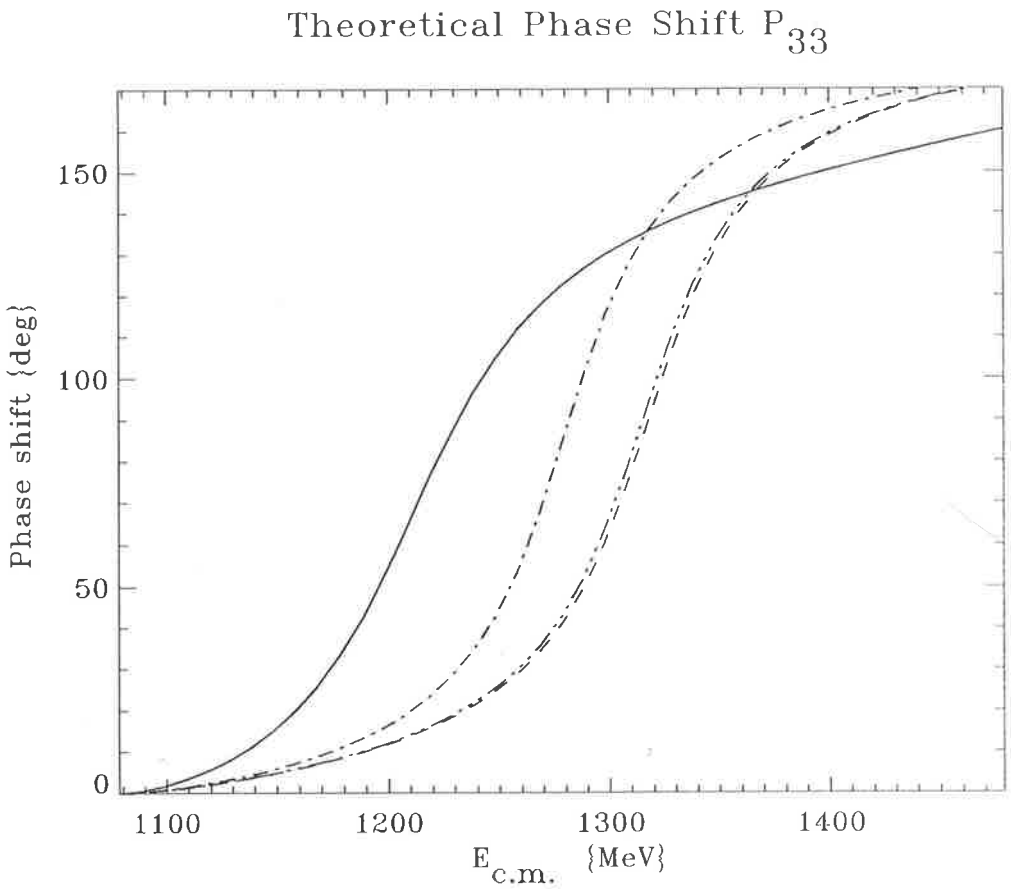

Figure 7.12: Theoretical P_{33} phase shifts; solid line experimental; long dash-dot line LS propagator; 3-dot-dash and dash lines CJ and BbS propagators respectively.

be different from those in Born approximation. Although previous authors do not mention the problem [Tho+80, Tho+86, PA 86, PA 89], we expect (and shown in Table 7.12) that the scattering volumes are not as good in agreeing with experiments.

Table 7.12: Theoretical scattering volumes(m_π^{-3}).

Propagator	P_{11}	P_{31}	P_{13}	P_{33}
LS	-0.0386	-0.0370	-0.0356	0.1024
CJ	-0.0715	-0.0407	-0.0365	-0.0954
BbS	-0.0785	-0.0414	-0.0366	-0.0943

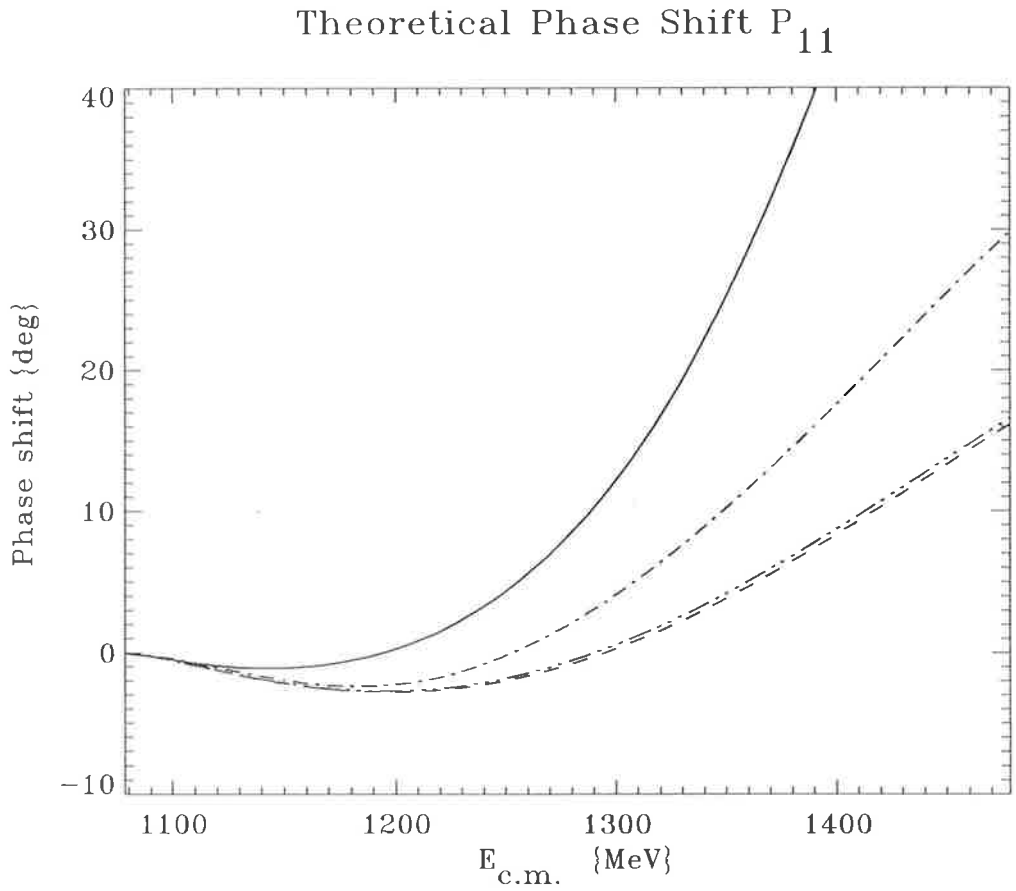

Figure 7.13: Theoretical P_{11} phase shifts; solid line experimental; long dash-dot line LS propagator; 3-dot-dash and dash lines CJ and BbS propagators respectively.

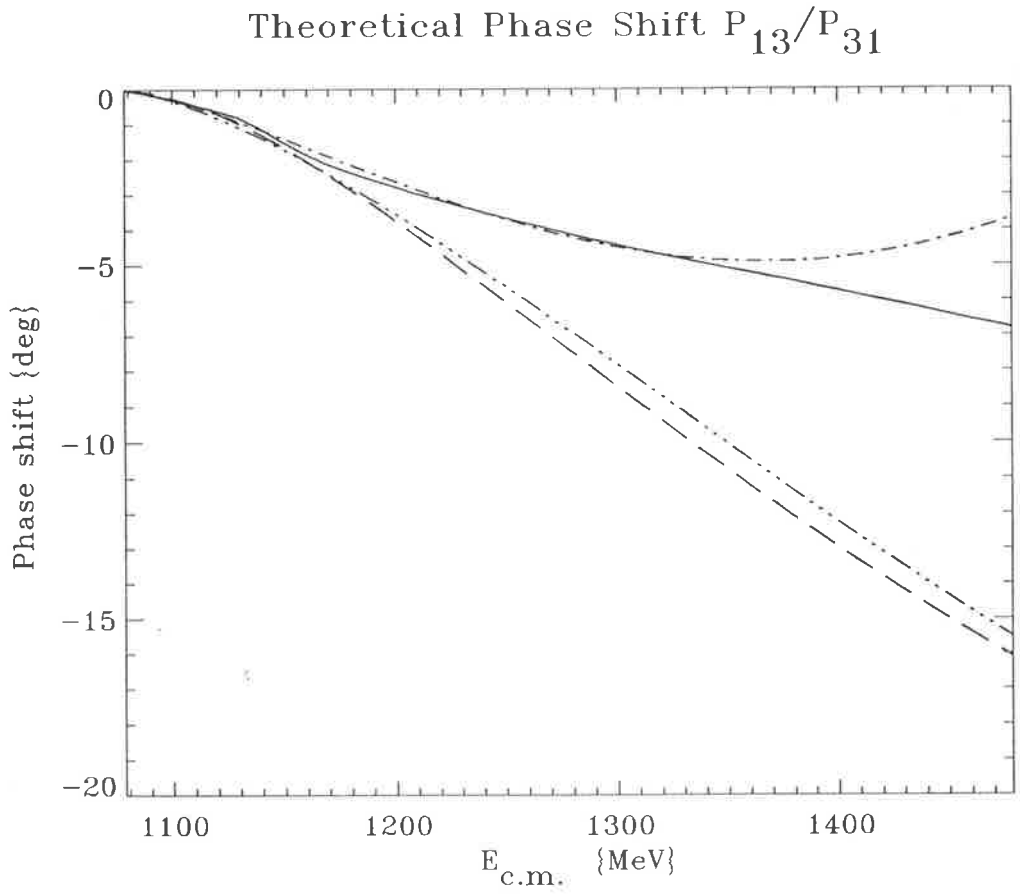

Figure 7.14: Theoretical P_{13}/P_{31} phase shifts; solid line experimental P_{13}; long-dash for experimental P_{31}; dash-dot theoretical P_{13}; 3-dot-dash theoretical P_{31}. LS propagator is used for this graph. The use of relativistic propagators do not change phase shifts significantly.

Chapter 8

Discussion and Outlook

In this chapter we present discussion of the result and give an outlook for the πN calculations. We will firstly look at the result of carrying out the calculation to order $\frac{1}{(2f)^4}$ in S-wave. In Born approximation, the scattering lengths are not improved by taking the calculation to higher order. In Table 7.6 we can see that the Adler consistency condition ($a_1 + 2a_3 = 0$, or that the threshold scattering lengths should be purely isovector) has been badly violated by this. It has also seen in Section 7.2.2 that in the soft pion limit, $m_\pi^2 \approx 0$, the badly behaved components(which become infinite in the soft pion limit) arise from v_b, v_c, v_e, v_f and v_g. The cancellation of the isoscalar piece, v_g, by the badly behaved piece of v_b and v_c can be proved explicitly [Gui 85]. We prove numerically that the badly behaved piece of v_f is not guaranteed to cancel exactly those of v_e. Nevertheless, these two diagrams at threshold energy do tend to cancel as advocated by Cooper and Jennings [CJ 86].

The phase shifts obtained by using higher order interactions are not much improved over the results of the leading order, Weinberg-Tomozawa term. However it is remarkable that the leading order results are not greatly altered by adding higher order graphs, as can be seen from Figs. 7.2 and 7.3. It is also seen that when we add the Δ contribution in the graphs, the overall magnitude over phase shifts is not greatly altered but the scattering lengths are improved (Table 7.7).

A nice feature of the CBM is that it treats the nucleon and Δ on the same footing as required by QCD [Tho+80, Tho 84]. This also prevents double counting in LS type equations [Hol+87]. The improvement over scattering lengths in Table 7.7 when we add the Δ contribution shows the Lagrangian of Kalbermann and Eisenberg has kept this nice feature of the CBM.

We therefore conclude that for Chiral Bag Lagrangians it is possible to guarantee convergence by adding higher order graphs. The overall magnitude of the phase shifts in Figs. 7.3 and 7.4 proves that the inclusion of higher order graphs does not induce significance alterations to the leading order result of Fig. 7.2.

One major drawback in our work is not including center of mass and recoil corrections to each higher order diagram. All graphs are calculated in the static approximation for the nucleon. While, those corrections are expected to be small [Tho 84] they may be very important in the rather subtle soft pion limit.

As for the question of unitarity, we compare the results from covariant 3-dimensional propagators and the Lippmann Schwinger propagators in Figs. 7.1,7.3 and Tables 7.4, 7.7. There are significant differences in results between LS and relativistic propagators in Figs. 7.1 and 7.3. There is some slight improvement when we use a smooth propagator with leading order, Weinberg-Tomozawa interactions, as has been speculated by Cooper and Jennings [CJ 88]. This is not the case when we use the full set of diagrams to calculate phase shifts and scattering lengths as shown in Fig. 7.4 and Table 7.7. The relativistic propagators underestimate a_1 and overestimate a_3 as we see in Table 7.7.

For completeness, we calculated the P-wave interaction and used it with various propagators. It was demonstrated that the P-wave phenomenological separable potentials are not reliable sources to learn potential strength and behaviour. This can be seen from Figs 7.8 and 7.10, where the P_{33} and P_{13} results are not well reproduced by relativistic propagators. In contrast, the theoretical P_{33} can be tested reliably by

both relativistic and LS propagators, as shown in Fig. 7.12 - although we need to fit the Δ mass for different propagators. There is still problem in scattering volumes for P-wave. Because of the richness of physical content of the higher order CBM diagrams that has been demonstrated in the S-wave calculations, one is encouraged to extend the calculation to order $\frac{1}{(2f)^4}$, including the resonances.

The renormalization for the S-wave Weinberg-Tomozawa term was calculated and tested numerically. The renormalised interaction over the Bag radius can be studied from Fig. 7.7 and Table 7.8. It is interesting to note that overall the phase shift is not significantly altered by changing the bag radius when the interaction gets renormalised. This is in contrast to the unrenormalised Weinberg-Tomozawa term, which shows a dependence on Bag radius as can be seen from Fig. 7.6.

From the overall picture of both S- and P-wave calculations, the CBM Lagrangian is reliable to calculate higher order graphs. This is not a new conclusion as previous workers, Kalbermann and Eisenbergs, [KE 83] pointed out a long time ago. Cancellations of higher order diagrams such as Fig. 4.1e and 4.1f can be considered as a major attribute of the chiral Lagrangians [Gro 82, CJ 86]. Numerically, the isoscalar contribution from v_e and v_f are large (Table 7.5). One of our dissatisfaction in calculating higher order graphs such as Fig. 4.1f is that we have to use an over simplified account of the $\pi\pi$ vertex. This kind of $\pi\pi$ interaction is also encountered in NN interaction as the correlated 2-pion resonance for the S-wave [Hol+87, PA 89]. In our calculation, the strength of v_f is greatly influenced by the assumption made on the $\pi\pi$ vertex. When we vary the form factor at the $\pi\pi$ vertex by altering pion radius, it shows a significant difference in the phase shifts, especially in the S_{11} channel in Fig. 8.2. Therefore a more careful analysis is necessary for the $\pi\pi$ interaction.

From Figs. 7.3, 7.4 and 8.2, the S_{31} channel calculations are in good agreement with the experiment. We therefore conclude that the remaining discrepancy in S_{11}

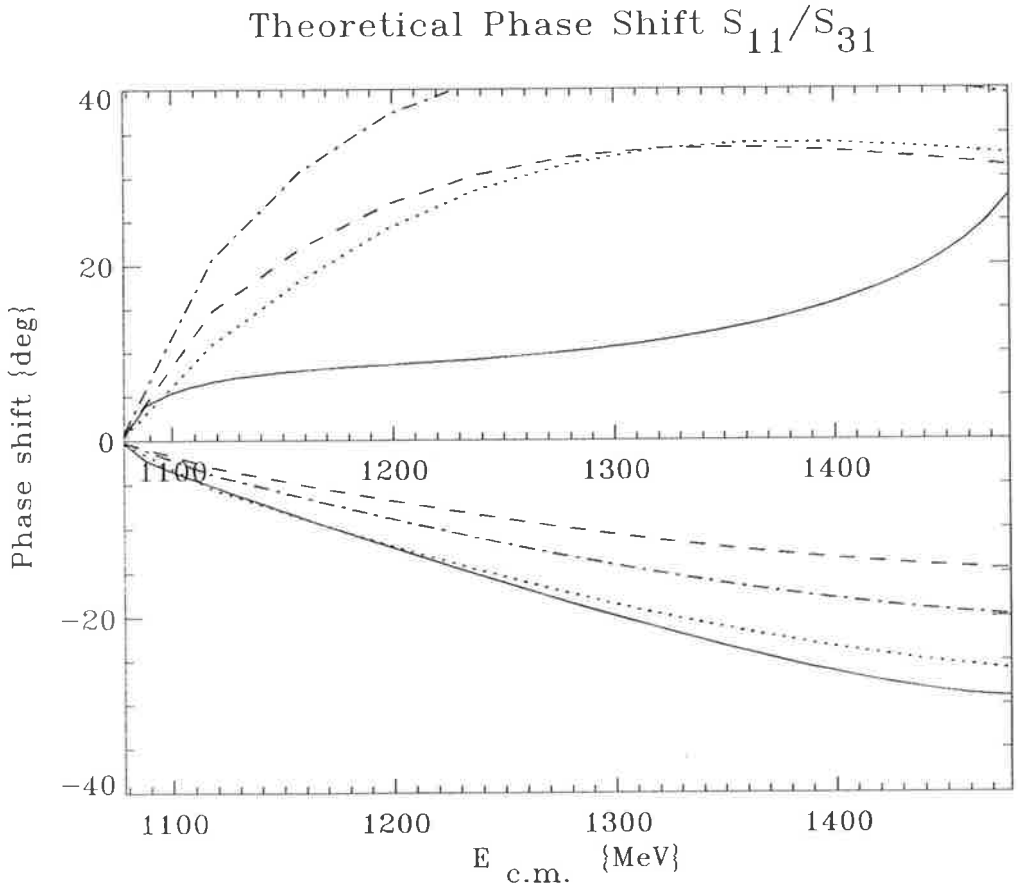

Figure 8.1: The phase shift obtained by turning off the isoscalar contributions from v_e and v_f; dashed line v_a only; dotted line full-set of driving potentials; dot-dash line, the isoscalar contribution from v_e and v_f turned off.

channel is due to N(1535) resonance and the strength of the $\pi\pi$ vertex.

The most challenging aspect of our work was to ensure that the Kalbermann and Eisenberg's Lagrangian does give the soft-pion limit. The troublesome part is clearly the isoscalar piece arising from Figs. 4.1e and f that would violate soft pion limit (becomes infinite in that limit). On the other hand, the isoscalar piece is necessary to produce scattering lengths and phase shifts at higher energies. This is shown in Fig.8.1 when we turn off the isoscalar contribution from v_e and v_f the phase shifts bend away from experiment.

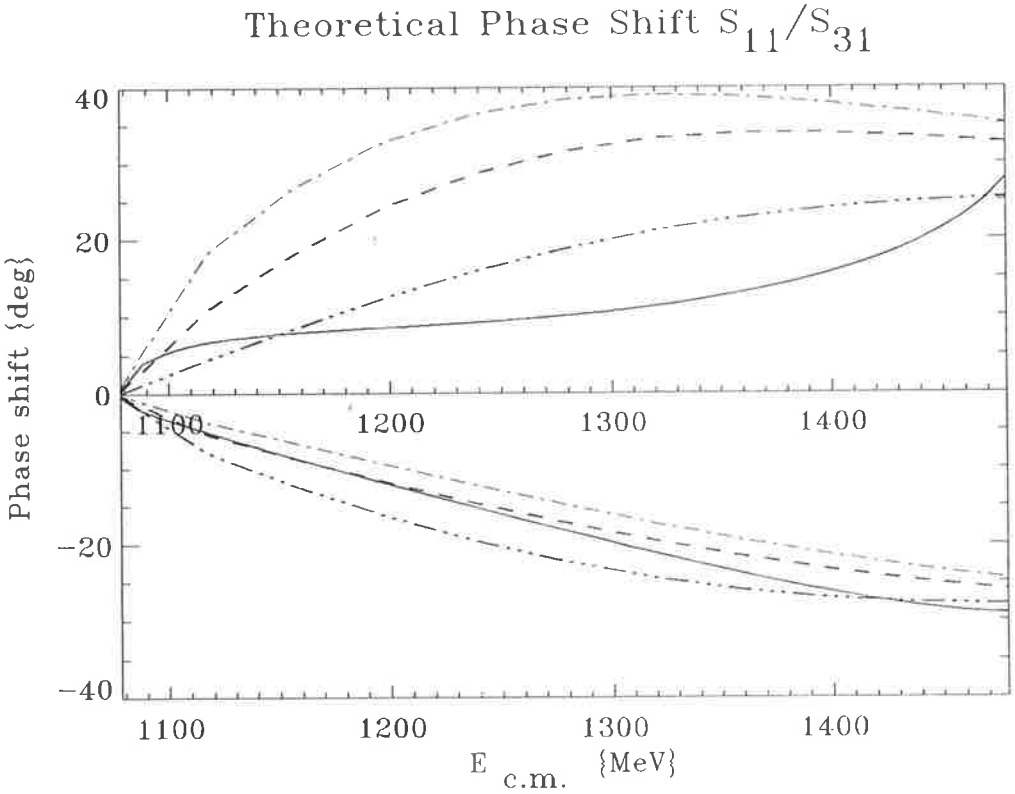

Figure 8.2: The phase shifts resulted from using different pion radius at 4-pion vertex at v_f. Dashed line $R_\pi = 0.4$;dot-dash $R_\pi = 0$ and 3 dot-dash $R_\pi = 0.6$.

Appendix A

The CBM Lagrangian and Wave function

A.1 MIT Bag wave functions

In this Appendix we give the quark wave functions which were used in calculating interaction matrix elements in Chapter 4. In the Cloudy Bag Model (CBM) quarks are treated as massless Dirac particles confined to a spatial region (Bag). Hence, the quark wave functions in CBM are the same as those of MIT. In this work, we only used the ground state wave function for quarks. The wave function for quark (a) is given by [Tho 84, Tho+83],

$$q_a(x) = \frac{N_s}{\sqrt{4\pi}} \begin{pmatrix} j_0(\frac{\Omega x}{R}) \\ i\boldsymbol{\sigma} \cdot \hat{x} j_1(\frac{\Omega x}{R}) \end{pmatrix} e^{-i\Omega t/R} \vartheta_a \tag{A.1}$$

Here $\Omega = 2.04$ is the quark eigen-frequency, R the bag radius N_s is the normalization constant

$$N_s^2 = \frac{1}{2R^3 j_0(\Omega)^2} \left(\frac{\Omega}{\Omega - 1} \right)$$

and ϑ_a is the combined spin-flavour wave function for quark (a). Pion field is treated as elementary particle (structureless). The pion field operators in orthogonal basis are given by

$$\phi_j(x) = \frac{1}{(2\pi)^{\frac{3}{2}}} \int \frac{d^3q}{\sqrt{2\omega_{\mathbf{q}}}} \left[a_j(\boldsymbol{q}) e^{i\mathbf{q}\cdot\mathbf{x}} + a_j^\dagger(\boldsymbol{q}) e^{-i\mathbf{q}\cdot\mathbf{x}} \right] \tag{A.2}$$

where $j = 1, 2, 3$ is the isospin index. The spherical basis for the pion field operators $(a_{\pm 1}, a_0)$ are built up from orthogonal basis according to eqns (C.1) and (C.2).

$$a_{\pm 1} = \mp \frac{1}{\sqrt{2}} (a_1 \pm i a_2) \tag{A.3}$$

$$a_0 = a_3 \tag{A.4}$$

A.2 The Non-Linear CBM Lagrangian

There are two types of chirally symmetric Lagrangians that describe πN interactions, namely σ and ρ types. It is also known that one can apply the unitarity transformation on σ type Lagrangians to yield ρ type coupling.

The Cloudy Bag Model Lagrangians are constructed from MIT Bag model in order to have chiral symmetric properties. This is achieved by incorporating the pion as a separate local field which couples with the quarks. Likewise in traditional nuclear physics, there have been Chiral Bag Lagrangians that include σ field [CT 75] and those reminisence of ρ type [Tho 81]. The latter type can be obtained by applying unitarity transformation on the σ type Lagrangians. All these Lagrangians are equivalent representation of the same basic theory and provide a freedom to choose for particular application.

In this thesis, we choose to work with the Lagrangian of Kalbermann and Eisenberg [KE 83]. The Hamiltonian density is written in such a way that the time derivative of pion field being replaced by its canonical momenta. This has the ad-

vantage of cancelling bad piece of the isoscalar component that arises from iterating lowest order (Weinberg-Tomozawa) term in Lippmann-Schwinger equation [Gui 85] (see the discussion in Section 7.2.2). The Lagrangian density is given by

$$\begin{aligned}\mathcal{L}(x) &= (\frac{1}{2}i\bar{q}\overleftrightarrow{\partial}q - B)\theta_v - \frac{1}{2}\bar{q}q\delta_s + \frac{\theta_v}{[1+\boldsymbol{\rho}_\pi]}\bar{q}\gamma^\mu\left(\gamma_5\frac{\boldsymbol{\tau}\cdot\partial_\mu\boldsymbol{\phi}}{2f} - \frac{\boldsymbol{\tau}\cdot(\boldsymbol{\phi}\times\partial_\mu\boldsymbol{\phi})}{(2f)^2}\right)q \\ &+\frac{(\partial_\mu\boldsymbol{\phi})^2}{2[1+\boldsymbol{\rho}_\pi]^2} - \frac{m_\pi^2\boldsymbol{\phi}^2}{2[1+\boldsymbol{\rho}_\pi]} \quad , \end{aligned} \tag{A.5}$$

where as in (A.5) θ_v is the step function, 1 inside the bag and 0 outside; B the bag pressure constant; δ_s the surface delta function and $\boldsymbol{\rho}_\pi = \frac{\boldsymbol{\phi}^2}{(2f)^2}$. By noting

$$\begin{aligned}F^\mu(\boldsymbol{\phi}) &= (F^0(\boldsymbol{\phi}), \vec{F}\,(\boldsymbol{\phi})) \\ &= \bar{q}\gamma^\mu\left(\frac{\gamma_5\boldsymbol{\tau}}{2f} - \frac{\boldsymbol{\tau}\times\boldsymbol{\phi}}{(2f)^2}\right)q\theta_v, \end{aligned} \tag{A.6}$$

the canonical momenta for the pion field is given as

$$\begin{aligned}\boldsymbol{\Pi}(x) &= \frac{\partial\mathcal{L}(x)}{\partial\boldsymbol{\phi}} \\ &= \frac{\partial_0\boldsymbol{\phi}}{[1+\boldsymbol{\rho}_\pi]^2} + \frac{F^0(\boldsymbol{\phi})}{[1+\boldsymbol{\rho}_\pi]}. \end{aligned} \tag{A.7}$$

Then, the Hamiltonian density can be written as

$$\begin{aligned}\mathcal{H} &= \boldsymbol{\Pi}\cdot(\partial_0\boldsymbol{\phi}) - \mathcal{L} \\ &= -\mathcal{L}_{Bag} - \frac{\vec{\nabla}\,\boldsymbol{\phi}\cdot\,\vec{F}\,(\boldsymbol{\phi})}{[1+\boldsymbol{\rho}_\pi]} + \frac{(\vec{\nabla}\,\boldsymbol{\phi})^2}{2[1+\boldsymbol{\rho}_\pi]^2} + \frac{m_\pi^2\boldsymbol{\phi}^2}{2[1+\boldsymbol{\rho}_\pi]} + \frac{(\partial_0\boldsymbol{\phi})^2}{2[1+\boldsymbol{\rho}_\pi]^2} \end{aligned} \tag{A.8}$$

We expand (A.8) for small pion field i.e. $\boldsymbol{\rho}_\pi = \frac{\boldsymbol{\phi}^2}{4f^2} < 1$, we have

$$[1+\boldsymbol{\rho}_\pi]^{-1} \approx 1 - \boldsymbol{\rho}_\pi + \boldsymbol{\rho}_\pi^2 - ...$$

$$[1+\boldsymbol{\rho}_\pi]^{-2} \approx 1 - 2\boldsymbol{\rho}_\pi + 3\boldsymbol{\rho}_\pi^2 - .....$$

The Hamiltonian density to order $(2f)^{-3}$ becomes

$$\begin{aligned}\mathcal{H} &= -\mathcal{L}_{Bag} - (\boldsymbol{\Pi}\cdot F^0(\boldsymbol{\phi}) + \vec{\nabla}\cdot\vec{F}\,(\boldsymbol{\phi})) + (\frac{\boldsymbol{\Pi}^2}{2} + \frac{m_\pi^2}{2}\boldsymbol{\phi}^2 + \frac{1}{2}(\vec{\nabla}\,\boldsymbol{\phi})^2) \\ &\quad -\boldsymbol{\rho}_\pi(\boldsymbol{\Pi}\cdot F^0(\boldsymbol{\phi}) - \vec{\nabla}\cdot\vec{F}\,(\boldsymbol{\phi})) + \boldsymbol{\rho}_\pi(\boldsymbol{\Pi}^2 - (\vec{\nabla}\,\boldsymbol{\phi})^2) - \boldsymbol{\rho}_\pi m_\pi^2\boldsymbol{\phi}^2 + \\ &\quad \frac{1}{2}(F^0(\boldsymbol{\phi}))^2 + \mathcal{O}(\frac{1}{(2f)^4}) \qquad\qquad (A.9) \\ &= \mathcal{H}_{MIT} + \mathcal{H}_{\pi 0} + \mathcal{H}_{int}\end{aligned}$$

In (A.9),

$$\mathcal{H}_{MIT} = \frac{i}{2}\bar{q}\boldsymbol{\gamma}\cdot(\overleftarrow{\nabla} - \vec{\nabla})q + B)\theta_v + \frac{1}{2}\bar{q}q\delta_s \qquad (A.10)$$

$$\mathcal{H}_{\pi 0} = \frac{1}{2}\left(\boldsymbol{\Pi}^2 + m_\pi^2\boldsymbol{\phi}^2 + (\vec{\nabla}\,\boldsymbol{\phi})^2\right) \qquad (A.11)$$

$$\mathcal{H}_{int} = \mathcal{H}_1 + \mathcal{H}_3 + \mathcal{H}_{WT}^t + \mathcal{H}_{WT}^{so} + \mathcal{H}' + \mathcal{H}_{4\pi} \qquad (A.12)$$

where the interaction Hamiltonian is given by

$$\mathcal{H}_1(\boldsymbol{x}) = -\frac{\theta_v}{(2f)}\bar{q}\boldsymbol{\gamma}\gamma_5\boldsymbol{\tau}q.\,\vec{\nabla}\,\boldsymbol{\phi} \qquad (A.13)$$

$$\mathcal{H}_3(\boldsymbol{x}) = \frac{\theta_v}{(2f)^3}\,\bar{q}\boldsymbol{\gamma}\gamma_5\boldsymbol{\tau}q\cdot\vec{\nabla}\,\boldsymbol{\phi}\;\;\boldsymbol{\phi}\cdot\boldsymbol{\phi} \qquad (A.14)$$

$$\mathcal{H}_{WT}^t(\boldsymbol{x}) = \frac{\theta_v}{(2f)^2}\,\bar{q}\gamma^0\boldsymbol{\tau}q\;\cdot(\boldsymbol{\phi}\times\boldsymbol{\Pi}) \qquad (A.15)$$

$$\mathcal{H}_{WT}^{so}(\boldsymbol{x}) = \frac{\theta_v}{(2f)^2}\,\bar{q}\boldsymbol{\gamma}\boldsymbol{\tau}q\;\cdot(\boldsymbol{\phi}\times\vec{\nabla}\,\boldsymbol{\phi}) \qquad (A.16)$$

$$\mathcal{H}'(\boldsymbol{x}) = \frac{1}{2}\,[\bar{q}\gamma_0(\frac{\gamma_5\boldsymbol{\tau}}{(2f)} - \frac{(\boldsymbol{\tau}\times\boldsymbol{\phi})}{(2f)^2})q]^2 \qquad (A.17)$$

$$\mathcal{H}_{4\pi}(\boldsymbol{x}) = \frac{1}{(2f)^2}\left(\boldsymbol{\Pi}^2 - (\vec{\nabla}\,\boldsymbol{\phi})^2 - m_\pi^2\boldsymbol{\phi}^2\right)\boldsymbol{\phi}\cdot\boldsymbol{\phi} \qquad (A.18)$$

The pion canonical momenta $\boldsymbol{\Pi}$ has the property,

$$-i\omega = [\boldsymbol{\Pi}, H_{\pi 0}]\ ,$$

and therefore the pion canonical momenta in (A.15) served as time derivative of the

pion field.

A.3 SU(6) Wave functions

In the following we will give SU(6) wave functions and matrix elements of transition spin-isospin operators. In studying the πN system, it is sufficient to consider only two flavours u, d. From this we can construct spin(flavour) symmetric $\chi_S(\phi_S)$, mix-symmetric $\chi_{M,S}(\phi_{M,S})$ and mixed-asymmetric $\chi_{M,A}(\phi_{M,A})$ (see Section 4 of F.E. Close) [Clo 79]. We will denote spin S,MS and A states as follows:

$$\begin{aligned}
|\chi^{\frac{3}{2}}_S\rangle &= |\uparrow\uparrow\uparrow\rangle \\
|\chi^{\frac{1}{2}}_S\rangle &= \frac{1}{\sqrt{3}}|\uparrow\uparrow\downarrow + \uparrow\downarrow\uparrow + \downarrow\uparrow\uparrow\rangle \\
|\chi^{\frac{1}{2}}_{M,S}\rangle &= \frac{1}{\sqrt{6}}|\uparrow\downarrow\uparrow + \downarrow\uparrow\uparrow - 2\uparrow\uparrow\downarrow\rangle \\
|\chi^{\frac{1}{2}}_{M,A}\rangle &= \frac{1}{\sqrt{2}}|\uparrow\downarrow\uparrow - \downarrow\uparrow\uparrow\rangle
\end{aligned} \tag{A.19}$$

The flavour S,MS,MA states are obtained by replacing $\uparrow$ ($\downarrow$) with $u(d)$ flavour.

The N, Δ spin-flovour states with particular spin(isospin) 3rd components can be constructed as follows.

$$\begin{aligned}
|N; I_z = \frac{1}{2}, S_z = \frac{1}{2}\rangle_{sf} &= \frac{1}{2}|\phi^{\frac{1}{2}}_{M,S}\chi^{\frac{1}{2}}_{M,S} + \phi^{\frac{1}{2}}_{M,A}\chi^{\frac{1}{2}}_{M,A}\rangle \\
|\Delta; I_3 = \frac{1}{2}, S_z = \frac{1}{2}\rangle_{sf} &= |\phi^{\frac{1}{2}}_S\chi^{\frac{1}{2}}_S\rangle \\
|\Delta; I_3 = \frac{3}{2}, S_z = \frac{3}{2}\rangle_{sf} &= |\phi^{\frac{3}{2}}_S\chi^{\frac{3}{2}}_S\rangle
\end{aligned} \tag{A.20}$$

The matrix elements of (1.25) can be obtained as

$$\begin{aligned}
\mathcal{M}_{P,P} &= {}_{sf}\langle N; I_3 = \frac{1}{2}, S_z = \frac{1}{2}|\sum_{a=1}^{3}\sigma_z^{(a)}\tau_3^{(a)}|N; I_3 = \frac{1}{2}, S_z = \frac{1}{2}\rangle_{sf} \\
&= \frac{5}{3}
\end{aligned} \tag{A.21}$$

Table A.1: The Quark spin isospin matrix element

$\alpha\backslash\beta$	N	Δ
N	$5/3$	$4\sqrt{2}/3$
Δ	$4\sqrt{2}/3$	$1/3$

When the transition involved only isospin, it is sufficient to determine the matrix element with flavour wave functions since spin functions are orthonormal. In this case we easily find that

$$ {}_{sf}\langle N; I_3 = \pm\frac{1}{2}|\sum_{a=1}^{3}\tau_3^{(a)}|N; I_3 = \pm\frac{1}{2}\rangle_{sf} = 1 \quad \text{(A.22)} $$

$$ {}_{sf}\langle \Delta; I_3 = \pm\frac{1}{2}|\sum_{a=1}^{3}\tau_3^{(a)}|\Delta; I_3 = \pm\frac{1}{2}\rangle_{sf} = 1 \quad \text{(A.23)} $$

$$ {}_{sf}\langle \Delta; I_3 = \pm\frac{3}{2}|\sum_{a=1}^{3}\tau_3^{(a)}|\Delta; I_3 = \pm\frac{3}{2}\rangle_{sf} = 3 \quad \text{(A.24)} $$

A.4 The Value for the Numerical Integrals

In this Appendix, we give the numerical integrals used in Section 7.2.2. We denote $\omega = \omega_{\mathrm{q}}, \Delta_m = m_\Delta - m_N, \mathcal{I}_t(qx) = \int_0^R dx x^2 \rho_t(x) j_0(qx)$ and $\mathcal{I}_{pv}(qx) = \int_0^R dx x^2 \rho_{pv}(qx)$.

symbol	Integral	Numerical value
$\mathcal{I}_t(x)$	$\int_0^R dx x^2 \rho_t(x)$	0.19436
$\mathcal{I}_0$	$\int_0^\infty dq q^2 \mathcal{I}_t^2(qx)$	0.1937
$\mathcal{I}_1$	$\int_0^\infty dq q^2 \frac{1}{\omega} \mathcal{I}_t^2(qx)$	0.08371
$\mathcal{I}_2^{(b)}$	$\int_0^\infty dq q^2 \frac{1}{\omega(\mathbf{k})-\omega} \mathcal{I}_t^2(qx)$	-0.16875
$\mathcal{I}_2^{(a)}$	$\int_0^\infty dq q^2 \frac{1}{\omega(\mathbf{k})+\omega} \mathcal{I}_t^2(qx)$	0.06138
$\mathcal{I}_e^{(N)}$	$\int_0^\infty dq \frac{q^4}{\omega^2} \mathcal{I}_{pv}^2(qx)$	0.06999
$\mathcal{I}_e^{(\Delta)}$	$\int_0^\infty dq \frac{q^4}{\omega} \left(\frac{1}{m_\Delta - m_N + \omega}\right) \mathcal{I}_{pv}^2(qx)$	0.04671
$\mathcal{F}_{1a}^{(N)}$	$\int_0^\infty dq \frac{q^4}{\omega^4} e^{-R_\pi^2 q^2/6} \cdot \mathcal{I}_{pv}^2(qx)$	0.01183
$\mathcal{F}_{2a}^{(N)}$	$\int_0^\infty dq \frac{q^4}{\omega^4} e^{-R_\pi^2 q^2/6} \cdot \mathcal{I}_{pv}^2(qx)$	0.005918
$\mathcal{F}_{(1a)}^{(\Delta)}$	$\int_0^\infty dq \frac{q^4}{\omega^2} \left(\frac{1}{m_\Delta - m_N + \omega}\right)^2 e^{-R_\pi^2 q^2/6} \cdot \mathcal{I}_{pv}^2(qx)$	0.003518
$\mathcal{F}_{2a}^{(\Delta)}$	$\int_0^\infty dq \frac{q^4}{\omega} \left(\frac{1}{m_\Delta - m_N + \omega}\right)^2 e^{-R_\pi^2 q^2/6} \cdot \mathcal{I}_{pv}^2(qx)$	0.001758
$\mathcal{F}_{3a}^{(N)}$	$\int_0^\infty dq \frac{q^4}{\omega^3} e^{-R_\pi^2 q^2/6} \cdot \mathcal{I}_{pv}^2(qx)$	0.02219
$\mathcal{F}_{3a}^{(\Delta)}$	$\int_0^\infty dq \frac{q^4}{\omega} \frac{e^{-R_\pi^2 q^2/6}}{(m_\Delta - m_N + \omega)^2} \mathcal{I}_{(pv)}(qx)$	0.007440
$\mathcal{F}_{1b}^{(N)}$	$\int_0^\infty dq \frac{q^4}{\omega^4} e^{-R_\pi^2 q^2/4} \cdot \mathcal{I}_{pv}^2(qx)$	0.01129
$\mathcal{F}_{2b}^{(N)}$	$\int_0^\infty \frac{q^4}{\omega^4} (\omega^2 + \lvert\boldsymbol{q}\rvert^2) e^{-R_\pi^2 q^2/4} \cdot \mathcal{I}_{pv}^2(qx)$	0.08211
$\mathcal{F}_{1b}^{(\Delta)}$	$\int_0^\infty dq \frac{q^4}{\omega^2} \frac{e^{-R_\pi^2 q^2/4} \cdot \mathcal{I}_{pv}^2(qx)}{(\Delta_m + 2\omega)(\Delta_m + \omega)}$	0.002125
$\mathcal{F}_{2b}^{(\Delta)}$	$\int_0^\infty dq \frac{q^4}{\omega^2} \frac{(\omega^2 + \mathrm{q}^2) e^{-R_\pi^2 q^2/4} \cdot \mathcal{I}_{pv}^2(\mathrm{qx})}{(\Delta_m + 2\omega)(\Delta_m + \omega)}$	0.018859
$\mathcal{I}_g(x)$	$\int_0^R dx x^2 \rho_t^2(x)$	0.12118
$\mathcal{I}_h^{(N)}(x)$	$\int_0^\infty dq \frac{q^4}{\omega^3} \mathcal{I}_{pv}^2(qx)$	0.02635
$\mathcal{I}_h^{(\Delta)}(x)$	$\int_0^\infty dq \frac{q^4}{\omega} \left(\frac{1}{m_\Delta - m_N + \omega}\right)^2 \mathcal{I}_{pv}^2(qx)$	0.00954

Appendix B

Relativistic Jacobi coordinates

The relativistic Jacobi coordinates for two particles with mass m_1 and m_2 , momenta p_1, p_2 are defined as follows. In the c.m. frame, the total 4-momentum, P, is related to the total energy squared, S, via

$$P = p_1 + p_2 = (\sqrt{S}, 0). \tag{B.1}$$

The energy of each particle when the square of total energy is S

$$\epsilon_1 = \epsilon_1(S) = \frac{S + m_2^2 - m_1^2}{2\sqrt{S}} \tag{B.2}$$

$$\epsilon_2 = \epsilon_2(S) = \frac{S + m_1^2 - m_2^2}{2\sqrt{S}} \tag{B.3}$$

We will denote the energy of particle 1 with total four momentum square $P'^2 = S'$ as $\epsilon_1' = \epsilon_1(S')$ etc. The relative 4-momentum is given by the relation

$$p = \frac{\epsilon_2 p_1 - \epsilon_1 p_2}{\epsilon_1 + \epsilon_2}. \tag{B.4}$$

By defining another energy variable $P' = \sqrt{\frac{S'}{S}}P$, one can show that

$$\left(\frac{\epsilon_1' P'}{\epsilon_1 + \epsilon_2} + p\right)^2 - m_1^2 = \epsilon_1'^2 + 2P \cdot p\frac{\epsilon_1'}{\sqrt{S}} - (m_1^2 - p^2) \tag{B.5}$$

$$\left(\frac{\epsilon_2' P'}{\epsilon_1 + \epsilon_2} - p\right)^2 - m_2^2 = \epsilon_2'^2 - 2P \cdot p\frac{\epsilon_2'}{\sqrt{S}} - (m_2^2 - p^2) \tag{B.6}$$

From (B.5) and (B.6), the two delta functions in eqn.(3.37) can be written as,

$$2\delta\left(\epsilon_1' - \epsilon_2' - \frac{(S_p + m_1^2 - m_2^2)^2}{4S_p} - \frac{(S_p + m_2^2 - m_1^2)^2}{4S_p} + 2P \cdot p\frac{\epsilon_1' + \epsilon_2'}{\sqrt{S}}\right)$$
$$\delta\left(\epsilon_1' + \epsilon_2' - \frac{(S_p + m_1^2 - m_2^2)^2}{4S_p} + \frac{(S_p + m_1^2 - m_2^2)^2}{4S_p} + 2P \cdot p\frac{\epsilon_1' - \epsilon_2'}{\sqrt{S}}\right). \tag{B.7}$$

By noting $m_1^2 - m_2^2 = M$, we can prove that

$$\epsilon_1'^2 - \epsilon_2'^2 = M \tag{B.8}$$

$$\epsilon_1'^2 + \epsilon_2'^2 = \frac{S'^2 + M^2}{2S'} \tag{B.9}$$

Using (B.8) and (B.9), the pair of delta functions in (B.7) become

$$2\delta\left(2P \cdot p\sqrt{\frac{S'}{S}}\right)\delta\left(\frac{S'^2 + M^2}{2S'} - \frac{S_p^2 + M^2}{2S_p} + 2P \cdot p\frac{\epsilon_1' - \epsilon_2'}{\sqrt{S}}\right). \tag{B.10}$$

Provided that

$$P \cdot p = 0,$$

by the 1st delta function the roots of 2nd delta function are S_p and M^2/S_p. We can therefore rewrite (B.10) by using the property

$$\delta(f(S')) = \frac{\delta(S' - S_p)}{\frac{\partial f(S')}{\partial S'}|_{S'=S_p}}$$

as

$$\frac{4S_p^2}{S_p^2 - M^2}\delta(2P \cdot p\sqrt{\frac{S'}{S}})\delta(S' - S_p) \tag{B.11}$$

By utilizing the relation in (B.11), the integration along the unitarity cut in the complex energy plane S', (3.37), can be carried out as

$$\begin{aligned} G_{gen}(p,P) &= \int_{m_1^2+m_2^2}^{\infty} \frac{dS'}{S-S'} f(S,S') \frac{4S_p^2}{S_p^2 - M^2} \delta\left(2P \cdot p\sqrt{\frac{S'}{S}}\right) \delta(S' - S_p) \\ &= \frac{f(S,S_p)}{S - S_p} \frac{\sqrt{SS_p}}{\epsilon_1(S_p)\epsilon_2(S_p)} \delta(2P \cdot p). \end{aligned} \tag{B.12}$$

By using one more relation,

$$(S - S_p) = (\boldsymbol{p}^2 - \boldsymbol{k}^2)\frac{4SS_p}{(S_pS - M^2)},$$

we rewrite (B.12) as,

$$G_{gen}(p,P) = \frac{f(S,S_p)}{\boldsymbol{p}^2 - \boldsymbol{k}^2} \frac{S_pS - (m_1^2 - m_2^2)^2}{4\sqrt{SS_p}\ \epsilon_1(S_p)\epsilon_2(S_p)} \delta(2P \cdot p) \tag{B.13}$$

Appendix C

Angular momentum relations

In this appendix, we give details of some of angularmomentum calculations done in Chapters 4,5 and 6.

C.1 Spherical tensors

The spherical basis $(\hat{\boldsymbol{e}}_{+1}, \hat{\boldsymbol{e}}_{-1}, \hat{\boldsymbol{e}}_0)$ can be defined from the orthogonal basis $(\hat{\boldsymbol{e}}_1, \hat{\boldsymbol{e}}_2. \hat{\boldsymbol{e}}_3)$ as [Rose57, Edm 57, Bri 68, Sch 87]

$$\hat{\boldsymbol{e}}_{\pm 1} = \mp\frac{1}{\sqrt{2}}(\hat{\boldsymbol{e}}_1 \pm i\hat{\boldsymbol{e}}_2) \tag{C.1}$$

$$\hat{\boldsymbol{e}}_0 = \hat{\boldsymbol{e}}_3 \tag{C.2}$$

These spherical tensors have the property

$$\hat{\boldsymbol{e}}^*_m = (-)^m \hat{\boldsymbol{e}}_{-m} \ , \tag{C.3}$$

and the scalar product

$$\hat{\boldsymbol{e}}_n \cdot \hat{\boldsymbol{e}}^*_m = \delta_{mn} \ . \tag{C.4}$$

We can write a vector $\boldsymbol{A} = (A_x\hat{x}, A_y\hat{y}, A_z\hat{z})$ as a spherical tensor of rank-1 [Rose57, Edm 57]

$$\boldsymbol{A} = \sum_m A_{1m}\hat{\boldsymbol{e}}^*_m \quad (m = \pm 1, 0) \tag{C.5}$$

where the components A_{1m} are given by

$$A_{1\pm 1} = \mp\frac{1}{\sqrt{2}}(A_x \pm iA_y) \tag{C.6}$$

$$A_{10} = A_z \ . \tag{C.7}$$

In particular we denote spin(isospin) operators in spherical representation as

$$\boldsymbol{\sigma} = \sum_m \sigma_{1m}\hat{\boldsymbol{s}}^*_m \quad (m = \pm 1, 0) \tag{C.8}$$

$$\boldsymbol{\tau} = \sum_n \tau_{1n}\hat{\boldsymbol{t}}^*_n \quad (n = \pm 1, 0) \tag{C.9}$$

It is useful to write a vector in cartesian coordinate $\boldsymbol{r} = \hat{r}|\boldsymbol{r}| = (\hat{x}x, \hat{y}y, \hat{z}z)$ by rank-1 spherical harmonic $Y_{1m}(\hat{r})$ as

$$|\boldsymbol{r}|\sqrt{\frac{4\pi}{3}}Y_{1\pm 1}(\hat{r}) = \mp\frac{1}{\sqrt{2}}(x \pm iy) \tag{C.10}$$

$$|\boldsymbol{r}|\sqrt{\frac{4\pi}{3}}Y_{10}(\hat{r}) = z \tag{C.11}$$

The scalar product of two vectors can be written in spherical notation as

$$\begin{aligned}\boldsymbol{A}\cdot\boldsymbol{B} &= \sum_{m,n} A_{1m}B_{1m}\hat{\boldsymbol{e}}^*_m \cdot \hat{\boldsymbol{e}}^*_n \\ &= \sum_m (-)^m A_{1m}\, B_{1,-m}\end{aligned} \tag{C.12}$$

$$\boldsymbol{\sigma}\cdot\hat{r} = \left(\frac{4\pi}{3}\right)^{\frac{1}{2}} \sum_{m_1} \sigma_{1m_1}Y^*_{1m_1}(\hat{r}) \tag{C.13}$$

$$\boldsymbol{k}\cdot\hat{r} \;=\; |\boldsymbol{k}|\left(\frac{4\pi}{3}\right)\sum_{m_2} Y_{1m_2}(\hat{k})Y^*_{1m_2}(\hat{r}) \qquad \text{(C.14)}$$

It is useful to describe the matrix element of spin(isospin) operators in the spherical representation. The matrix element of a spin vector can be decribed, for example, using reduced matrix elements as

$$\begin{aligned}\langle S_{B'}m_{B'}|\boldsymbol{\sigma}|S_Bm_B\rangle &= \langle S_{B'}m_{B'}|\sum_m \sigma_{1m}\hat{\boldsymbol{s}}^*_m|S_Bm_B\rangle \\ &= C^{m_Bmm_{B'}}_{S_B1S_{B'}}\frac{\langle S_{B'}||\boldsymbol{\sigma}^{(1)}||S_B\rangle}{\sqrt{2S_{B'}+1}}\,\hat{\boldsymbol{s}}^*_m \qquad \text{(C.15)}\end{aligned}$$

C.2 Proof of Eqn. (4.19)

By using the equations (C.13) and (C.14), we can write (4.19) as

$$\begin{aligned}\int d\hat{x}\;\boldsymbol{\sigma}\cdot\hat{r}\;\boldsymbol{k}\cdot\hat{r}\;e^{i\mathbf{k}\cdot\mathbf{x}} \;=\; \left(\frac{4\pi}{3}\right)^{\frac{3}{2}}\sum_{lmm_1m_2}\int d\hat{x}\sigma_{1m_1}Y^*_{1m_1}(\hat{r})|\boldsymbol{k}|Y_{1m_2}(\hat{k})Y^*_{1m_2}(\hat{r}) \\ (4\pi)(i)^l j_l(kx)Y^*_{lm}(\hat{k})Y_{lm}(\hat{x}) \qquad \text{(C.16)}\end{aligned}$$

Since we have (Edmonds: eqn (4.6.3) [Edm 57])

$$\begin{aligned}\int d\hat{x}Y^*_{1m_1}(\hat{r})Y^*_{1m_2}(\hat{r})Y_{lm}(\hat{r}) \;=\; & \qquad \text{(C.17)} \\ (-)^{m_1+m_2}\left[\frac{3^2(2l+1)}{4\pi}\right]^{\frac{1}{2}}&\begin{pmatrix}1 & 1 & 1\\ 0 & 0 & 0\end{pmatrix}\begin{pmatrix}1 & 1 & l\\ -m_1 & -m_2 & m\end{pmatrix},\end{aligned}$$

and (Edmonds: (4.6.5))

$$Y_{1m_2}(\hat{k})Y^*_{lm}(\hat{k}) \;=\; \sum_{l'm'}\left[\frac{3(2l+1)(2l'+1)}{4\pi}\right]^{\frac{1}{2}}\begin{pmatrix}1 & l & l'\\ 0 & 0 & 0\end{pmatrix}\begin{pmatrix}1 & l & l\\ m_2 & -m & m'\end{pmatrix}(-)^{m'}Y^*_{l'm'}(\hat{k})\ , \tag{C.18}$$

we can write eqn (C.16) as

$$\left(\frac{4\pi}{3}\right)^{\frac{3}{2}}(4\pi)|\boldsymbol{k}|\sum_{lm}(i)^l j_l(kx)\left[\frac{3^2(2l+1)}{4\pi}\right]^{\frac{1}{2}}\left[\frac{3^2(2l+1)}{4\pi}\right]^{\frac{1}{2}} \tag{C.19}$$
$$\frac{1}{3}\sigma_{1m_1}Y^*_{1m_1}(\hat{k})(-)^l\begin{pmatrix}1 & 1 & l\\ 0 & 0 & 0\end{pmatrix}\begin{pmatrix}1 & l & 1\\ 0 & 0 & 0\end{pmatrix}$$

Since $l = 0$ and $l = 2$ are allowed, eqn (C.16) becomes

$$\int d\hat{x}\ \boldsymbol{\sigma}\cdot\hat{r}\ \boldsymbol{k}\cdot\hat{r}\ e^{i\mathbf{k}\cdot\mathbf{x}} = \left(\frac{4\pi}{3}\right)(j_0(kx) - 2j_2(kx))\boldsymbol{\sigma}\cdot\boldsymbol{k} \tag{C.20}$$

C.3 Proof of Eqn. (4.90)

We can calculate the isospin relations (4.90) and (6.29) with the help of graphical methods [See Brink [Bri 68] for details]. First, we write (4.90) as

$$\frac{1}{(2I+1)}\sum_{i_M i_{M'}}\sum_{n,I_3}(-)^n C^{i_{\alpha_4} i_{M'} I_3}_{I_{\alpha_4} I_{M'} I}\, C^{i_{\alpha_3} - n i_{\alpha_4}}_{T_{\alpha_3} l_1 I_{\alpha_4}}$$
$$\langle I_{\alpha_3} i_{\alpha_3}; I_{M'} i_{M'}|\boldsymbol{\tau}\cdot\boldsymbol{\theta}|I_{\alpha_2} i_{\alpha_2}; I_M i_M\rangle C^{i_{\alpha_1} n i_{\alpha_2}}_{I_{\alpha_1} l_1 I_{\alpha_2}}\, C^{i_{\alpha_1} i_M I_3}_{I_{\alpha_1} I_M I}\ . \tag{C.21}$$

Since we can write in spherical representation

$$\boldsymbol{\tau}\cdot\boldsymbol{\theta} = \sum_q (-)^q \tau_{1q}\theta_{1,-q}\ ,$$

we write the eqn (C.21) in terms of reduced matrix elements as (c.f. eqn (C.15))

$$\frac{\langle I_{\alpha_3}||\tau^{(1)}||I_{\alpha_2}\rangle}{\sqrt{2I_{\alpha_3}+1}}\frac{\langle I_{M'}||\theta^{(1)}||I_M\rangle}{\sqrt{2I_{M'}+1}}\frac{1}{(2I+1)} \tag{C.22}$$
$$\sum_{allm}(-)^{n+q}C^{i_{\alpha_4}i_{M'}I_3}_{I_{\alpha_4}I_{M'}I}C^{i_{\alpha_1}i_MI_3}_{I_{\alpha_1}I_MI}C^{i_{\alpha_3}ni_{\alpha_4}}_{I_{\alpha_3}l_1I_{\alpha_4}}C^{i_{\alpha_1}-ni_{\alpha_2}}_{I_{\alpha_1}l_1I_{\alpha_2}}C^{i_{\alpha_2}qi_{\alpha_3}}_{I_{\alpha_2}l_2I_{\alpha_3}}C^{i_M-qi_{M'}}_{I_Ml_2I_{M'}}$$

The Clebsch-Gordan coefficients in eqn (C.22) can be represented graphically as [Bri 68]:

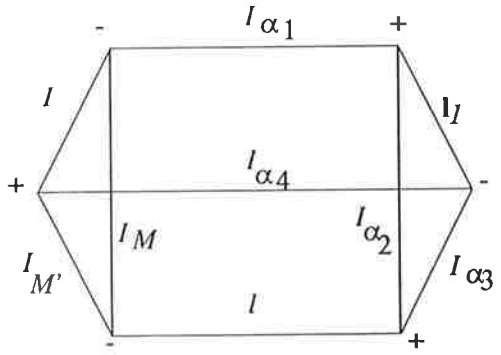

This can be further decomposed into two 6-j symbols(See Brink[Bri 68] Section 7.)

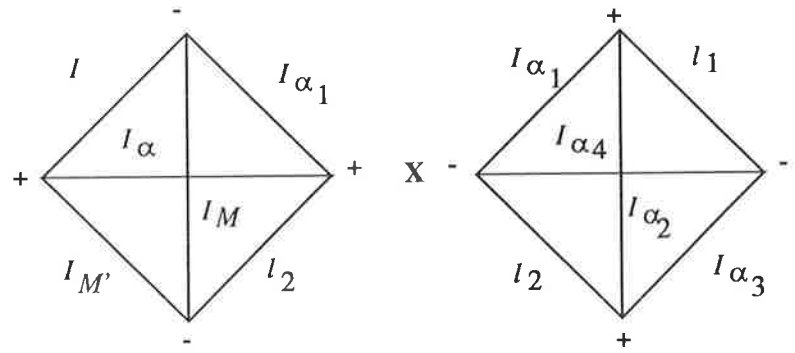

This process is described by algebraic methods as follows. We first transcribe the Clebsch-Gordan coefficients in 3-j symbols. Equation (C.22) then becomes

$$\langle I_{\alpha_3}||\boldsymbol{\tau}^{(1)}||I_{\alpha_2}\rangle\langle I_{M'}||\boldsymbol{\theta}^{(1)}||I_M\rangle\hat{I}_{\alpha_4}\hat{I}_{\alpha_2}$$

$$\sum_{allm}(-)^{-2I_3+I_{M'}-2I_{\alpha_1}-I_{\alpha_2}-I_{\alpha_3}-I_{\alpha_4}-i_{M'}-i_{\alpha_2}-i_{\alpha_3}-i_{\alpha_4}+2l_1+2l_2+n+q}$$

$$\begin{pmatrix} I_{\alpha_4} & I_{M'} & I \\ i_{\alpha_4} & i_{M'} & -I_3 \end{pmatrix}\begin{pmatrix} I_{\alpha_3} & l_1 & I_{\alpha_4} \\ i_{\alpha_3} & -n & -i_{\alpha_4} \end{pmatrix}\begin{pmatrix} I_{\alpha_2} & l_2 & I_{\alpha_3} \\ i_{\alpha_2} & q & -i_{\alpha_3} \end{pmatrix} \tag{C.23}$$

$$\begin{pmatrix} I_M & l_2 & I_{M'} \\ i_M & -q & -i_{M'} \end{pmatrix}\begin{pmatrix} I_{\alpha_1} & l_1 & I_{\alpha_2} \\ i_{\alpha_1} & n & -i_{\alpha_2} \end{pmatrix}\begin{pmatrix} I_{\alpha_1} & I_M & I \\ i_{\alpha_1} & i_M & -I_3 \end{pmatrix}.$$

Since we can write, using (Edmonds:(6.2.8)),

$$\sum_{-i_{M'},-i_{M'},-I_3}\begin{pmatrix} I_{\alpha_1} & I_M & I \\ i_{\alpha_1} & i_M & -I_3 \end{pmatrix}\begin{pmatrix} I_{\alpha_4} & I_{M'} & I \\ i_{\alpha_4} & i_{M'} & -I_3 \end{pmatrix}\begin{pmatrix} I_M & l_2 & I_{M'} \\ i_M & -q & -i_{M'} \end{pmatrix}$$

$$= (-)^{-I+I_3-2I_{M'}+I_{\alpha_1}-I_{\alpha_4}+i_M+i_{M'}}\begin{pmatrix} I_{\alpha_1} & I_{\alpha_4} & l_2 \\ -i_{\alpha_1} & i_{\alpha_4} & -q \end{pmatrix}\begin{Bmatrix} I_{\alpha_1} & I_{\alpha_4} & l_2 \\ I_{M'} & I_M & I \end{Bmatrix} \tag{C.24}$$

We use eqn (C.24) in (C.23). We Finally have

$$\sum_{allm}(-)^{-I-I_3-I_{M'}-I_{\alpha_1}-I_{\alpha_2}-I_{\alpha_3}-2I_{\alpha_4}+i_M-i_{\alpha_2}-i_{\alpha_3}-i_{\alpha_4}+2l_1+2l_2+n+q}$$

$$\begin{pmatrix} I_{\alpha_1} & I_{\alpha_4} & l_2 \\ -i_{\alpha_1} & i_{\alpha_4} & -q \end{pmatrix}\begin{pmatrix} I_{\alpha_3} & l_1 & I_{\alpha_4} \\ i_{\alpha_3} & -n & -i_{\alpha_4} \end{pmatrix}\begin{pmatrix} I_{\alpha_2} & l_2 & I_{\alpha_3} \\ i_{\alpha_2} & q & -i_{\alpha_3} \end{pmatrix}\begin{pmatrix} I_{\alpha_1} & l_1 & I_{\alpha_2} \\ i_{\alpha_1} & n & -i_{\alpha_2} \end{pmatrix}$$

$$\begin{Bmatrix} I_{\alpha_1} & I_{\alpha_4} & l_2 \\ I_{M'} & I_M & I \end{Bmatrix}\langle I_{\alpha_3}||\boldsymbol{\tau}^{(1)}||I_{\alpha_2}\rangle\langle I_{M'}||\boldsymbol{\theta}^{(1)}||I_M\rangle\hat{I}_{\alpha_4}\hat{I}_{\alpha_2} \tag{C.25}$$

$$= (-)^{I+I_{\alpha_1}+1}\langle I_{\alpha_3}||\boldsymbol{\tau}^{(1)}||I_{\alpha_2}\rangle\langle I_{M'}||\boldsymbol{\theta}^{(1)}||I_M\rangle\hat{I}_{\alpha_4}\hat{I}_{\alpha_2}$$

$$\begin{Bmatrix} I_{\alpha_1} & I_{\alpha_4} & l_2 \\ I_{M'} & I_M & I \end{Bmatrix}\begin{Bmatrix} l_1 & I_{\alpha_4} & I_{\alpha_3} \\ l_2 & I_{\alpha_2} & I_{\alpha_1} \end{Bmatrix}$$

C.4 Proof of Eqn. (5.10)

Since $(\boldsymbol{\sigma}\boldsymbol{\sigma}\cdot\hat{x}-\boldsymbol{\sigma}\cdot\hat{x}\boldsymbol{\sigma})=-2i(\boldsymbol{\sigma}\times\hat{x})$, we can write

$$\begin{aligned}&\int d\hat{x}(\boldsymbol{\sigma}\boldsymbol{\sigma}\cdot\hat{x}-\boldsymbol{\sigma}\cdot\hat{x}\boldsymbol{\sigma})\cdot(\boldsymbol{k}'+\boldsymbol{k})e^{-i(\mathbf{k}-\mathbf{k}')\cdot\mathbf{x}}\\ =\;&-2i\int d\hat{x}(\boldsymbol{\sigma}\times\hat{x})\cdot\{(\vec{\nabla}\,e^{i\mathbf{k}'\cdot\mathbf{x}})e^{-i\mathbf{k}\cdot\mathbf{x}}-(\vec{\nabla}\,e^{-i\mathbf{k}\cdot\mathbf{x}})e^{i\mathbf{k}'\cdot\mathbf{x}}\}\end{aligned}\tag{C.26}$$

Since we can write [Edm 57, Rose57, Bri 68],

$$\begin{aligned}(\boldsymbol{\sigma}\times\hat{x})\cdot\vec{\nabla}\,Y_{lm}(\hat{x}) &= (\boldsymbol{\sigma}\times\hat{x})\cdot(\hat{x}\frac{\partial}{\partial x}-i\frac{\hat{x}\times\boldsymbol{L}}{|x|})Y_{lm}(\hat{x})\\ &= \frac{-i}{|x|}(\boldsymbol{\sigma}\times\hat{x})\cdot(\hat{x}\times\boldsymbol{L})Y_{lm}(\hat{x})\\ &= \frac{i}{|x|}\boldsymbol{\sigma}\cdot\boldsymbol{L}Y_{lm}(\hat{x})\\ &= \frac{i}{|x|}\sqrt{l(l+1)}\,\boldsymbol{\sigma}\cdot\boldsymbol{\mathcal{Y}}_{llm}(\hat{x})\\ &= \frac{i}{|x|}\sqrt{l(l+1)}\sum_{m'm''}C^{m'm''m}_{l\;1\;l}Y_{lm'}(\hat{x})\;\hat{e}_{m''}\cdot\boldsymbol{\sigma}\\ &= \frac{i}{|x|}\sqrt{l(l+1)}\sum_{m'm''}C^{m'm''m}_{l\;1\;l}Y_{lm'}(\hat{x})\sigma_{1m''}\end{aligned}\tag{C.27}$$

we can then write (C.26) as

$$\begin{aligned}&(-2)\frac{1}{|x|}(4\pi)^2\sum_{lm}\sum_{m'm_2}j_l(k'x)j_l(kx)Y^*_{lm'}(\hat{k}')Y_{lm}(\hat{k})\sqrt{l(l+1)}\\ &\qquad\sigma_{m_2}\{C^{mm_2m'}_{l\;1\;l}-(-)^{m+m'}C^{-m'm_2-m}_{l\;1\;l}\}\\ =\;&\frac{-4}{|x|}(4\pi)^2\sum_{lm}\sum_{m'm_2}j_l(k'x)j_l(kx)Y^*_{lm'}(\hat{k}')Y_{lm}(\hat{k})\sqrt{l(l+1)}\sigma_{m_2}C^{mm_2m'}_{l\;1\;l}\end{aligned}\tag{C.28}$$

Bibliography

[Adl 65] S.L. Adler, *Phys. Rev.* **137** (1965) B1022.

[AD 68] S. Adler and A. Dashen, *Current Algebra and applications to particle Physics* (Benjamin, New York, 1968).

[AH 84] I.J.R. Aitchison and A.J.G. Hey, *Gauge Theories in Particle Physics* (Adam Hilger, Bristol, 1984).

[AZR 80] R.N. Arndt, V.S. Zidell and L.D. Roper, *Phys. Rev.* **D 21** (1980) 1289.

[BbS 66] R. Blankenbecler and R. Sugar, *Phys. Rev.* **142** (1966) 1051.

[BD 62] J.D. Bjorken and S.D. Drell, *Relativistic Quantum Mechanics* (Associated Press, New York, 1962).

[Bie 62] E. Bierman, *Phys. Rev.* **127** (1962) 599.

[Bri 68] D.M. Brink and G.R. Satchler, *Angular Momentum* (Clarendon Press, Oxford, 1968).

[Bro 69] A.D. Jackson, G.E. Brown and T.T.S.Kuo, *Nucl. Phys.* **A133** (1969) 481.

[Bro+74] G.E. Brown, S. Barshay and M. Rho, *Phys. Rev. Lett.* **32** (1974) 787.

[Bro 79] G.E. Brown, *Nucleon Nucleon Interaction* (North Holland, Amsterdam, 1979).

[Bro 90] G. E. Brown in, *Lectures on Hadron Physics* (World Scientific, Singapore, 1990).

[BS 51] E.E. Salpeter and H.A. Bethe, *Phys. Rev.* **84** (1951) 1232.

[BW 75] G.E. Brown and W. Weise, *Phys. Rep.* **C 22** (1975) 279-337.

[CJ 86] E.D. Cooper and B.K. Jennings, *Phys. Rev.* **D 33** (1986) 1509.

[CJ+86] E.D. Cooper and B.K. Jennings, *Nucl. Phys.* **A 458** (1986) 717.

[CJ 88] E.D. Cooper and B.K. Jennings, *Nucl. Phys.* **A 483** (1988) 601.

[CJ 89] E.D. Cooper and B.K. Jennings, *Nucl. Phys.* **A 500** (1989) 553.

[Clo 79] F.E. Close, *An Introduction to Quarks and Partons* (Academic Press, New York, 1979).

[Coh 70] H. Cohen, *Phys. Rev.* **D 2** (1970) 1738.

[CT 75] A. Chodos and C.B. Thorn, *Phys. Rev.* **D 12** (1975) 2733.

[Don 66] R.A. Donald, *Proc. Phys. Soc.* **88** (1966) 1047.

[Edm 57] A. R. Edmonds, *Angular Momentum in Quantum Mechanics* (Oxford University Press, 1957).

[Erk 74] K. Erkelenz, *Phys. Rep.* **C 13** (1974) 191.

[Eric70] T.E.O. Eriscon, *Proceedings of the BANFF Summer School* (BANFF, Alberta, Canada, 1970).

[EW 88] T.E.O. Ericson and W. Weise, *Pions and Nuclei* (Oxford University Press, 1988).

[Fis 59] G.E. Fisher and E.W. Jenkins, *Phys. Rev.* **116** (1959) 116.

[GL 60] M. Gell-Mann and M. Levy, *Nuovo Cimento* **16** (1960) 53.

[Gro 82] Franz Gross, *Phys. Rev.* **C 26** (1982) 2203; *Phys. Rev.* **C 26** (1982) 2226.

[Gui 85] P.A.M. Guichon, Private Communications. (1985).

[Ham 63] J. Hamilton and W.S. Woolcock, *Rev. Mod. Phys.* **35** (1963) 737.

[Hey 77] A.J. Hey, Proc. 8th Int. Seminar **77** (1977).

[Hol+87] K. Holinde, R. Machleidt and Ch.Elster, *Phys. Rep.* **149** (1987) 1-89.

[HT 70] Michael I. Haftel and Frank Tabakin, *Nucl. Phys.* **A 158** (1970) 1-42.

[IZ 88] C. Itzykson and J.B. Zuber, *Quantum Field Theory* (McGraw-Hill, New York, 1988).

[Jaf 79] R.L. Jaffe, *Lectures at the 1979 Eric Summer School.* MIT preprint, Oct. (1979).

[KE 83] G. Kalbermann and J.M. Eisenberg, *Phys. Rev.* **D 28** (1983) 66; *Phys. Rev.* **D 28** (1983) 71.

[Klu 91] W. Kluge, *Rep. Prog. Phys.* **54** (1991) 1251.

[Kol 69] D.S. Koltun, *Adv. in Nucl. Phys. Vol.* **3** (1969) 71.

[Lee 88] T.D. Lee, *Particle Physics and Introduction to Field Theory* (Harwood Academic Publishers, New York, 1988).

[McK 63] J.M. McKinley, *Rev. Mod. Phys.* **35** (1963) 788.

[MS 88] F. Mandl and G. Shaw, *Quantum Field Theory* (John Wiley and Sons, New York, 1988).

[PA 86] B.C. Pearce and I.R. Afnan, *Phys. Rev.* **C 34** (1986) 991.

[PA 89] B.C. Pearce and I.R. Afnan, *Phys. Rev.* **C 40** (1989) 220.

[PJ 90] B.C. Pearce and B.K. Jennings, *TRIUMF preprint-PP-90-27* (1990).

[PL 70] M.Hossein Partovi and Earle L. Lomon, *Phys. Rev.* **D 2** (1970) 1999.

[PT 87] A. Picklesimer and P.C. Tandy, *Phys. Rev.* **C 35** (1987) 1174.

[Rose57] M.E. Rose, *Elementary Theory of Angular Momentum* (John Wiley and Sons, New York, 1957).

[Sca 79] M.D. Scadron, *Advanced Quantum Field Theory and its application* (Springer-Verlag, New York, 1979).

[Sca 81] M.D. Scadron, *Rep. Prog. Phys.* **44** (1981) 215.

[Sch 87] L.I. Schiff, *Quantum Mechanics (Third Edition)* (McGraw-Hill, New York, 1987).

[Stah] Karlsruhe J.Stahov, Karlsruhe Report No. TKP82-16, Unpublished.

[Thi 85] M. Thies, *Phys. Lett.* **162B** (1985) 255.

[Thi 86] M. Thies, *Phys. Lett.* **166B** (1986) 23.

[Tho 76] A.W. Thomas, *Nucl. Phys.* **A 258** (1976) 417.

[Tho 77] A.W. Thomas: Editor *Mordern Three Hadron Physics* (Springer-Verlag, Berlin, 1977).

[Tho+80] A.W. Thomas, S. Theberge and G.A. Miller, *Phys. Rev.* **D 22** (1980) 2838.

[Tho 81] A.W. Thomas, *J. Phys.* **G 7** (1981) L283.

[Tho+81] A.W. Thomas, L.R. Dodd and R.F. Alvarez-Estrada, *Phys. Rev.* **D 24** (1981) 1961.

[Tho+83] S. Theberge and A.W. Thomas, *Nucl. Phys.* **A 393** (1983) 252-282.

[Tho 84] A.W. Thomas, *Adv. in Nucl. Phys. Vol.* **13** (1984) 1.

[Tho+86] B.K. Jennings, E.A. Viet and A.W. Thomas, *Phys. Rev.* **D 33** (1986) 1859.

[Tho*86] G.A. Miller, M.A. Morgan and A.W. Thomas, *Phys. Rev.* **D 33** (1986) 817.

[Tho+87] P.A.M. Guichon, E.D. Cooper, B.K. Jennings and A.W. Thomas, *Nucl. Phys.* **A 469** (1987) 717-725.

[Thom70] R.H. Thomson, *Phys. Rev.* **D 1** (1970) 110.

[Wei 67] S. Weinberg, *Phys. Rev. Lett.* **18** (1967) 188.

[Wei 69] S. Weinberg, *Phys. Rev.* **177** (1969) 2604.

[Wei 79] S. Weinberg, *Physica* **96 A** (1979) 327-340.

[Wick55] G.C. Wick, *Rev. Mod. Phys.* **27** (1955) 339.

[WJ 73] R.M. Woloshyn and A.D. Jackson, *Nucl. Phys.* **B 64** (1973) 269.

[Wool65] V.K. Samaranayake and W.S. Woolcock, *Phys. Rev. Lett.* **15** (1965) 936.